

ABSTRACT

Title of dissertation: INDUCED SOIL LIQUEFACTION FOR THE
FREEING OF GROUNDED SHIPS

Jeffrey Cerquetti, Doctor of Philosophy, 2017

Dissertation directed by: Professor M. Sherif Aggour (Chair/Advisor)
Department of Civil and Environmental Engineering

The objective of this study is to determine the feasibility of freeing a grounded ship by liquefying the surrounding soils. Ships either moored or traveling in near-shore waters and subjected to storm events, will experience waves energetic enough to direct the ship toward the shore. The ship can then become embedded in the soils (grounded) close to the shore.

The study included two phases. Phase one was an experimental study where models of three ship sections representing standard classes of ships were constructed. These models were embedded in a saturated sand in an especially constructed tank. Pull tests were done initially to establish benchmark freeing forces and then air blasts were used to produce the dynamic force needed to liquefy the surrounding soils. The models subsequently regained buoyancy. The second phase of the study utilized the data obtained from the testing program to extrapolate those data to a response of an actual-size ship.

The conclusion showed that ships grounded can be freed by liquefaction of the surrounding soils. This novel technique of restoring a ship's buoyancy and thus refloating

it was demonstrated experimentally on model ships and analytically by determining the air pressure needed to free an actual ship in a grounding event. This new technique will have an economical value for the shipping industry and could provide an environmentally safe approach in dealing with grounded ships.

INDUCED SOIL LIQUEFACTION FOR THE
FREEING OF GROUNDED SHIPS

by

Jeffrey Cerquetti

Dissertation submitted to the Faculty of the Graduate School
of the University of Maryland in fulfillment
of the requirements for the degree of
Doctor of Philosophy
2017

Advisory Committee:

Professor M. Sherif Aggour (Chair/Advisor)
Professor Chung Fu
Professor Allison Reilly
Professor Michael E. McCormick
Professor Amr M. Baz

©Copyright by

Jeffrey Cerquetti

2017

ACKNOWLEDGEMENTS

I want to thank my wife of 33 years, Rena Marie Cerquetti, first and foremost for her tireless and inspirational efforts in support of me during the many years I have worked on this study. This accomplishment is as much hers as it is mine. Much thanks also to my father Hervey H. Smith III, a Johns Hopkins educated Civil Engineer, who worked with me hand and hand through all the hard work of the experiment over nearly 3 years. Thanks to my three beloved children, Francesca Marie, Deanna Rose and Dominic Anthony for all their support and prayers over the many years their father has toiled over this work. I am also very grateful to my faculty advisor, Prof. M. Sherif Aggour who has worked tirelessly with me over the course of years. My most sincere gratitude to my longtime advisor and mentor, Prof. Michael E. McCormick, who has navigated and encouraged me through all the turbulent waters of my academic life, both academically and mentally, leading to this zenith. I would like to thank Mr. Robert Murtha for all his help and support and use of his facility for my experimentation – he is truly an honorable friend. Thanks to Dr. Patrick J. Hudson for all his advice and consul.

Additional thanks to Mr. Clifford Stearns who worked with me over many weekends through several of the technical snarls in constructing my experiment. Thanks to Mr. James Wilson, PE, who generously contributed his many years of engineering expertise in working with the air cannon during the experiment. Special thanks to Mr. Mark Schroeder, formerly of Wartsila NSD, and Mr. Frank Morabito, PE, of Morabito Consultants, Inc. for their financial support during my tenures at both firms. Other thanks go out Ms. Danielle Lambert for her help with the MathCAD modeling and Mr. Michael

Hild, PE, for his support and consul both of JMT, Inc. Thanks also to Prof. Zenon Medina Cetina of Texas A&M who I have had the benefit of having as a friend and councilor since we were both students at Johns Hopkins. I wish to express special gratitude to Dr. John Rosero for all his masterful help and assistance with the many technical post-processing issues he tirelessly helped resolve over many months. I gratefully acknowledge the financial support provided by my employer Johnson, Mirmiran and Thompson, Inc.. I would like to gratefully acknowledge the members of my University of Maryland committee; Prof. M. Sherif Aggour (Chair), Prof. Allison Reilly, Prof. Chung Fu and Prof. Amr M. Baz as well as Prof. Michael E. McCormick of the United States Naval Academy.

I would like to finally dedicate this work to the memory of my mother,

Virginia Adelia Cerquetti Smith

Who instilled the will and drive in me to persevere through life's hazardous waters to achieve any goal – through God's grace....

Contents

ACKNOWLEDGEMENTS	ii
LIST OF TABLES	vi
LIST OF FIGURES	vii
SYMBOLS AND ABBREVIATIONS	xii
1. INTRODUCTION	1
2. PROBLEM DEFINITION	4
2.1 Mechanics of Grounded Ship Motions	4
2.2 Ocean Wave Mechanics – The Energy for Grounded-Ship Motions	7
2.2A Linear (Sinusoidal) Waves – Contributions to Ship Embedment	7
2.2B Solitary Waves – The Cause of Ship Migration	18
2.3 Existing Methods Employed to Free a Grounded Ship:.....	20
2.3A Brute-Force Pulling:.....	21
2.3B Sand-Jetting:.....	21
2.3C Load Reduction:	22
3. PRIOR EXPERIMENTAL STUDIES	24
4. EXAMPLES of ACTUAL SHIP GROUNDINGS	26
5. SOIL LIQUEFACTION	32
5.1 Definition of Soil Liquefaction	33
5.2 Soil Liquefaction as a Mode of Release.....	34
5.3 Blast-Induced Liquefaction (BIL).....	36
5.3A Experiments at Treasure Island.....	36
5.3B USAF Office of Scientific Research	37
6. EXPERIMENTAL APPROACH.....	39
6.1 Experimental Facilities	39
6.1A Model Tank	39
6.1B Ancillary Equipment	41
6.1C Reaction Frame	43
6.2 Ship Section Models	43
6.3 Blast Simulation: Compressed Air Device	51
6.4 Detection of Shock Intensity by Hydrophones	54
6.5 Baseline and Blast Tests	57
6.5A Baseline Tests	58
6.5B Blast Tests	59
6.6 Experimental Setup.....	64
6.6A Model Positioning and Alignment	65

6.7 Measurement and Recordings.....	69
6.7A Blast Pressure and Spectra	72
6.7B Blast-Pressure Effects on Pull-Out Loads	75
7. RESULTS	79
8. DISCUSSION	85
9. PROJECTION FORWARD: CONCEPT-to-IMPLEMENTATION	89
9.1 Dimensional Analysis	89
9.2 Implementation	96
10. CONCLUSIONS and RECOMMENDATIONS	101
APPENDIX.....	103
Appendix A: Experimental Photograph Record	103
Appendix B: Sample Case Studies	118
Case 1 – M/V Pasha Bulker:	118
Case 2 – TK Bremen:.....	120
Case 3 – M/V Victoria:	121
Appendix C: Design and Construction of the Experimental Equipment	124
Model Tank Construction:	124
Ship Models:	127
Cofferdam and Vibrator System:	131
Reaction Frame:	132
Appendix D: Additional Equipment Listing	134
Appendix E: Sound Recording Equipment Diagrams	138
Appendix F: Hydrophone Construction Design.....	147
Appendix G: Model Testing Log Sheets (Baseline and Blast Test)	159
Appendix H: Pressure Trace Plots and Spectrum Plots	162
Appendix I: Results Description related to the Theorem of Buckingham Pi.....	183
REFERENCES	185
PHOTO REFERENCES	191
REFERENCES (APPENDIX B)	192

LIST OF TABLES

Table 1	Signal Response Data Taken from Figure 35.....	61
Table 2	Ship Model Embedment Depths in Tank.....	65
Table 3	Table of Sand Properties used in the USAF Study by Fragaszy, <i>et al</i> (1981).....	66
Table 4	Model Sand Gradation Curve.....	68
Table 5	Model Pull-Out Baseline Test Results.....	71
Table 6	Blast Test Results from Written Logs for SS1, SS2, and SS3.....	77
Table 7	Results for Model Surface Area Pull-Out Pressures.....	87

LIST OF FIGURES

Figure 1.	The Cargo Ship TK Bremen stranded on a beach near Erdeven, France (from <i>Marine Nationale</i> : “T. K. Bremen Grounding”, On-Line, 2011).....	5
Figure 2.	Principal Ship Motions (from <i>Modern Ship Design</i> ; Gillmer 1975).....	6
Figure 3.	Three Phases of Ship Grounding	7
Figure 4.	Notation for a Linear Right-Running Wave	14
Figure 5a.	Standing Wave Profile Using the Method of Images from a Perfect Reflection (from <i>Ocean Engineering Mechanics</i> ; McCormick 2014).....	15
Figure 5b.	Ship Embedment, (d), Rocking Motion – Bow View	16
Figure 6a.	Wave Profiles in Various Sea States	17
Figure 6b.	Solitary Wave Profile	18
Figure 7.	Migratory Shoreward Wave Force Acting on a Grounded Ship (from image by <i>Paul J. Gallie</i> : “M/V SeaLand Express Grounding”, On-Line, 2003	20
Figure 8.	M/V Sealand Express in Port in Table Mountain, Cape Town, South Africa (from image by <i>Paul J. Gallie</i> : “M/V SeaLand Express Grounding”, On-Line, 2003).....	27
Figure 9.	M/V Sealand Express Lies in Sturrock Drydock in Cape Town (from image by <i>Paul J. Gallie</i> : “M/V SeaLand Express Grounding”, On-Line, 2003)	28
Figure 10.	APL Panama Shown here Grounded from a Navigational Error (from the <i>San Diego Tribune</i> : “APL Panama Grounding”, On-Line, 2008).....	29
Figure 11.	APL Panama Being Unloaded from a Constructed Landside Jetty (from the <i>San Diego Tribune</i> : “APL Panama Grounding”, On-Line, 2008)	30
Figure 12.	Fishing Vessel <i>Mar-Gun</i> shown here being driven aground near beach off the Alaska coast from storm surge (photo credit N. Huddleston - ADEC: “F/V Mar-Gun”, On-Line, 2009).....	30
Figure 13.	Table from Seed and Idriss (<i>Analysis of Soil Liquefaction</i> , 1967).....	32

Figure 14.	Soil Liquefaction Mechanism (from <i>Univ. of Washington CE Dept.</i> , Webpost 2010)	33
Figure 14a.	Laboratory Testing of Sand Under Cyclic Loading on Loose and Dense Sands (research of <i>Shannon and Wilson; 2011</i>).....	35
Figure 15.	Detonation Sequence used for BIL at NGES on Pile Load Tests	36
Figure 16.	Tank, Restraint Cable and Platform Assembly.....	40
Figure 17.	Drain Valve Installed in Tank Corner	41
Figure 18.	Aluminum Cofferdam before and after use with Burying Model	42
Figure 19.	Reaction Frame Assembly over Model Tank	43
Figure 20.	Ship Sections Model Geometry	45
Figure 21.	Ship Models in the process of being built (Note hollow interior for ballast additions	46
Figure 22.	Lifting Arrangements	47
Figure 23.	Model Fiberglass Covering/Coating Operation	48
Figure 24.	Model Ballast with Wood Sub-Frame, Lifting Lanyard and Painted Exterior View	49
Figure 25.	SS2 Flotation Test being performed after Low-Keel Ballast Added	50
Figure 26.	Lead Sinkers being melted into Steel Pipe Fittings for Keel Ballast	50
Figure 27.	Low Keel Permanent (Buckshot) Ballast placed into SS2 Model	51
Figure 28a.	Air Cannon Schematic	52
Figure 28b.	Air Cannon with Pressure Gage and Quick Release Valve	53
Figure 29.	Assembling of Hydrophones from Parts	54
Figure 30.	Assembled Hydrophone	55
Figure 31.	PVC Pipe Diaphragm, Blast Nozzles (left) and Hydrophone Port (right).	56
Figure 32.	Schematic of Tank with Buried Equipment	57

Figure 33.	Guywires for Consistent Model Positioning within the Tank.....	59
Figure 34.	Positioning of Hydrophones into Ports adjacent to Blast Nozzles	60
Figure 35.	Hydrophone(s) Signal Record and Sound Spectrum from DA-88 Recorder.....	63
Figure 36.	Tascam DA-88 Recorders (Bottom Left) and Input Soundboard (Right).	69
Figure 37.	Plotted Results of the Effects of Pull-Out Force on each of the Three Ship Models.....	72
Figure 38.	Setup and Arrangement for Blast Tests	76
Figure 39.	Baseline (Brute Force) Pull-Out Test	79
Figure 40.	Pull-Out Test Plot Results	81
Figure 41a.	Effect of Air Pressure Variations on the Pull-Out Ratio (SS1) during Liquefaction Segment.....	82
Figure 41b.	Effect of Air Pressure Variations on the Pull-Out Ratio (SS2) during Liquefaction Segment.....	83
Figure 41c.	Effect of Air Pressure Variations on the Pull-Out Ratio (SS3) during Liquefaction Segment.....	84
Figure 42.	Model Surface Contact Areas	86
Figure 43.	Bunkering Tank ARCA 1 grounded off Cape Breton beach. Nova Scotia, Canada (from <i>Fisheries and Oceans Canada</i> : On-Line, 2017).....	91
Figure 44.	Values for Field Scaled Pressures compared to the ARCA 1 Ship Example.....	94
Figure 45.	Draft Definition of Midship Section.....	95
Figure 46.	Ship Draft (depth) vs. Blast Pressure at the Site.....	96
Figure 47.	BIL Equipped Rescue Barge in Position Around a Grounded Ship.....	98
Figure B1.	M/V Pasha Bulker Taking on Heavy Seas (from <i>1233 ABC Newcastle News</i> , “M/V Pasha Bulker Grounding”, On-Line, 2012)	119

Figure B2.	M/V Pasha Bulker Grounded off the coast of Nobbys Beach, Australia, (from <i>1233 ABC Newcastle News</i> , “M/V Pasha Bulker Grounding”, On-Line, 2012)	119
Figure B3.	TK Bremen is Stranded on Kerminihy beach. Rescue Measures begun. (from <i>Marine Nationale</i> : “T. K. Bremen Grounding”, On-Line, 2011)..	120
Figure B4.	TK Bremen is Broken Apart on January 7, 2012 at Erdeven, France (from <i>Marine Nationale</i> : “T. K. Bremen Grounding”, On-Line, 2011)..	121
Figure B5.	Liberian Flagged M/V Victoria Grounded at Fladen (from <i>World Maritime News</i> : M/V Victoria Grounding,” On-Line, 2016).....	122
Figure B6.	Tug Towing / Fuel Unloading following to Night-Time Salvage Attempts (from <i>World Maritime News</i> : M/V Victoria Grounding,” On-Line, 2016)	123
Figure C1.	Tank During Construction and Water Leak Testing	124
Figure C2.	Model Tank Schematic with Sidewall Stiffeners	125
Figure C3.	Completed Model Tank with Lexan Sides, Stiffeners and Tension Cable.....	126
Figure C4.	Ship Models showing Geometry and Embedment Lines	127
Figure C5.	Ship Model Wooden Subframe Construction	128
Figure C6.	Model Foam Gluing Procedures with Nylon Strap-Chains	129
Figure C7.	Section of Model Subframe with Aluminum Straps and Eyebolt Rod Assembly	130
Figure C8.	Vibrator Used with Sideslide Mounts for Insertion of Cofferdam Into Tank Sand	131
Figure C9.	Screw Dredge for Sand Removal during Model Trials	132
Figure C10.	Reaction Frame in Mobile Position Over Model Tank	133
Figure G1.	Typical Baseline (Pullout) Test Field Record	160
Figure G2.	Typical Blast (Compressed Air) Test Field Record	161
Figure H1.	Tape No. 1, Blasts 1, 2 and 3	164

Figure H2.	Tape No. 2, Blasts 1, 2 and 3	165
Figure H3.	Tape No. 3, Blast 1	166
Figure H4.	Tape No. 4, Blasts 1, 2 and 3	167
Figure H5.	Tape No. 5, Blasts 1, 2 and 3	168
Figure H6.	Tape No. 7, Blasts 1, 2, 3, 4 and 5	169
Figure H7.	Tape No. 8, Blasts 1, 2 and 3	170
Figure H8.	Tape No. 9, Blasts 1 and 2	171
Figure H9.	Tape No. 10, Blasts 1, 2 and 3	172
Figure H10.	Tape No. 11, Blasts 1, 2 and 3	173
Figure H11.	Tape No. 12, Blasts 1, 2 and 3	174
Figure H12.	Tape No. 13, Blasts 1, 2, 3 and 4	175
Figure H13.	Tape No. 14, Blasts 1, 2, 3 and 4	176
Figure H14.	Tape No. 15, Blasts 1, 2, 3 and 4	177
Figure H15.	Tape No. 16, Blasts 1, 2, 3 and 4	178
Figure H16.	Tape No. 17, Blasts 1, 2, 3, 4 and 5.....	179
Figure H17.	Tape No. 18, Blasts 1, 2, 3 and 4	180
Figure H18.	Gaussian Spectrum Log Plots of Tape 1 Blast 1 on all 4 Hydrophones..	182

SYMBOLS AND ABBREVIATIONS

Abbreviations

AFB	Airforce Base
ASCE	American Society of Civil Engineers
ASTM	American Society of Testing Materials
BIL	Blast Induced Liquefaction
CFD	Computational Fluid Dynamics
DWT	Dead Weight Tonnage
HP	designation for dimensionally square steel pile
Hz	Hertz (cycles per second)
ISO	International Standards Organization
LL	Liquid Limit
M/V	Motor Vessel
MWL	Mean Water Level
NGES	National Geotechnical Experimentation Site
PL	Plastic Limit
PVC	Polyvinyl Chloride
S.G.	Specific Gravity
SM	Silty Sand (USCS Classif.)
SP	Sand, Poorly graded (USCS Classif.)
SW	Sand, Well graded (USCS Classif.)
SWL	Still Water Level
TILT	Treasure Island Liquefaction Test
USAF	United States Air Force
USCS	Unified Soil Classification System per ASTM D2487

Mathematical Symbols

c	Wave Celerity, phase velocity (feet/sec.)
C	Solitary Wave Speed (feet/sec.)
C_c	Coefficient of Curvature; of the soil mass (USCS Desig.)
C_u	Coefficient of Uniformity; of the soil mass (USCS Desig.)
d	Depth of Embedment (ft.)
D_{xx}	Grain Dia. at sieve where xx percent passes; of the soil mass (mm)
e	Void ratio; of the soil mass
E	Modulus of Elasticity, Young's Modulus (pounds/sq. in.)
F_b	Flexural Bending Stress (pounds/sq. in.)
F_c	Compressive Strength (pounds/sq. in.)
F_y	Yield Stress (pounds/sq. in.)
f	Frequency (Hertz)
g	Acceleration of Gravity (32.2 feet/sec. ²)
$G_{x,s}$	Specific gravity of the material (sand = 2.65)
$h, h(x)$	Water depth (feet)
h_b	Water Depth at Break (feet)
H	Wave Height (feet)
H_b	Breaking Wave Height (feet)
k	Wave Number
n	Porosity (of the soil mass)
p	Pressure (pounds/sq. in.)
Q	Quality Factor
R	Damping Coefficient
R_u	Excess Pore Pressure Ratio
S_t	Strouhal Number (dimensionless)

T	Wave Period (seconds)
V, v, w	Velocity (feet/sec.)
V_S	Volume of the soil solids (cu. ft.)
V_T	Volume total; of the soil mass (cu. ft)
V_V	Volume of the voids; of the soil mass (cu. ft.)
W_S	Weight of the soil solid material (lbs.)
W_T	Weight total; of the soil mass (lbs.)
W_W	Weight of the water within the soil mass (lbs.)
x, y, z	Spatial coordinates (feet; inches, meters)

Greek Letter Symbols

β_T	Isothermal Bulk Modulus of water
Δu	Excess Pore Pressure (at the depth of study)
λ	Wavelength (feet)
γ_w	Unit weight of the water (62.4 lbs./cu. ft.)
$\eta, \eta(x)$	Wave Free Surface Profile
ρ, ρ_0	Density (pounds/feet ³)
σ'_0	Effective Vertical Stress (in the soil)
ω	Circular (wave) Frequency (Hertz)
ϕ	Velocity Potential

1. INTRODUCTION

Grounded ships are sources of both environmental and navigational problems in the coastal zone. The severity of these problems depends on the time taken to re-float these ships. To reduce this time, a method to quantify the forces and reactions associated with the release of grounded ships could prevent adverse effects to the environment as well as to the naval community and the shipping industry. This dissertation presents the results of experimental studies of a novel technique designed to free grounded ships from pliable seabeds typically associated with near-shore locations. This technique referred to employs the use of *blast-induced soil liquefaction*.

In many cases, a ship may have to be dismantled or “broken” down. This process often involves beach cleanup, spill containment and remediation, and hazmat disposal utilizing teams of workers and equipment over the ensuing months of an incident. Oil spills and washup can be devastating to wildlife and plant life with long-term effects.

Results of the present study have several possible implications for the maritime industry as well as for Navy and Coast Guard ships. Salvage operations could be enhanced once a grounding situation was identified and assessed as to location, type of grounding (bow or broaching), soil type and soil condition (saturated and/or compacted). The present-day standard salvage technique is to, first, remove the ship’s contents (of particular importance when carrying certain types of liquids) in order to increase the buoyancy as much as possible. Lines are then attached seaward of the grounded vessel, and the ship is pulled by one or more tugboats during high-tide. Unfortunately, this type of freeing operation could compromise the ship’s structure. Depending on the amount of fuel onboard and the nature of the cargo, a rupture of the hull would pose a bio-hazard. A grounded ship

is not fully buoyant, and remains partially embedded. This poses a hazard to the hull viability. It should be noted that the standard freeing operation must be performed within 24 hours of the grounding event to be successful.

Again, the premise of the present study is that it should be possible to aide in the regaining of the ship's buoyancy by making use of blast-induced soil liquefaction (BIL) technique. The success of the operation would, naturally, depend on the nature and size of the cargo. When one hears the term "blast", explosives such as dynamite come to mind. This type of BIL is normally unacceptable because of the inherent dangers to the ship, cargo and sea life. The BIL method proposed in the present study is a more acceptable method since only the sea bed materials are affected. That is, the soil surrounding an embedded vessel could be induced to liquefy using compressed air (blasts) administered from a buried pipe diaphragm within the sand. This would be during a high-tide event. The high-tide combined with the liquefaction could instantaneously result in the ship being brought back to a total-buoyant condition. It was hypothesized and, subsequently, demonstrated that several ship shapes were able to regain buoyancy once the compressed-air blast-induced liquefaction occurred. This was successfully done on three ship-section models, including a flat-bottom section and two with dihedral angles. These are ship-sectional shapes that bear naval similarities to typical sea-going vessels.

The research undertaken investigates a release mechanism for a grounded ship. The research is primarily experimental in nature, where the model-scale naturally depends on the prototype dimensions. The model sectional geometries are *apropos* to cargo ships and tankers. The experimentation study is designed to examine the feasibility of introducing a concussive shock pressure into the soil surrounding a stranded vessel that induces

liquefaction. This methodology is a function of ship configuration and blast or concussion force determination needed to cause the soil to liquefy. Ship-shape models were built for these experiments to simulate standard-vessel sectional geometries. The goal of the study is to determine the potential release characteristics in a known bed material – for this study sand is used.

The research involved in this study is organized such that there is a clear understanding of the process undertaken in a logical format. It starts from the problem-definition following to the setup and implementation of the experiment to the mechanics of liquefaction induction in this marine environment. Sequentially, Section 2 discusses the mechanics of grounded ships and background on waves followed by present methods used free grounded ships. Section 3 is prior experimental studies in the area of grounded ships. Section 4 describes examples of ship groundings and pertinent Case studies to support the premises on which the experimentation and the data analyses are based. Section 5 is background on soil liquefaction and an introduction of Blast-Induced research and testing. A detailed discussion of the experimental approach is presented in Section 6, highlighting the constructs used along the way. Section 7 is a presentation of the experiment results and Section 8 is a discussion of those results which are collected and synthesized. Section 9 is a discussion of a proposed implementation method using dimensional analysis scaling with the experimental results and Section 10 is Conclusions and Recommendations.

In general, this sequence of sections, augmented by appendices, follows the thought process leading to the design of the experiment to what results ensued and how to implement those results for future work on actual ship grounding release.

2. PROBLEM DEFINITION

Ship groundings over the years are a source of continued nautical problems in both rivers and coastal waterways. Ships and their cargoes, which become lodged in channels and watercourses have navigational and spill-containment detrimental effects, pose issues to agencies charged with physical security like the U.S. Coast Guard. Ship groundings are due to extreme environmental effects, propulsion failures and human error. Normally, two of these are coupled to produce the grounding event which, in turn, affects all sectors of the maritime theater - industrial, military and private. When a ship drags anchor due to a storm event or loses power in a seaway, the ship migrates landward due to wave action. There are two waves that contribute to the problems associated with grounded ships. These are (a) linear or sinusoidal waves, which can rock a grounded ship, causing further embedment and (b) solitary-type (or long-period) waves, which cause the migration of the grounded ship towards shore. When a ship loses power, it becomes subject to the waves which normally cause the ship to broach. That is, the centerline of the ship becomes approximately parallel to the wave crest, and the ship is then in a beam-sea condition. The broached ship then becomes embedded in the seabed. Normally, once a ship is grounded, it stays grounded and the wave action will cause it to be more embedded into the seabed.

2.1 Mechanics of Grounded Ship Motions

Traditional freeing methods are often ineffective, and can cause structural damage to the ship in the process. The releasing method investigated in this work proposes a process of effectively changing the “state” of the seabed material in which the grounded vessel is embedded from granular to *quasi*-liquid. When this local seabed state-change is achieved

during a high-tide, the vessel's buoyancy has a high probability of being regained. The vessel would, in turn, be safely dislodged and/or refloated in a more cost-effective way.

One example of this type of costly ship grounding is that of the Maltese-flagged *TK Bremen* - a 2,000 DWT cargo ship with 220 tons of fuel oil traveling along the northwest coast of France. This ship ran aground in 2011 on Kerminihy Beach in a high-wind, heavy-sea condition. A photograph of this grounded ship is presented in Fig. 1.



Fig. 1 – The Cargo Ship TK Bremen stranded on a beach near Erdevén, France (from Marine Nationale: “T. K. Bremen Grounding”, On-Line, 2011)

The TK Bremen lost power and, subsequently, was brought parallel to the shoreline (broached) as waves slammed against her side. Once grounded, the wave-induced rocking of the ship caused the hull to further embed into the beach sand. There was an associated fuel-oil spill with extensive environmental consequences. The ship was damaged so severely as a result of the grounding that a decision was made to dismantle and remove it from the site. This effort was conducted over the next three weeks. Environmental cleanup had to be done on the beach at an estimated loss of over \$13 million. If the blast-induced

soil liquefaction (BIL) method was available during the TK Bremen grounding, the ship could have been freed and refloated within 24 hours, resulting in far-less economic and environmental costs.

A three-phase grounding scenario for this event was first described by McCormick (1999) and later by McCormick and Hudson (2001). According to these authors, the grounding process of a ship consists of (1) the bow coming into contact with the seabed usually from a loss of power or anchor slippage (2) wave action altering the ship's orientation to a coast-parallel position of the ship's centerplane and (3) the wave induced motions resulting in the migration of the vessel landward (see Fig. 3). These principal ship motions are *sway* (lateral, linear motion along the transverse axis) and *roll* (rotation about the longitudinal axis) as the hull becomes embedded in the soil, as sketched in Fig. 2.

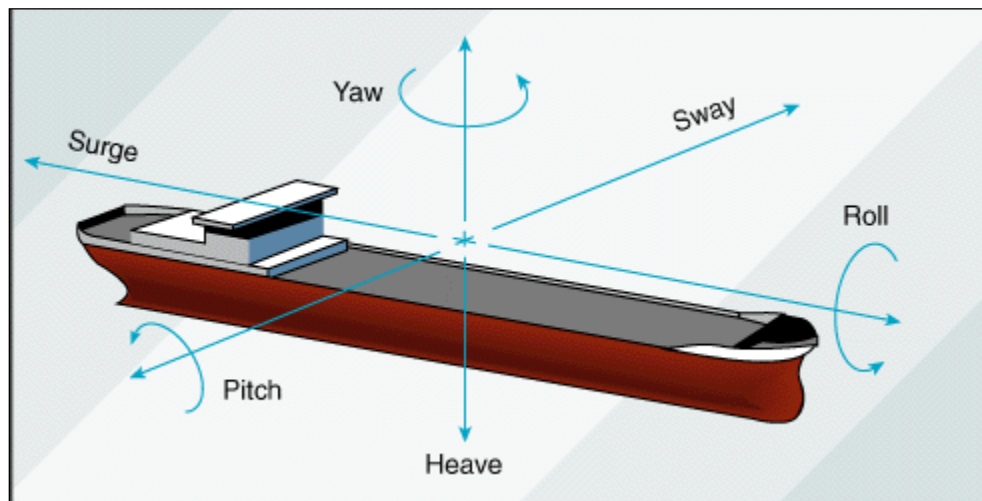


Fig. 2 – Principal Ship Motions (from *Modern Ship Design*; Gillmer 1975)

Once the ship hull is in contact with the soil, the nature of the vessel changes. That is, the soil now partially supports the ship as does the water by reduced buoyancy. Hence, the nature of remediation (ship freeing) changes from a hydromechanics problem to a hybrid soil-fluid problem. This complicates matters since the soil (solid) mechanics must

be simultaneously addressed with the hydromechanics. The goal of the present study is to use BIL as a means to return to the hydromechanics realm.

2.2 Ocean Wave Mechanics – The Energy for Grounded-Ship Motions

As previously stated, ocean waves collectively are the primary problem for a ship that has lost power or lost its anchorage. The waves in open water will rotate the ship until the centerline of the ship is parallel to the shoreline. Once grounded, the ship is either rocked by non-breaking linear waves, or driven shoreward by nonlinear waves of long-period. Theoretically, the longest breaking wave is called the *solitary wave*. See Fig. 6b. These waves are briefly discussed in the following sub-sections.

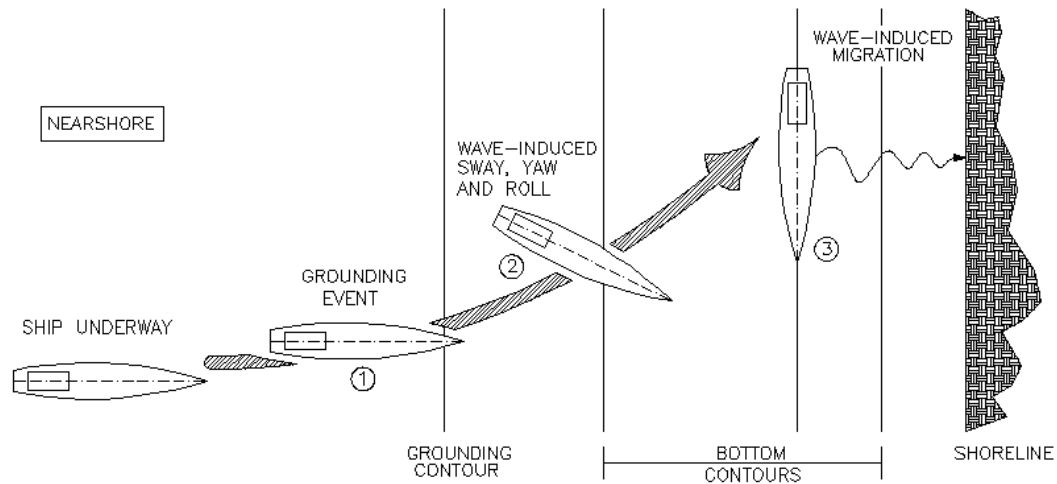


Fig. 3 – Three Phases of Ship Grounding

2.2A Linear (Sinusoidal) Waves – Contributions to Ship Embedment

George B. Airy (1845) introduced the linear wave theory, sometimes referred to as the “Airy wave theory”. As noted by McCormick (2010, 2014), the theory is somewhat basic; however, the kinematic wave properties derived from the theory well-agree with those that are actually observed. The only proviso is that the wave steepness is small. The

wave steepness is defined as the ratio of the wave height (H) and the wavelength (λ). In what follows, the basic results of the theory that are applicable to the ship-grounding problem are reviewed.

Basic Linear Wave Theory:

The linear wave is one with a *sinusoidal profile* which is shown in Fig. 4. This is based on a *traveling sinusoidal wave* which is linear in nature – therefore the term “linear” is used for purposes of general derivation. The roots of this theory go back to the 19th century where wave mechanist George B. Airy formulated the *linear or Airy wave theory*. Airy based the theory on two equations in fluid dynamics. The first is *the equation of continuity*:

$$\mathbf{V} \cdot \nabla \mathbf{V} = \nabla (V^2/2) - 0 \quad (2.1)$$

Where ∇ is the *del operator* : $\frac{\partial}{\partial x} + \frac{\partial}{\partial y} + \frac{\partial}{\partial z}$

To simply the general form of the continuity equation, Airy assumed the flow under water waves to be two-dimensional, **inviscid**, **irrotational** and **incompressible** resulting in the following equation, known as ***Laplace’s Equation*** as:

$$\nabla \cdot \mathbf{V} = \partial^2 \phi / \partial y^2 + \partial^2 \phi / \partial z^2 = \nabla^2 \phi = 0 \quad (2.2)$$

Where, ϕ , is the velocity potential, a scalar quantity whose partial derivative with respect to y is the horizontal velocity component, v , and with respect to z is the vertical velocity component, w .

The second equation is:

$$\rho \frac{\partial \phi}{\partial t} + \frac{1}{2} \rho V^2 + \rho g z + p = f(t) \quad (2.3)$$

where, ρ , is the mass density, a function of neither time nor space; V is the fluid velocity; z is the vertical position and g is the acceleration of gravity.

This is known as ***Bernoulli's Equation*** which is an expression of the conservation of energy per unit mass. To apply this equation to water with a *free surface*, consider a simplification case to water on a calm surface or no motion bringing the *time-function* in that equation, $f(t)$, equal to zero:

$$\rho \frac{\partial \phi}{\partial t} + \frac{1}{2} \rho V^2 + \rho g z + p = 0 \quad (2.4)$$

which is *non-linear* due to the velocity-squared term.

In order to obtain a method of analysis for the general solution to these two equations, Airy applied boundary conditions on both the sea floor and the free surface.

a. Sea Floor Condition

The seafloor condition assumes that there are usually impermeable layers of rock, silt and clay on the bottom. This condition states that there can be *no flow across the seafloor (or bed)*. So the vertical velocity component at $z = -h$ (from Fig. 4 notation) will be zero. Expressed mathematically, the condition is:

$$-\frac{\partial \phi}{\partial z} = 0 \quad \text{on } z = -h \quad (2.5)$$

b. Kinematic Free-Surface Condition

A water wave will displace the free-surface as it passes, and this displacement can be described as a function η , of y and t . A statement of this condition is *particles on the free surface always remain on the free surface*. This physically means the particles are not allowed to jump up into the air. The kinematic free-surface boundary condition may be expressed as:

$$w = \frac{\partial y}{\partial x} + v \frac{\partial y}{\partial x} \text{ at } z = \eta (y, t) \quad (2.6)$$

or in terms of the velocity potential as:

$$-\frac{\partial \phi}{\partial z} = \frac{\partial \eta}{\partial t} - \frac{\partial \phi}{\partial y} \frac{\partial \eta}{\partial y} \text{ at } z = \eta (y, t) \quad (2.7)$$

c. Dynamic Free-Surface Condition

The water surface freely responds to pressure distribution changes across it which is where the term *free-surface* comes from. The pressure everywhere on the free-surface is then uniform and equal to atmospheric pressure. A statement of this condition is *the pressure on the free-surface is uniform, constant and equal to zero (gauge; $p = 0$)*. We apply this condition to Bernoulli's equation (2.3) to the free-surface of a wave to *linearize* the equation by allowing the velocity-squared term to be of *second-order*. The assumption of this condition is that the *kinetic energy* (in the second term; i.e. the velocity-squared term in the Bernoulli equation) is an order of magnitude less than the other energies within the equation. Considering this assumption that the amplitude of the waves, η , is very small since maximum value is the wave amplitude, it follows that the velocities v and w are likewise small and can surmise that the square of these velocities can be taken as negligible. So with very small η , the pressure at $z = \eta$ is approximately that at $z = 0$. Using this assumption, the following expression can be obtained from the simplified Bernoulli's equation:

$$\eta = \frac{1}{g} \frac{\partial \phi}{\partial t} \text{ at } z = 0 \quad (2.8)$$

d. Linearized Free-Surface Condition

The third free-surface condition is obtained by making use of a combination of equations 2.7 and 2.8, and is termed the *linearized free-surface condition*. This continues, as above, on the premise that the wave steepness (H/λ) is small. The free-surface conditions are now combined by eliminating η to ascertain the linearized free-surface condition which is now:

$$\frac{1}{g} \frac{\partial^2 \varphi}{\partial t^2} \Big|_{z=\eta=0} + \frac{\partial \varphi}{\partial z} \Big|_{z=\eta=0} = 0 \quad (2.9)$$

$$\left\{ \frac{1}{g} \frac{\partial^2 \varphi}{\partial t^2} + \frac{\partial \varphi}{\partial z} \right\} \Big|_{z=\eta=0} = 0$$

Since the flow in the wave is assumed to be irrotational, the equation of continuity expressed as Laplace's equation (2.1) can be solved using a product solution. This is of the form:

$$\varphi = X(x)Z(z)T(t) \quad (2.10)$$

When this product solution is for a *traveling wave*, it will be in the form:

$$\varphi = X(x \pm ct)Z(z) = X(\xi)Z(z) \quad (2.11)$$

The coordinate system for (2.10) is fixed at a point, whereas that of (2.11) is transported with the wave. For a traveling wave the expression of (2.10) is substituted into that of (2.1) and separate terms of the same variables become:

$$\frac{1}{X} \frac{d^2 X}{d\xi^2} = - \frac{1}{Z} \frac{d^2 Z}{dz^2} = -k^2; \text{ (k is a constant)} \quad (2.12)$$

The negative sign comes about because the free-surface profile follows the shape of a sine-wave in the ξ – direction. The general solutions of the differential equations in the ξ – and z – directions respectively are of the form:

$$X(\xi) = C_\xi \sin (k \xi + \alpha) \quad (2.13)$$

$$Z(z) = C_z \cosh (k z + \beta) \quad (2.13)$$

where C_ξ , C_z and β are constants that are determined by the boundary conditions. Because the origins of the horizontal coordinates ξ and x are arbitrary, the constant α can be assigned a value of zero without loss of generality. Equation (2.13) can therefore be reduced to:

$$X(\xi) = C_\xi \sin (k \xi) \quad (2.14)$$

To determine the constant β , apply the sea-floor condition of (2.5) to the velocity potential expression resulting from the combination of equations (2.11) and (2.13). Assuming the sea floor is flat and horizontal, only the z -term is affected by the boundary condition. That is, the sea-floor condition results in the equation:

$$\left. \frac{dZ}{dz} \right|_{z=-h} = k C_z \sinh (-kh + \beta) = 0 \quad (2.15)$$

From which $\beta = kh$. The expression in Eq. C1.13 is then:

$$Z(z) = C_z \cosh [k(x + h)] \quad (2.16)$$

The combination of the expressions of equations (2.14) and (2.16) with that of (2.10) results in:

$$\varphi = C_\varphi \cosh [k(z + h)] \sin(k\xi) \quad (2.17)$$

where $C_\varphi = C_\xi C_z$. If the nature of the horizontal coordinate, ξ , is now considered, we can surmise from (2.10) that its' coordinate is defined as:

$$\xi = x \pm ct \quad (2.18)$$

The origin of the coordinate corresponds to:

$$x = \pm ct \quad (2.19)$$

From this it can be seen that the value of x decreases as the time, t , increases for the upper sign (-). As such, the wave must travel in the $x -$ direction at a celerity or phase velocity, c . The waves corresponding to the upper signs in equation (2.18) and (2.19) are called *left-running waves*. Following the same line of thinking, the lower signs in those equations correspond to *right-running waves*.

Returning to the expression for the velocity potential in (2.17), the arbitrariness of the coefficient C_ϕ in the equation can now be removed. In order for this to be accomplished, combine the expressions in (2.8) and (2.17) by eliminating the velocity potential, ϕ . This combination yields the following expression for the free-surface displacement of a sinusoidal wave:

$$\eta^\pm = \frac{ck}{g} C_\phi^\pm \cosh(kh) \cos(k\xi^\pm) = \frac{H}{2} \cos(k\xi^\pm) \quad (2.20)$$

where the last equality results from knowing that the wave is sinusoidal in both time and space. In the right term of (2.20), H is the wave height. Comparing the terms of the last equality of (2.20), we obtain the expression for the coefficient C_ϕ^\pm , which is:

$$C_\phi^\pm = \pm \frac{H}{2} \frac{g}{kc} \frac{1}{\cosh(kh)} \quad (2.21)$$

Combining this expression and that of (2.18) with that of (2.17) to obtain the final expression for the velocity potential of a traveling wave as:

$$\phi^\pm = \pm \frac{H}{2} \frac{g}{kc} \frac{\cosh[k(z+h)]}{\cosh(kh)} \sin[k(x \pm ct)] \quad (2.22)$$

The velocity potential yields the velocity components of the particles in the irrotational flow beneath traveling waves. The velocity potential expression in (2.22) is the primary

result of the Airy wave theory. All the other properties mentioned earlier starting from (2.1) following to (2.7) follow from this methodology can now be derived.

Results from the Linear Wave Theory:

From the analysis above, applicable results are now presented.

At a point x in space and t is time, a passing linear wave will cause the free-surface to be displaced (raised or lowered) from equilibrium. See wave notation as shown in Fig.

4. The free-displacement of a traveling wave, η , according to the linear theory, is given by

$$\eta = H/2 \cos [k(x - ct)] \quad (2.23)$$

Where k is the wave number, defined as:

$$k = 2\pi / \lambda \quad (2.24)$$

and c is the phase velocity (wave celerity)

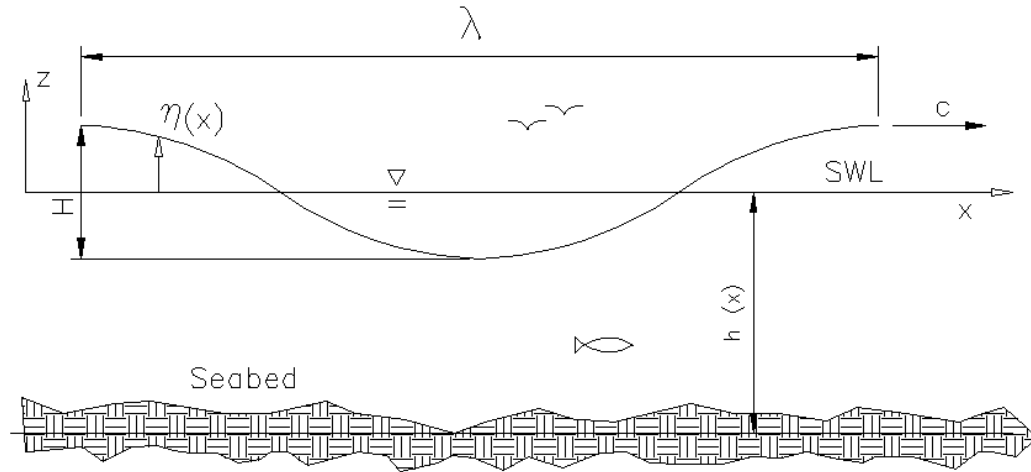


Fig. 4 – Notation for a Linear Right-Running Wave

In the figure, SWL is the acronym for still-water level.

As a linear wave comes in contact with a vertical wall, such as the hull of the ship, it reflects. It is more easily understood if one considers two traveling waves (one being a mirror image of the other) having the same heights, celerity (c^+ and c^- respectively) and periods passing each other in the x-z plane. As they pass each other in opposite directions with equal magnitudes, they cancel each other out when superimposed. The resulting pattern, formed from a perfect reflection (as stated earlier from a seawall or wall-sided ship), that remains has zero celerity, or becomes a *standing wave*. When this happens, the incident wave height (H) doubles, resulting in the standing wave having twice the height of the incident wave. This can be seen in Fig. 5a. Mathematically, the free-surface displacement for a standing wave is:

$$\eta = H \cos(kx) \cos(\omega t) \quad (2.25)$$

Where ω is the circular wave frequency, defined as:

$$\omega = 2\pi / T \quad (T = \text{wave period in seconds}) \quad (2.26)$$

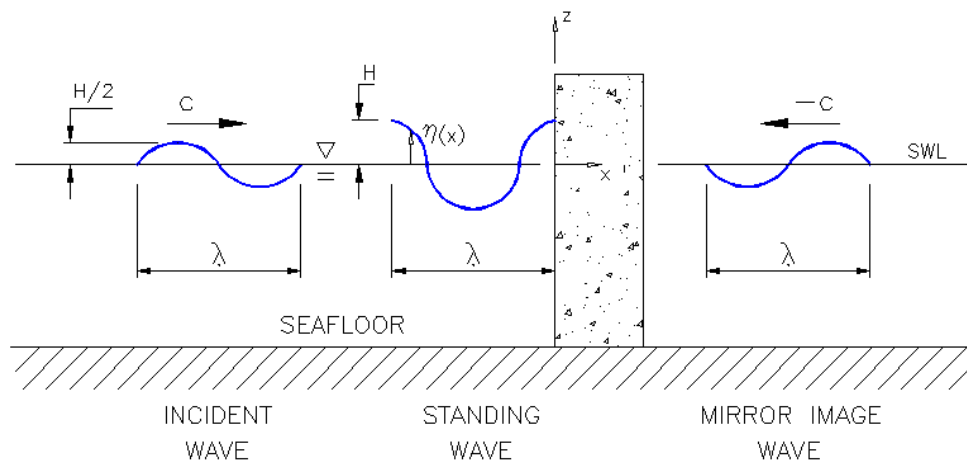


Figure 5a – Standing Wave Profile Using the Method of Images from a Perfect Reflection (from *Ocean Engineering Mechanics*; McCormick, 2014)

Note: The value of x at the hull can be equal to zero. So, on the seaward side of the hull, the free-surface displacement adjacent to the hull is:

$$\eta|_{x=0} = H \cos(\omega t) \quad (2.27)$$

On the leeward side, the wave climate is much smaller. This causes a rocking (rolling) moment which, in turn, causes the ship to embed itself into the soil. See Fig. 5b.

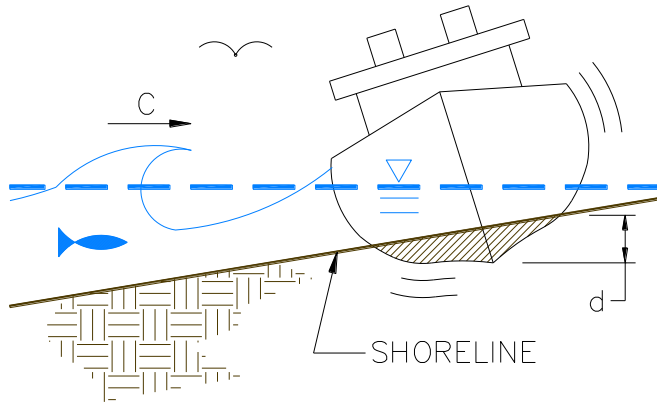


Fig. 5b – Ship Embedment, (d), Rocking Motion – Bow View

In terms of coastal engineering and further references contained in this work, it is common practice to partition the ranges of the wave steepness (h/λ) into three regions, which are:

1. Deep Water: $h/\lambda \geq 1/2$
2. Intermediate Water: $1/20 < h/\lambda < 1/2$
3. Shallow Water: $h/\lambda \leq 1/20$

These regions correspond to different wave profiles. For example, the deep-water wave profile is sinusoidal. These profiles are sketched in Fig. 6a.

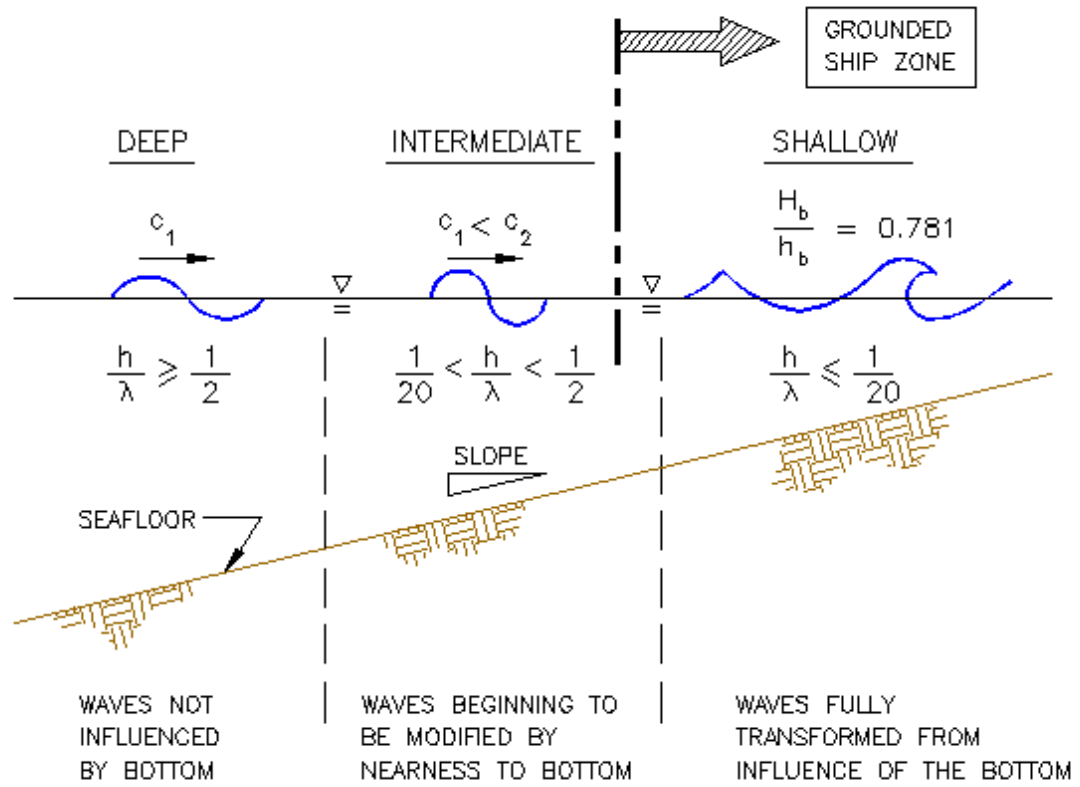


Figure 6a – Wave Profiles in Various Sea States

In Fig. 6b, the profile of the solitary wave is presented. This wave is an ultra-shallow-water wave. Breaking wave conditions occur at the seaward boundary of the surf zone, the region where ships become grounded in our study. The *breaking condition* is defined as that for which the horizontal particle velocity of the crest equals the celerity of the wave. Mathematically, the breaking condition is:

$$\mathbf{u}_{crest} \equiv \mathbf{u}_c = c \quad (2.28)$$

Breaking waves drive the grounded ship further ashore and compound the embedment process in Fig. 5b. They produce unintended forces on the vessel structure and complicate

rescue efforts. A progression follows from the previous sub-section where *non-linear* wave theory is generally discussed in light of a limiting case of a non-linear *cnoidal* wave, namely; the Solitary Wave.

2.2B Solitary Waves – The Cause of Ship Migration

Recent studies by Hudson (2001) and McCormick and Hudson (2001) show that the *solitary-type wave* is the greatest single contributory factor causing the shoreward migration in groundings. This type of wave is an extremely-long shallow-water wave that typically results because of a far-off storm.

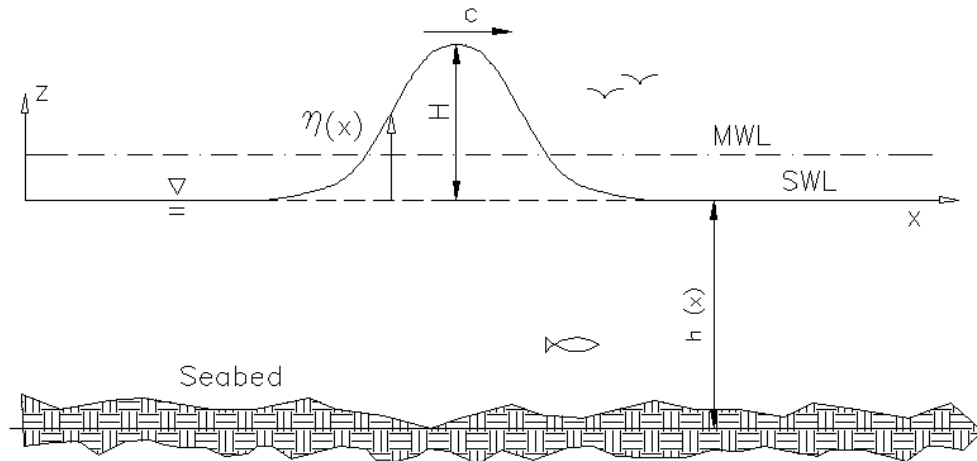


Fig. 6b – Solitary Wave Profile

The geometry of the wave is unusual in that the high-energy water volume is principally above the still-water level as it travels. Historically, J. Scott Russell (*circa* 1832) first called attention to the existence of this wave form. According to Russell (1833), he observed a wave form that was wholly above the still-water level, and consisted of a “single intumescence” which propagates at a constant velocity and unaltered in form.

According to the solitary wave theory, the free-displacement is predicted by

$$\eta = H \operatorname{sech}^2[(3H/4h^3)^{1/2}(x-ct)] \quad (2.29)$$

where c is the phase velocity (celerity) of the traveling wave. The horizontal water particle on and beneath the crest is given by

$$u = (g/h)^{1/2}(1 + H/h) \eta \quad (2.30)$$

From this equation, one sees that the horizontal particle velocity is uniform from the seabed to the crest. Furthermore, comparing the free-surface equation of the solitary wave with that of the linear wave, we see that the solitary wave is not repetitive in time or space. This is characterized by an infinite period and wavelength. When the crest hits a vertical hull, the water in the wave acts as if it was in a flume, and the momentum of the wave is diverted vertically upward.

The speed of the solitary wave is given by:

$$C = [g (h + H)]^{1/2} \quad (2.31)$$

It can be noted here that larger (higher) solitary waves travel faster.

As stated earlier in linear wave theory, there is consideration needed as to the breaking conditions necessary for solitary waves which have been proven to be the primary wave type responsible for groundings of ships. When the breaking wave condition listed in (2.28) is applied to a solitary wave, the ratio of the breaking wave height (H_b)-to-water depth (at break; h_b) value is somewhat different. At the wave crest (where $\eta = H_b$), the resulting wave height-to-water depth value is:

$$H_b / h_b = 0.780776 \dots \cong 0.781 \quad (2.32)$$

From the momentum theory of fluid mechanics, a resulting large horizontal hydrodynamic load acts on the seaward side of the hull; while, little or no dynamic load is on the leeward side. As a result, there is a strong migratory force shoreward on the hull. See Fig. 7. A discussion and derivation of the solitary wave is found in the book by McCormick (2010, 2014) and elsewhere.



Fig. 7 – Migratory Shoreward Wave Force Acting on a Grounded Ship (from image by Paul J. Gallie: “M/V SeaLand Express Grounding”, On-Line, 2003)

2.3 Existing Methods Employed to Free a Grounded Ship: As stated earlier, if ships lose power in a seaway, they tend to broach (be moved parallel to the coast) and are subject to beam waves. Presently, there are three conventional methods of ship freeing. Those are (a) the brute-force pulling on the stranded vessel with lines attached to a series of tugboats positioned in deeper water, (b) sand – jetting of the areas near the grounded hull using pumped-water with both high volume and velocity to displace the sand and (c) to lighten the load by decreasing the draft. These methods are discussed in the following sub-sections.

There are a number of problems with each of these methods, although only a few are identified and discussed. See, for example, the U. S. Navy “Ship Salvage Manual”, Vol. 4. Naval Sea Systems Command, 1 August 1993.

2.3A Brute-Force Pulling: The first event in this method is to attach the anchor chain (or line) to a tugboat in an attempt to dislodge the hull. Unfortunately, this has a low probability of success, unless performed within several hours of grounding. The method is also rather dangerous in that it is susceptible to snap failure of the chain. Because of the high energy stored in the taut chain, when a snap failure occurs, the chain can actually slice through the ship, cargo and one or more crew members. If the leeward water is of sufficient depth to safely accommodate the tug, a tug can simultaneously be positioned to push the hull seaward.

As one can expect, hull damage can occur during the brute-force process, depending on the nature of the seabed material. For example, a cobble beach can rip the hull skin as the ship is towed and pushed. If the ship is single-walled, then a rip will cause in internal flooding or, depending on the type of ship, a loss in liquid cargo or fuel.

2.3B Sand-Jetting: First, a drill-rig must be put in position. This is a time-consuming operation. As stated earlier, for a freeing process to be successful, it must be conducted within 24 hours of the grounding. Physically, the soil beneath the hull is displaced in the process. If enough soil is removed, then the hull can be momentarily buoyant. The problem is that the displaced bed will eventually migrate back under the hull due to wave action. Hence, the time-factor is critical.

Also resulting from the material displacement are unwanted moments caused by a loss of bed support on one side of the hull. To illustrate: A broached and grounded hull will

have a high rolling moment resulting from the loss of the bed material. This can cause a rolling motion which will result in a cargo shift that can overload different hull structural elements. If the loads become super-critical (structurally speaking), then failure is possible.

2.3C Load Reduction: This is only feasible with containerized cargo, since helicopters and large cranes are required. In general, unloading of a grounded vessel is perilous and involves skilled coordination and planning, not to mention great expense. This is generally done by airlifting of cargo and containers or with land-based salvage operations parallel to the nearshore if the wave climate and the time allow. In order to position a large crane, two methods are used. First, the crane can be on a long, broad spud-barge of shallow draft. The large deck area is required for rolling stability. The shallow-draft is required to prevent the barge itself from grounding. The second method is to construct a causeway from the shore as a path for a ground-based crane and trucking operation. As one can expect, this is a time-consuming method to be used in a time-critical situation. Certain types of ship grounding dislodgement and recovery operational typical methods and procedures are referenced in the U.S. Navy *Salvage Engineer's Handbook*.

For bulk cargo, such as grain, coal or oil, this type of unloading is impractical. To illustrate: The *M/V New Carissa* (ref. in Appendix B) was grounded off the Oregon coast in 1993. This ship was carrying petroleum, and was unable to be unloaded by any means, since the Pacific wave climate at the site is rather hostile. What was done to prevent a fuel spill was environmentally unacceptable. That is, the fuel was actually ignited in the hope that all of the fuel would be burned off. During operation, the hull fractured and the fuel was lost to the ocean. As reported by Hudson (2001) and others, it took several years to reclaim the beach.

In the following chapter, background analytical and experimental studies are described. Results of these studies are incorporated in whole or in part in the present study.

3. PRIOR EXPERIMENTAL STUDIES

Previous work devoted to the wave-induced motions affecting the grounded condition was focused on the midship section, where the geometric section was consistent and “box-like”. Rotational effects were neglected as they were of smaller order than the two principal motions previously mentioned. The results of the previous studies show that the vessel buoyancy diminishes with time due to the grounding on the nearshore bed and as the ship’s longitude becomes parallel to the shoreline. The works of McCormick (1999), Hudson (2001) and McCormick and Hudson (2001) provide a base from which a study of the relationships of the bed material properties and the aspects of the release methods can be launched.

The experimental work done by Hudson (2001) was the first of its kind. Up to that time, it was thought that breaking waves of any length contributed to the migration of a grounded ship towards the shore. Based on a ship having a beam of 40 feet (12.2 meters), the scale of the Hudson (2001) experiment was 1/40. The experiment was conducted in a wave-sediment tank specifically designed and constructed for the study. See Hudson, McCormick and Browne (2002) for the details of the wave-sediment tank. Although the experiment was of small-scale, the results showed that sinusoidal waves tend to rock grounded ships in place, but do not cause migration. The rocking motions cause the ship to be more embedded in the soil. Hudson (2001) found that the migration of a ship towards the shore is caused by the long waves that are near or at breaking. The long-wave (solitary wave) breaking condition is mathematically described in Eq. 2.10. This was the first experimental evidence of the wave-structure interaction for the migration process. The

Hudson (2001) studies were the inspiration for the present study of the freeing of grounded ships.

Some of the past work was centered on laboratory experiments, where the soils were confined to cell-testing. That is, the sands, cell pressure and other parameters were varied in order to understand the mechanism characterization of Blast Induced Liquefaction. In a few full-scale studies, BIL was used as part of pile-release behavior investigations in an effort to determine ways to reinforce structural systems during seismic events. In these studies, efforts were made to the avoid soil liquefaction. Although some attention was directed to considering a mechanism for blast induced liquefaction, quantitative or empirical results concerning the effects of liquefaction on embedded ship shapes nor how liquefaction would play into releasing possibilities.

Other studies done by *Shannon and Wilson* did testing of various soil types under cyclic loadings that show a buildup of pore water pressure and associated deformation. This cyclic loading over time culminated in liquefaction in both loose and dense sands which is shown later in Chapter 5 - Fig. 14a.

4. EXAMPLES of ACTUAL SHIP GROUNDINGS

Historically, a multitude of ships groundings along the Eastern U.S. coast have been documented for two centuries. Recorded ship grounding and sinkings go back to the 1700's and continue to the present day. Many types of vessels have been involved, which include sailing ships, passenger liners, trawlers, tugs, barges and military ships of varying types.

Along the Delaware, Maryland and Southern New Jersey mid-Atlantic coastal area, there are over one thousand recorded locations of all types of grounded/sunken vessels. A great percentage of these groundings was never raised or salvaged because of the complexities involved with freeing operations associated with the coastal soil interactions.

In the following, two specific case studies of ship groundings are described. Because of these groundings, considerable financial losses were incurred, as well as delays in delivering and unloading the cargo that remained undamaged. The financial repercussions were substantial and amounted to many times the value of the vessels themselves. Fortunately, several of the referenced ships did not end up releasing any hazardous materials to the environment, although the risk was certainly present. Other ship grounding incidents have not been as environmentally fortunate and have been proven to be detrimental in terms of oil or hazmat spills. See Appendix B for other ship-grounding examples.

4.1 Motor Vessel Sealand Express

The first case study of a ship grounding is the M/V Sea-Land Express in Cape Town, South Africa in 2003. See Fig. 8 below.



Fig. 8 - M/V Sealand Express in Port in Table Mountain, Cape Town, South Africa (from image by *Paul J. Gallie*: “M/V SeaLand Express Grounding”, On-Line, 2003)

The *M/V Sea-Land Express* was a 33,000 DWT cargo carrier with 1,037 sea containers, crude oil and other volatile substances including drums of propyl acetate and uranium oxide. The ship anchored offshore near Cape Town, South Africa, on a delivery voyage in order to weather high winds and heavy seas. During the night, the anchors slipped and the Sea-Land Express was driven landward by the intense wind and waves. By morning, she had her bow embedded in the near-shore sandy bottom and had been broached alongshore. The vessel was being pounded by heavy broad-side swell, and eventually rested parallel to the shore. Within hours after the bow came in contact with the beach, salvage tugs were dispatched, but were unable to pull the *M/V Sea-Land Express* free.

The *M/V Sea-Land Express* was lodged on the beach of Cape Town for 25 days after the initial grounding event. Salvage efforts were carried out, that included continued efforts to pull her free with tugs and air-lifting the hundreds of sea containers off the ship utilizing heavy-lift helicopters. The latter eventually allowed sufficient weight reduction to re-establish buoyancy during a high-tide, enabling three oversize tugs to pull her free. The

M/V Sea-Land Express had to be dry-docked to be evaluated structurally following the near month-long salvage operation. See Fig. 9.



Fig. 9 - M/V Sealand Express Lies in Sturrock Drydock in Cape Town (from image by Paul J. Gallie: “M/V SeaLand Express Grounding”, On-Line, 2003)

4.2 M/V APL Panama

A second ship grounding event was the *M/V APL Panama* in Mexico in 2005, which was a 40,360 DWT container vessel with 1,100 sea containers stacked over ten stories high. A grounding occurred with circumstances similar to those of the *M/V Sea-Land Express*. A navigational piloting error was made when the ship was off the Ensalada Harbor of Mexico that caused the ship to ground, bow-first, in shallow water. The bulbous bow of the ship was then the pivot point for the rotation of the ship caused by the nearshore energetic wave action that subsequently caused her to broach. The vessel began to list due to the combined effects of its’ cargo burden and the pounding of the shoaling waves. Tugboats were dispatched in an attempt to pull the *M/V Panama* from the shoal. Freeing

efforts were once again ineffective and the ship remained grounded even though the tug's response was quick and during a high tide.



Fig. 10 – APL Panama Shown here Grounded from a Navigational Error (from the *San Diego Tribune*: “APL Panama Grounding”, On-Line, 2008)

The experience of the *M/V APL Panama* was somewhat different than that of the *M/V Sealand Express*. A jetty had to be constructed from the shore to access the ship, and track crawler-cranes were used to unload her cargo. These combined land and air-lift salvage measures left *M/V APL Panama* stranded on the Ensalada Harbor coast for three months from the time of the initial grounding. See Fig. 11. The vessel also had to undergo structural damage repair as a result of the incident. Other ship grounding cases are presented in Appendix B.



Fig. 11 - APL Panama Being Unloaded from a Constructed Landside Jetty (from the *San Diego Tribune*: “APL Panama Grounding”, On-Line, 2008)

4.3 F/V Mar-Gun

Ship groundings are not limited to only larger type vessels such as have been described in the previous two examples. Smaller ships frequently experience similar grounding events as was the case for the diesel engine fishing vessel, *Mar-Gun*, based out of Seattle, WA. The *Mar-Gun* was a 112-foot-long (34-foot beam) fishing trawler that ran aground off of St. George Island, Alaska on March 7, 2009 due to heavy seas.



Fig. 12 – Fishing Vessel *Mar-Gun* shown here being driven aground near beach off the Alaska coast from storm surge (photo credit N. Huddleston - *ADEC*: “F/V Mar-Gun”, On-Line, 2009)

The U.S. Coast Guard was initially called in to safely evacuate the crew but there was 19,000 gallons of diesel fuel aboard which posed a potential spill hazard to the waters of the Bering Sea. Salvors were then dispatched to free the ship and unload the cargo. The salvage effort took nearly two months and ended, with much difficulty and risk, with the Mar-Gun being dislodged and towed to nearby Dutch Harbor for extensive repairs.

5. SOIL LIQUEFACTION

Most nearshore and beach soils in temperate climates are composed of granular sands with little significant cohesive properties. The reason for the lack of cohesiveness is that the sands are composed of quartz and feldspar. According to the Unified Soil Classification System (USCS), the sands are classified as SW (Well-graded Sands), SP (Poorly-graded Sands) or SM (Silty Sands, Sand-Silt mixtures). This information is paramount to the present study, since there is precedent for inducing soil liquefaction in this classification of soil. See Fig. 13.

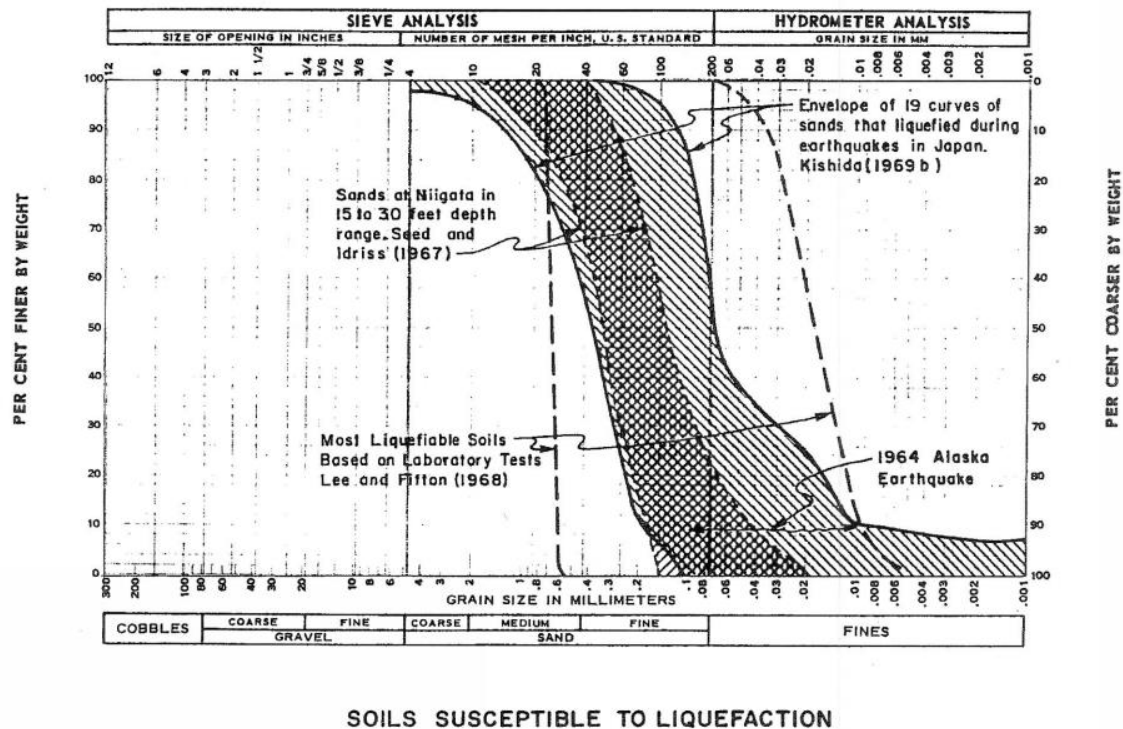


Fig. 13 – Table from Seed and Idriss (*Analysis of Soil Liquefaction*, 1967)

Other sands subject to cyclic loadings have been studied by *Casagrande* and *Seed* resulting in liquefaction under these conditions as well as shock loads from explosions. Tests done

by *Castro* (1969) on the behavior of sands under cyclic loadings have shown that certain sands subjected to Tri-axial apparatus testing were susceptible to liquefaction in the ranges shown in Fig 13. Castro tested a *Banding* sand in this study (see Table 3 for properties of sand used in example case study by the USAF and in this dissertation) which liquefied during the cyclic tests loadings.

5.1 Definition of Soil Liquefaction

In general, liquefaction is defined as a phenomenon whereby a saturated soil substantially loses strength and stiffness in response to an applied stress or other sudden change in stress condition, causing it to behave like a liquid. The American Society of Civil Engineers defines liquefaction as “the act or process of transforming any substance into a liquid. In cohesionless soils, the transformation is from a solid state to a liquid state as a consequence of increased pore pressure and reduced effective stress.” Further, Terzaghi, Peck and Mesri (1996; third edition) in Soil Mechanics in Engineering Practice, define the general case of liquefaction as “The sudden drop of shear strength under undrained conditions from the yield strength...”

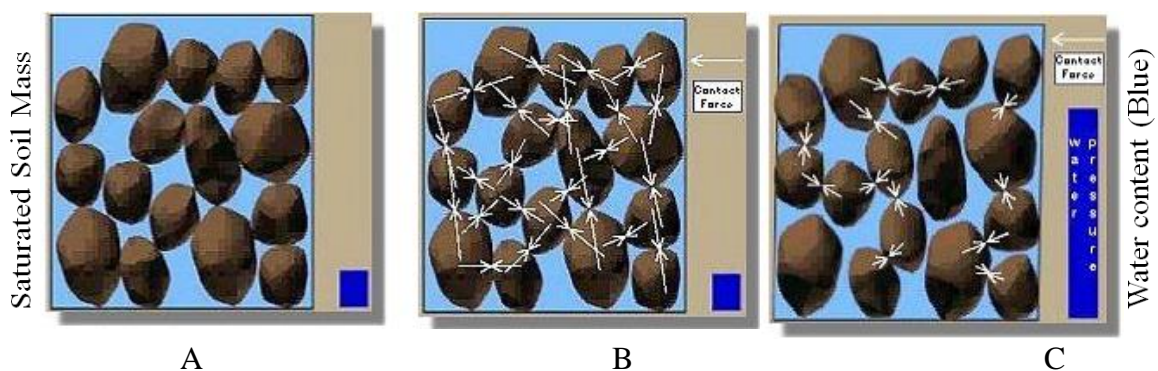


Fig. 14 – Soil Liquefaction Mechanism (from Univ. of Washington CE Dept., Webpost 2010)

In terms of soil parameters, when the *Excess Pore Pressure Ratio*, defined as:

$$R_u = \Delta u / \sigma'_0 \quad (5.1)$$

is 100% or 1.0, the soil is indicated as being completely liquefied (where Δu is the excess pore pressure and σ'_0 is the initial vertical effective stress).

5.2 Soil Liquefaction as a Mode of Release

The weight of overlaying soil particles (in fine-to-medium particles such as in beaches sands) produces constant forces between the particles that give soil its strength. When the contact pressure is high, the pore-water pressure is low. With a sudden force or shock, such as that produced by a blast, there is an uprush (buildup) of pore-water pressure. This, in turn, reduces the effective pore-solid pressure, and the water is “trapped” between particles. The inter-particle contact forces decrease and, subsequently, the soil strength is reduced. In other words, the soil is i.e. “liquefied”, and or behaves more like a liquid. The process to induce liquefaction can have a time-dependent cyclic buildup component. This can be seen in the following two figures where cyclic tests were performed on loose and dense sands:

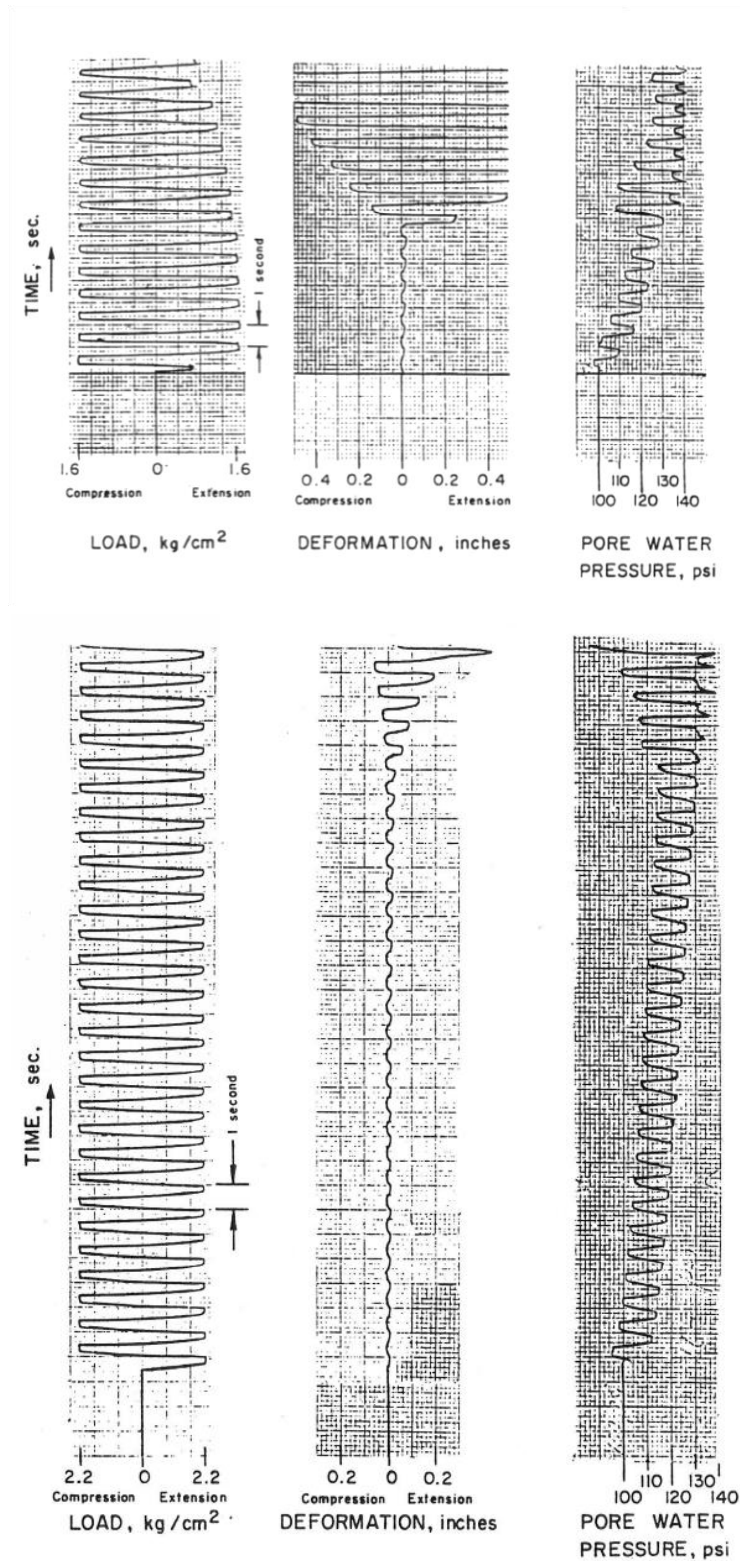


Fig. 14a – Laboratory Testing of Sands Under Cyclic Loading on Loose (upper part) and Dense (bottom part) Sands (research of *Shannon and Wilson; 2011*)

This type of induced soil liquefaction is advantageous in re-establishing a floatable substrate under an embedded body, i.e. such as a grounded ship – the focus of this study.

5.3 Blast-Induced Liquefaction (BIL)

One method of liquefying a soil is to create some type of pressure shock. This has been previously done by using explosives, which is a rather dangerous method with possible disastrous consequences. The method proposed here is to create the shocks using compressed air. These are discussed in this sub-section.

5.3A Experiments at Treasure Island

The explosion technique was documented in reports resulting from several full-scale experiments done in 2004 and 2005 by Scott A. Ashford et al (2004). These experiments were conducted on the Yerba Buena Island outcrop in San Francisco Bay, at the Treasure Island National Geotechnical Experimentation Site (NGES), where piles were being used in lateral pull-trials under liquefied soil conditions. Charges were placed in the soil surrounding the subject Cast-in-steel-shell (pipe) pile(s) and detonated in a peripheral sequence to liquefy the sand.

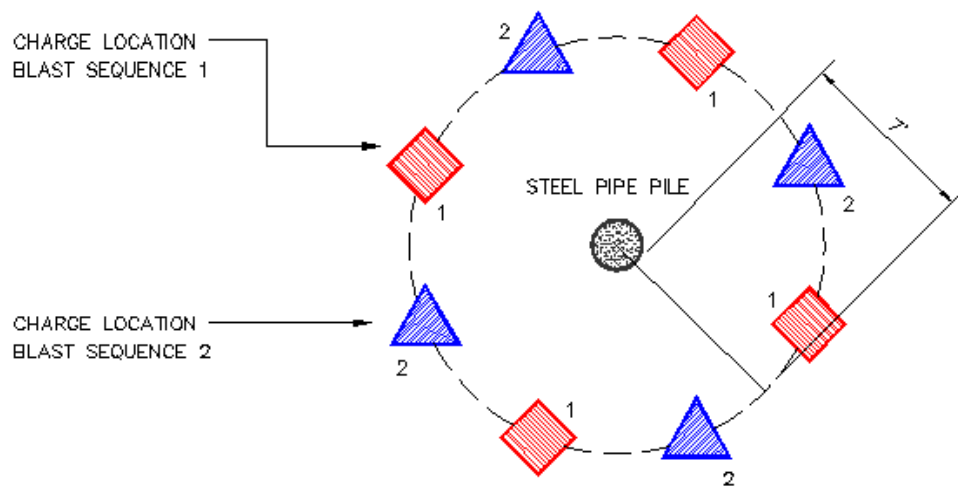


Fig. 15 – Detonation Sequence used for BIL at NGES on Pile Load Tests

This testing program, known as the Treasure Island Liquefaction Test (TILT), successfully used controlled blasting of buried explosive charges to liquefy a study area around full-scale pile and pile groups to evaluate pile-soil-pile interaction effects. In this series of trials using blast-induced liquefaction, the pore-water pressure was near-instantaneously increased by compression waves generated from the explosions.

5.3B USAF Office of Scientific Research

In 1981, the Air Force Office of Scientific Research (at Bolling AFB, Washington DC) administered a grant to the Civil Engineering Department of the San Diego State University to determine a metric to quantify the mechanism for blast-induced soil liquefaction from explosives. See Fragaszy and Voss (1981). The Air Force's interests were with understanding the effects of weapon detonations on geologic materials at or near the ground surface. Tests were carried out by the investigators on saturated samples of Eniwetok beach sand and Ottawa sands (Flintshot, Sawing and Banding) with quasi-static

isotropic loadings. See Fragaszy and Voss (1981). Laboratory testing was done on the sample sands using a constant pressure pump. In that study, a high pressure steel tri-axial cell with varying cell and pore-water pressures was used. Results were graphically presented, and the pore-water pressure was found to be larger at the end of the cycle than at the beginning. There was liquefaction of the sands in varying sample pressures as well as residual increases in pore-water pressure throughout the induced stress cycles.

In the present study, the soil surrounding an embedded vessel is induced to be liquefied with compressed air administered from a buried pipe diaphragm within the sand in order for it to be brought back to a buoyant condition. With the exception of the method of shock introduction, the method is similar to that of Ashford et al. In this way, it was hypothesized and subsequently proven that several types of ship-shapes were able to regain buoyancy once liquefaction occurred. This is performed with three types of model ship shapes that bear naval similarities to typical sea-going vessels.

6. EXPERIMENTAL APPROACH

A model tank was constructed for the experimental part of the present research study. The tank weight with the required sand and water is approximately 3,000 pounds. The tank was used for each of the two phases of the experiment setup and repeat trials. Along with this newly created ship model tank, a moveable reaction frame and a leveling platform were also constructed as the base integral parts of the work system. There were ship models also constructed that are the interactive parts of the experiment along with data recording equipment and methodology. In this section, the design, assembly and testing procedure of the model tank and all associated parts are described. The physical details of the model tank, the ship models and other equipment pertinent to the performance of the experiment are found in Appendix C.

6.1 Experimental Facilities

The experimental facility had to be specifically designed and constructed for the study due to the uniqueness of the project.

6.1A Model Tank

The model tank was designed to ensure that the ship models to be used had adequate sidewall clearances and to satisfy sand-depth embedment requirements. The final working dimensions of the tank were set at 5'W x 5'L x 2'D (inside depth). The tank is composed of 1/2" thick clear acrylic Lexan as the primary material. The structural properties of the Lexan were evaluated for their selection as to hydrostatic pressure and concussion resistance effect. The structural properties of the acrylic lexan, per ASTM D 638 and D 695 were:

1. $F_b = 9.0 \times 10^3$ psi Flexural Bending

2. $F_c = 16.0 \times 10^3 \text{ psi}$ Compressive Strength
3. $E = 0.55 \times 10^6 \text{ psi}$ Modulus of Elasticity

Based on ship model testing precedents, a clearance of 1.5 times the model body width (beam) in the short direction was maintained to mitigate the effects of reflection from the tank boundary walls. These were the criteria used in determining the dimensions of the tank. From a depth standpoint, enough sand was needed on the bottom to allow for a uniform clearance between the tank bottom and the bottom of the deepest model (SS3). This is calculated to be between 9" – 11", depending on the various model geometries and embedment requirements shown later. A tank sidewall depth of 2' allows sufficient sand and water to be placed to accurately conduct the ship model embedment experiment trials. The tank has enough volume to insure that the displaced water from the models does not have an impact on the overall water depth.



Fig. 16 – Tank, Restraint Cable and Platform Assembly

6.1B Ancillary Equipment

The tank rests on an 8' x 7'-9" timber platform. The purpose of this platform is to provide a level, absorptive base on which the tank is supported. The model tank and platform were designed for transportability.

To facilitate water level control in the tank as each sequence of trials was performed, a tank sidewall valve that could be fitted with a hose for drainage was installed. A water spigot fixture was obtained that had a threaded turn-wheel valve handle with strainer and nylon filter.



Fig. 17 - Drain Valve Installed in Tank Corner

An obstacle that needed to be addressed was how to bury the model in the saturated sand without the perimeter sand collapsing the excavated hole. In addition, water needed to be prevented from entering the hole and causing premature buoyancy of the model. After many trials and alternative methods of burying the model for a pull-trial, it was decided that a framed structure (or cofferdam) was needed so that sand could be evacuated while being held back.



Fig. 18 - Aluminum Cofferdam before and after use with burying Model

The actual material for the cofferdam is weldable $\frac{1}{4}$ " thick structural Grade 6061-T6 aluminum ($F_y = 35,000$ psi; $E = 10.1 \times 10^6$ psi). This was chosen to be durable and strong yet lightweight for lifting and positioning around the models within the tank. Each of the four sides of the cofferdam were welded at a fabrication shop to fit the plan size and depth required for the experiment per design drawings and lifting criteria (32" L x 20" W x 18" D). This included having to use the cofferdam in conjunction with a vibrator and side holsters that are further explained in Appendix C and as seen in Photo Record images P12-87, P12-94 and P12-95.

6.1C Reaction Frame

To facilitate the multiple lifting/hoisting operations of the various ship models, an overhead lifting frame was built. This reaction frame functions as the support structure to lift the models in and out of the model tank. In addition, it provides an access walkway for maneuvering equipment needed during the experimentation. A full description of the reaction frame and its components are contained in Appendix C.

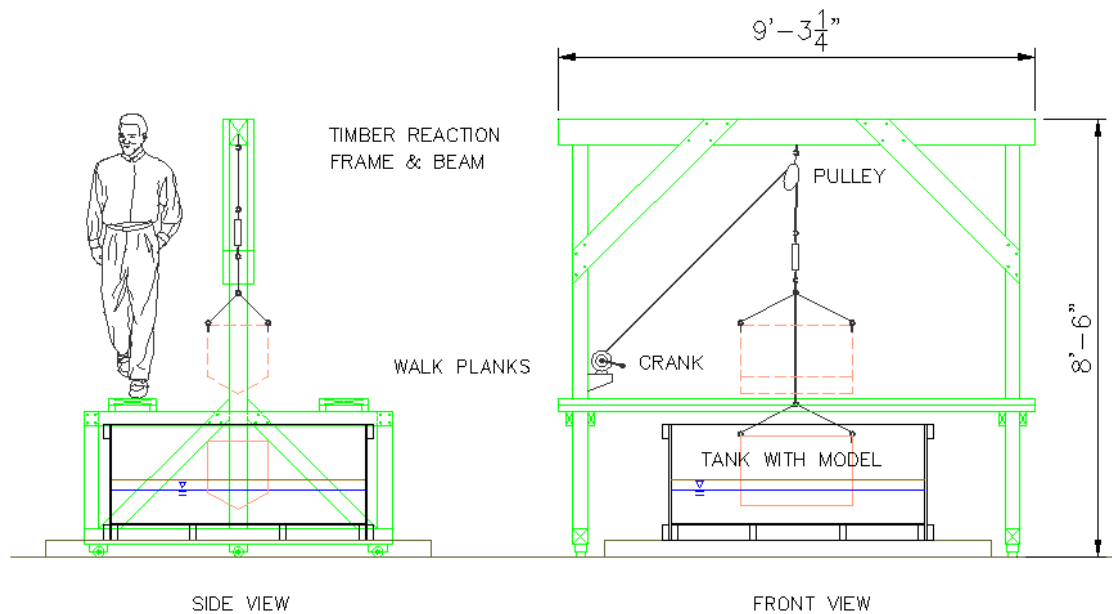


Fig. 19 – Reaction Frame Assembly over Model Tank

6.2 Ship Section Models

The experiment requires the use of ship-section models. If one slices a ship hull across the widths at various longitudinal stations, the vertical cross-sections of the slices are called *ship-sections*. The sections of the model are uniform in the longitudinal (fore-to-aft) direction. Their placement was in the center of the tank, with spaces between each model side and the opposite wall. Three models were created that represent standard classes of ships. These models are specifically made to be geometrically symmetric in both the

longitudinal and athwartships directions. The geometries are functionally simple so that any later computational fluid dynamics (CFD) analyses of the results can be readily performed. Each of the three models is referred to as Ship-Shapes (SS1, 2 or 3). The inside of the models is made hollow and accessible from the top for the ability to add weight ballast. Sectional drawings of the three sections are presented in Fig. 20. Photographs of the models are contained in Appendix C. The specifics of the three model sections are as follows:

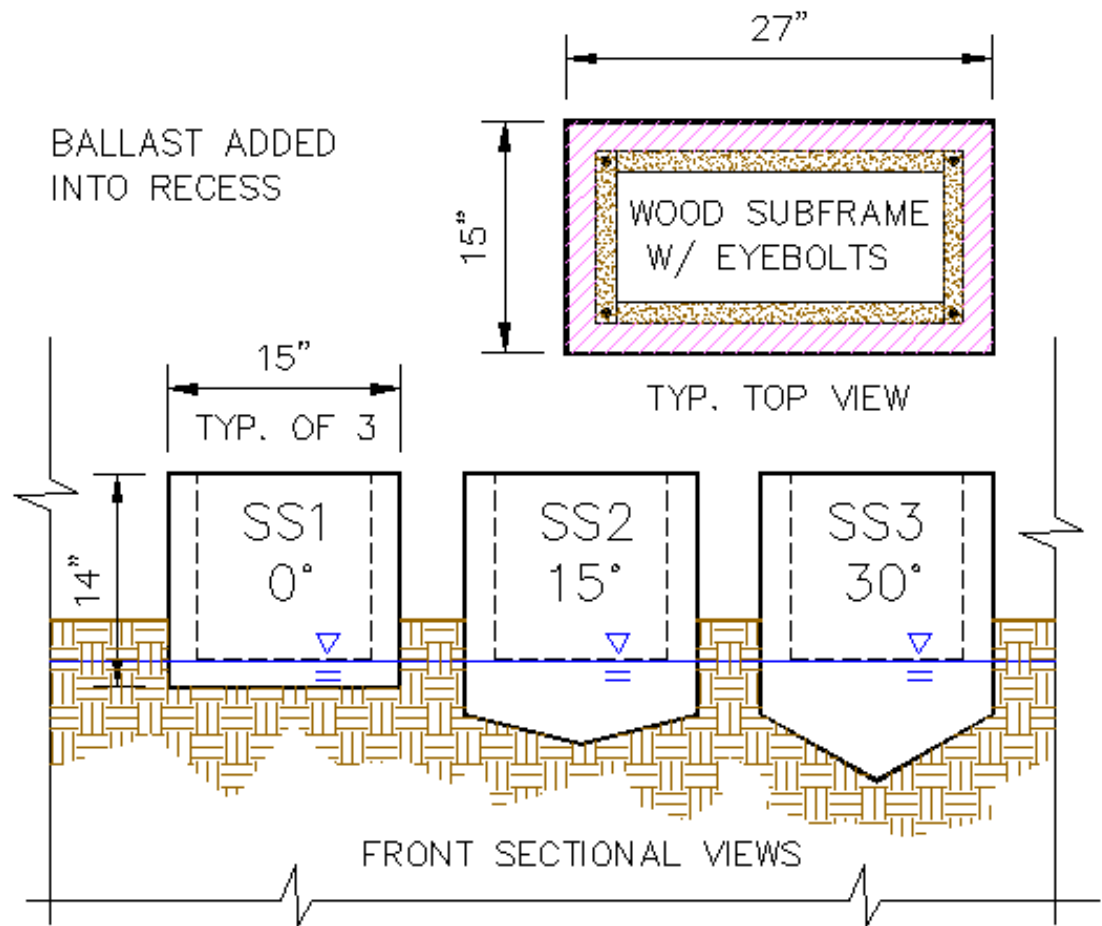


Fig. 20 – Ship Sections Model Geometry

Model SS1 – This model has a flat bottom and vertical wall sides similar to a barge.

Model SS2 – The unit has a 15 degree dihedral shape and is indicative of a low-draft vessel or skiff.

Model SS3 – This unit has a 30 degree dihedral shape, and is modeled after a deeper-draft vessel.



Fig. 21 - Ship Models in the process of being built (Note hollow interior for ballast additions)

These models are also needed to hold up under many repeat trails in all phases of the experiment. This included the use of removable/adjustable bottom ballast as well as built-in ballast described later. These are shown in the lifting arrangements in Fig. 22.



Fig. 22 – Lifting Arrangements

In order to make the models able to be floatable and watertight, the exterior insulation “skin” was covered with a multi-layer covering of fiberglass. This was done for each model and was composed of a marine fiberglass fabric glued to the insulation with an epoxy-resin topcoat mix done in 3 coats. Each coat was sanded, filled and filed such that a fully waterproof outer model surface resulted.



Fig. 23 - Model Fiberglass Covering/Coating Operation

The final step in the model building was to paint each model with a marine paint. Several coats were applied and a waterline was painted and stripped to identify the center of buoyancy of each respective model after a flotation test was done (see Fig. 25). The flotation test included the addition of brick primary ballast into the hollow of the model frame.



Fig. 24 - Model Ballast with Wood Sub-Frame, Lifting Lanyard and Painted Exterior View

From a stability standpoint, the models were able to be floated to a suitable operational depth. Because of the dihedral angles at the keel, the SS2 and SS3 models needed additional low-keel weight to ensure overturning stability. A method of adding low-keel weight was designed and implemented for these two units. For the SS2 model, a series of partial depth holes were drilled in the triangular Styrofoam hull and filled with copper buckshot. Once this procedure was done, the holes were capped with Styrofoam plugs and glued in place. The hydrostatic stability flotation test was, then, done to ensure the effects of the low ballast.



Fig. 25 - SS2 Flotation Test being performed after Low-Keel Ballast Added

For the SS3 (deeper 30-degree dihedral), the low-keel weight issue was more severe for stability. The addition of buckshot into drilled keel holes was not sufficient based on repeated flotation tests. A heavier low base weight was needed for this model and so lead was considered for a ballast because of greater density.



Fig. 26 - Lead Sinkers being melted into Steel Pipe Fittings for Keel Ballast

Another flotation test was done (similar to that shown in Fig. 25) for SS3 which then resolved the stability / rotation issue making it ready for trials in the main tank.



Fig. 27 – Low Keel Permanent (Buckshot) Ballast placed into SS2 Model

6.3 Blast Simulation: Compressed Air Device

As a preparation to this part of the experiment, the water level was pre-determined, and was visible through the Lexan window – one side of the tank. First, water was poured into the tank. Then, the sand is mixed with this water to prevent stratification. Following this, a time delay was needed to allow the sand level to become stable. The cofferdam was vibrated into position for the setting of the ship model. The sand-water level would, again, rise in response to the cofferdam installation. Following another time delay, the model was set by removing all sand from the cofferdam, and the remaining sand was packed around the model. Finally, the cofferdam was removed.

Following the method of the previously referenced work at the NGES at Treasure Island (see References Section), submerged explosive charges were placed at buried locations in a peripheral array around a study area in order to produce a shock wave in the saturated soil. This shock wave, or concussion force, produced from a series of sequenced detonations, induced the soil to locally liquefy.

It was found during this study that a similar effect could be produced using compressed air instead of buried explosives. A device, which is referred to here as an “Air Cannon” was built and utilized for the same purpose and similar effects using compressed air.

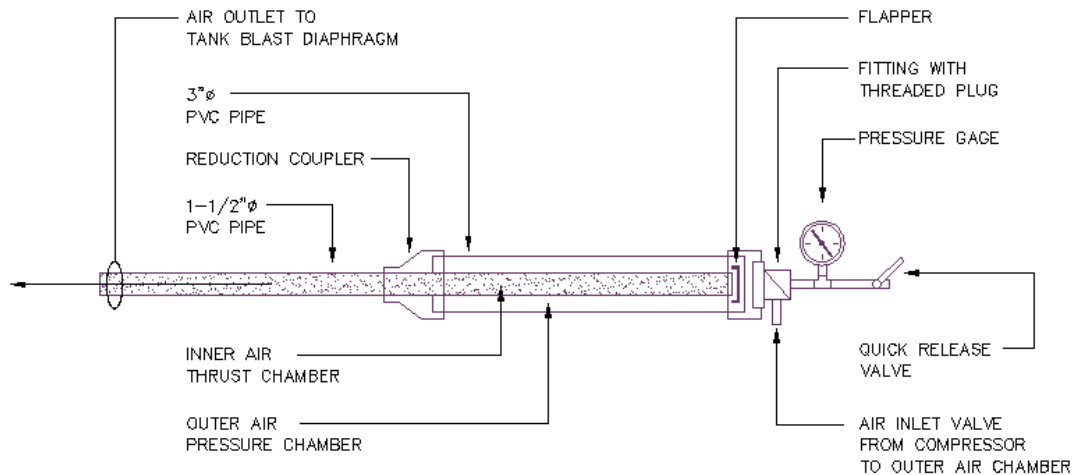


Fig. 28a – Air Cannon Schematic



Fig. 28b – Air Cannon with Pressure Gage and Quick Release Valve

The Air Cannon was able to be charged to designated pressure, *via* an air compressor assembly. Following the charging, the compressed air could be released near-instantly into the soil surrounding the buried SS models to cause liquefaction. So the technique in this experiment is using a controlled volume of relatively high pressure air, discharged through four peripheral nozzles at the end of a buried PVC diaphragm. This sets off a compression wave propagation surrounding the embedded model and causes the saturated sand to liquefy.

6.4 Detection of Shock Intensity by Hydrophones

The means to record and synthesize information associated with the soil–water condition as affected by the compressed air concussive forces from the air cannon was done with a series of underwater microphones (hydrophones). It was decided for the arrangements in the tank and positioning of the models that four hydrophones would be used to record omni-directionally. This hydrophone arrangement matches the four-sided plan-orientation of each of the three models.



Fig. 29 – Assembling of Hydrophones from Parts

The hydrophones were specifically constructed for these experiments based on instructions from construction by the University of Connecticut (COSEE TEK). See Appendix F for details. Parts were obtained locally and assembled into five hydrophones (4+ one spare). Each hydrophone has the capacity to transmit a full spectrum of sound to a recorder. This ties in well with how the blast force from each nozzle facilitates *liquefaction*.

These interaction phenomena were observed dozens of times during the experiment. (See Photo Record Images P13-26, 27, 28)



Fig 30 – Assembled Hydrophone

The hydrophones, blast nozzle ports and the air cannon all work in conjunction with each other around the model within the sand of the tank for each trial of the experiment. Reference Fig. 32. The buried PVC pipe blast diaphragm is situated near the outer walls of the tank. The air blast is administered to this pipe network to distribute the air to each of the four nozzles. One section of the diaphragm on the right-hand side of the tank is actually valved off to enable air flow to be optimized. Alongside each nozzle, four larger (three-inch diameter; 90-degree elbow) PVC sleeves were built to be able to place and retract the hydrophones as each set of the experiment proceeded.



Fig. 31 – PVC Pipe Diaphragm, Blast Nozzles (left) and Hydrophone Port (right)

The sleeves, or hydrophone ports, enabled the hydrophones to be slid down into them and positioned close to the nozzle blast outlet locations so that there could be an accurate recording from each of the four hydrophones to the DA-88 recorder. Each end of the hydrophone port being buried, was fitted with a fine nylon screen so that sand was not in direct contact with the recorder end of the hydrophone. The PVC pipe sleeve was flooded

with water into which the hydrophones were submerged. The placement of each of these three interactive parts, with respect to each other and the model locations, underwent several rounds of trials before a viable long term arrangement was arrived at. See images from Photo Record P13-41 through P13-46.

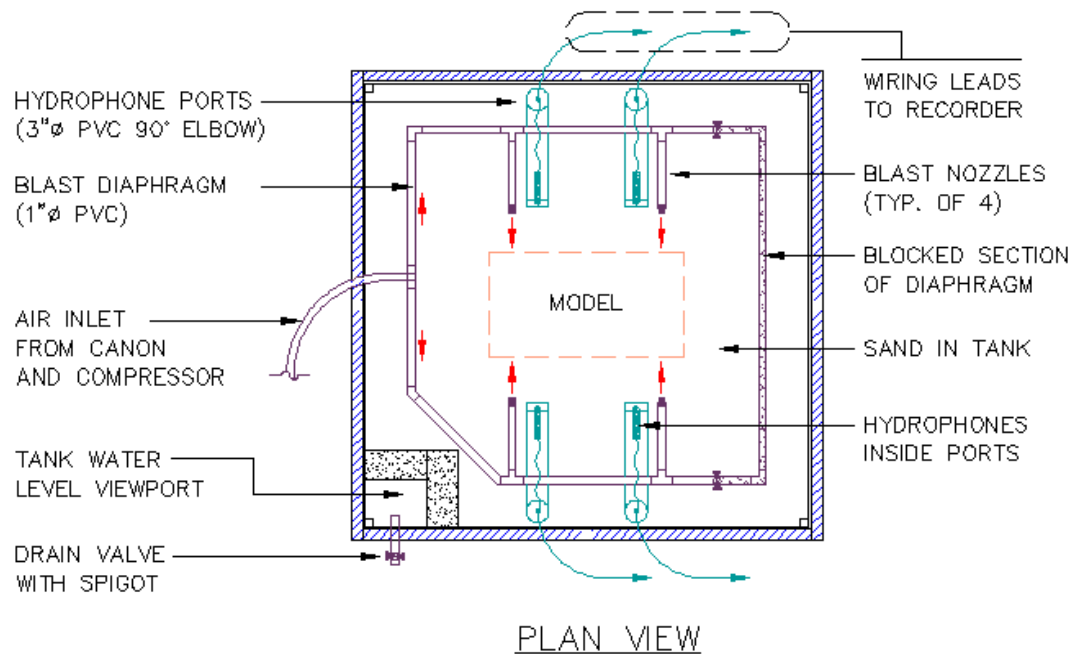


Fig. 32 – Schematic of Tank with Buried Equipment

6.5 Baseline and Blast Tests

The model tank and reaction frame work together to allow the placing, embedding and raising of the various ship shape models for this experiment. The process involves multiple trials of each of the (three) ship models used in the study. The number of trials of each model must be sufficient to provide a statistically credible sample size. The two tests are called the Baseline and Blast tests. The former is the pull-test, whereby the embedded model is freed from the soil by direct application of a vertical load. The latter test is the

reduction of the soil-induced vacuum force using the compressed-air blast. These are described in the following sub-sections.

6.5A Baseline Tests

The first part of the experiment is to run the model embedment tests using each of the three model types constructed. The sand layer, water depth and positioning of the models within the tank are standardized/normalized, so that in each repeat trial the results can be compared with accuracy. The initial trials are designed to determine the force required to dislodge the embedded model from the natural sand with no other factors at play.

Prior to the embedment, the waterline of each model was determined as a result of a buoyancy test as further explained below. This waterline was the same for both the free-floating and the embedded models.

In order to produce results that have statistical accuracy, the testing protocol was standardized with certain aspects constant with each trial. The sand height was set at a height of 11-1/2" (from the bottom of the tank) and the water level was controlled and adjusted to be at a free surface height of 8-1/2" within the sand. The arrangement is characteristic of the typical relationship of a grounded ship hull depth to the mudline or subaqueous water level on a beach.

The depth of the embedment was chosen (via painted line on each ship model) based on tare weight plus ballast flotation level done previously and described as a "Buoyancy Test". The waterline, then, was the same for both the free-floating and the embedded model.

To insure horizontal placement consistency, a series of guywires were used to align the models in the tank. These were strung from four wooden side brackets made to fit the tank walls during operation. Each guywire had a horizontal spring at the end to maintain tension during model placements. See photo record images P12-80, P12-89 as well as Fig. 33.

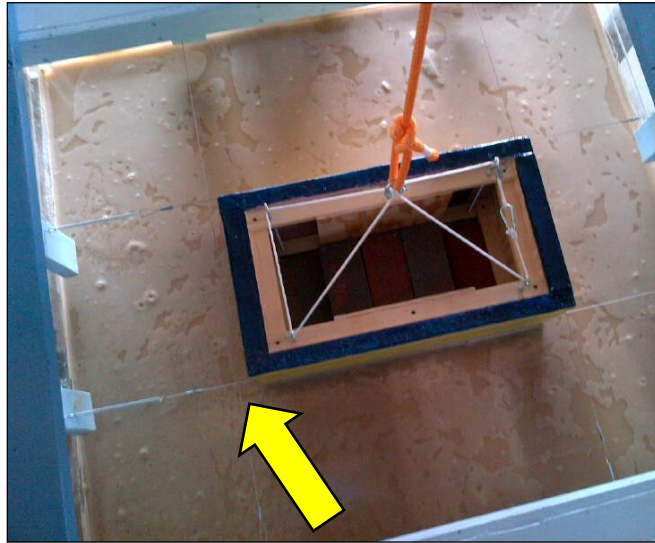


Fig. 33 – Guywires for Consistent Model Positioning within the Tank

The sand / water consistency was also adjusted at the start of each day's trials through the addition/mixing of water and monitoring the sand and water level at the clear view end of the tank.

The tensiometer used was tested / tuned periodically against a known benchmark weight. The brick and steel ballasts used during the trials were the same each time as well as the soil and water depth used throughout for each respective model.

6.5B Blast Tests

The second part of the experiment is to run the same model embedment tests on each of the three models with the soil being in a liquefied state. This is a blast-induced soil procedure involving air-blasting from an air cannon nozzle in the saturated soil around the

model embedment area. The air-blasts are designed to cause the soil to sequentially liquefy. As in the first series of trials, the experimentation determines the force required to dislodge the embedded model from the artificially liquefied sand. In each of the trials, the reaction frame makes use of an in-line scale that measures the force or tension in the rope assembly as it pulls the model free of the sand mass.

There are hydrophones positioned in the soil to measure the full spectrum of the blast intensity as affected by both their relative location and the soil liquefaction. This is demonstrated in Fig. 34.



Fig 34 – Positioning of Hydrophones into Ports adjacent to Blast Nozzles

A sample record of the hydrophone results is presented in Fig. 35 through the use of Audacity audio multi-track recording and editing software. In the top figure, the blast signal is recorded for three sequential blasts of one hydrophone. The blasts are identified by A, B and C in that figure. It can be seen from these results that the initial A blast has the highest signal amplitude response corresponding to the lowest inlet pressure. The pressure is steadily increased with each successive blast as can be seen in Table 6. There is a time interval of 1 to 3 minutes between blasts as recorded in the log sheets represented in

Appendix G. This indicates that the sand surrounding the model is being modified with continuing blasts. Even though the air cannon pressure per blast is increasing, the recorded signal amplitudes are not as high, and in some instances such as this one, are lower. A further discussion of this trend subsequently undertaken and as also seen in many other trials and depicted in the table below:

Blast ID	Relative Maximum Amplitude	Pressure (PSI)
A	+/- 0.4	90
B	+/- 0.2	92
C	+/- 0.1	95

Table 1 - Signal Response Data Taken from Figure 35

In the bottom of Figure 35, a *Gaussian* (linear) spectrum is presented from the same signal data containing blasts A, B and C. There is a majority clustering of frequency content in the range of 100-1000 Hz (200 -300 Hz highest recorded values) with a smaller secondary grouping at 10,000 Hz and another larger amount grouped at the 20,000 Hz range. An examination of all the recorded hydrophone and blast data reveals that this pattern of frequency content grouping is consistent throughout with individual or multiple blast records. Another example of these groupings can be seen in Fig. H18 showing a (log) Gaussian spectrum for all 4 hydrophones of an individual blast. It should be noted that there is line “noise” from the signal acquisition that potentially corresponds to the center 10,000 Hz spike seen in the bottom of Figure 35 and elsewhere (namely the blast spectral

plots of the signal records in Appendix H). This was observed during an examination of records where no blasts were administered during experiment setup and initial testing.

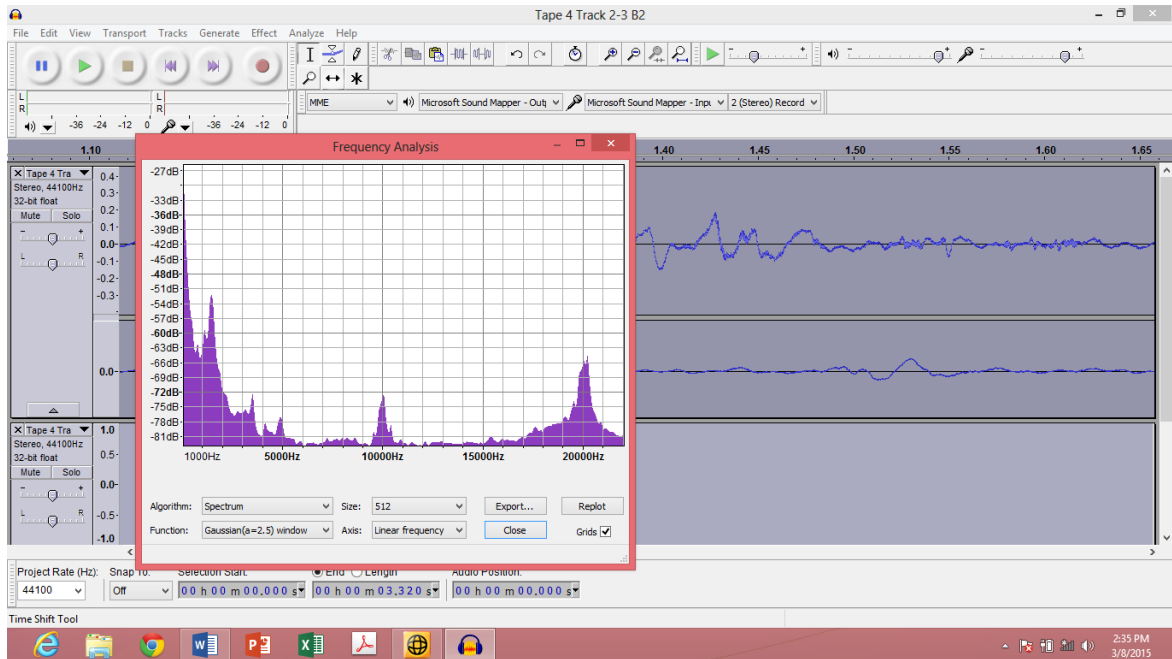
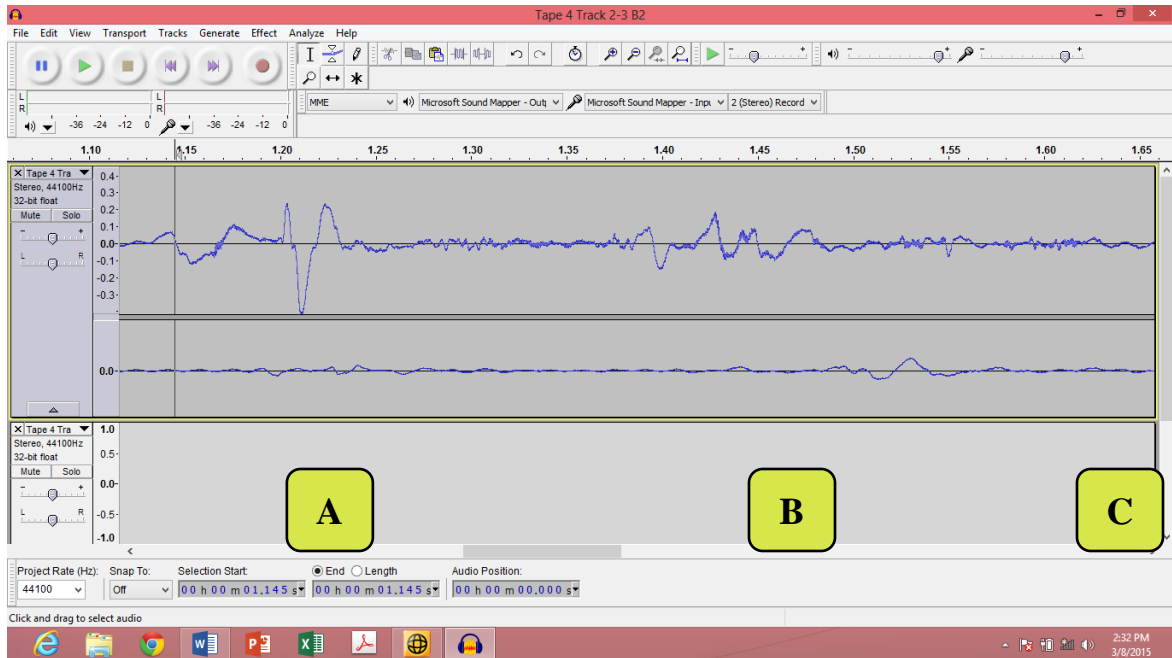


Fig. 35 – Hydrophone(s) Signal Record and Sound Spectrum from DA-88 Recorder

These pressure signals allow for the determination of the wave celerity (phase velocity) and, thereby, the mass-density of the soil which is derived from the general form as based on the text by Kinsler and Frey (1982):

$$c = (\partial P / \partial \rho)^{1/2} |_{adiabatic} \quad (6.1)$$

The wave celerity in water, or the speed of sound in water, is no longer a function of the properties of an ideal gas and so a derivation using the *Isothermal Bulk Modulus*, β_T , which can be empirically measured for liquids yields a convenient expression for the speed of sound in liquids which is:

$$c = (\gamma \beta_T / \rho_0)^{1/2} \quad (6.2)$$

where γ , β_T , and ρ_0 all vary with temperature and pressure of the liquid. These variations can be expressed as a numerical formula:

$$c(P,t) = 1402.7 + 488t^2 + 135t^3 + (15.9 + 2.8t + 2.4t^2)(P_G/100) \quad (6.3)$$

where P_G is the gauge pressure and t is the temperature. Using standard temperature and pressure values, the wave celerity or speed of sound in water is 1,500 m/s. Full derivations of this value can be found in the above reference and other texts.

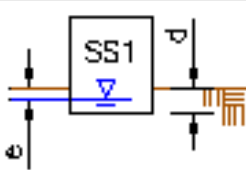
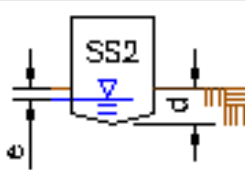
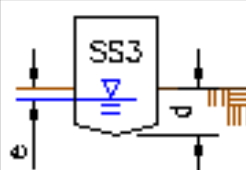
6.6 Experimental Setup

As previously written, the models described in Section 6.2 are positioned in the tank to ensure proper water and soil depths, as well as plan location. The methodology in assuring exactness in each task is presented in the following sub-sections.

6.6A Model Positioning and Alignment

The first two considerations must be those involving soil depth and water depth. In combination, these must be determined for each model type based on net model buoyancy (buoyancy and ballast). The two depths must be such that the embedded resting model is negatively buoyant. This is the initial condition for the accompanying analysis. Following the blast, the soil-water combination must allow for the model to be positively buoyant. The embedment depths are presented in Table 2 for each of the models.

The second category of the experimental setup is the horizontal alignment within the tank. That is, model sides must be equidistant between opposite walls of the tank. To accomplish this, wire guides were stretched between opposite walls. The wires were adjacent to the model sides. This alignment is important because of reverberation considerations described in Section 6.5. (See Fig. 33).

MODEL EMBEDMENT DEPTHS			
MODEL NO.			
d [IN]	4.0	5.5	8.0
e [IN]	3.0	3.0	3.0

d = EMBEDMENT DEPTH IN THE SAND WITH BALLAST

e = WATER DEPTH FROM THE SOIL SURFACE

Table 2 – Ship Model Embedment Depths in Tank

6.6B Sand – Sieve Analysis

In section 5.3B, the Eniwetok and Ottawa soil types, normally found on beaches, are discussed. As stated, there are numerous data on these soil types. For the experiments described herein, it is important that the experimental sand has properties similar to the real-world beach sands. For later comparison, the properties of the Eniwetok and Ottawa sands are presented in Table 3.

Sand	Min. Dry Density (g/cm³)	Mean Grain Size (mm)	Cu*	S.G.
Eniwek	1.31	0.35	1.6	2.71
Ottawa (Flintshot)	1.57	0.60	1.4	2.66
Ottawa (Sawing)	1.56	0.50	1.3	2.66
Ottawa (Banding)	1.47	0.25	2.0	2.66

* *Coefficient of Uniformity* – a comparative indication of the range of soil particle sizes

Table 3 – Table of Sand Properties used in the USAF Study by Fragaszy, <i>et al</i> (1981)
--

The experiment requires the use of a layer of sand (simulation of shoreline beach sand in which ships have historically grounded). This sand mass was placed in the model tank base with a sand depth designed for the ship-model embedment. The sand used was sifted into its relative particle sizes using the ASTM D422 *Standard Test Method for Particle-Size Analysis of Soils* (1963) grain sieve size analysis procedure in order to produce an accurate size distribution. The sand layer depth is maintained throughout the experiment at a depth

of 11-1/2". Filtering of impurities was done on an ongoing basis when water was added to the tank by way of using a wet-dry vacuum and skimming the surface. The gradation results are presented in table 4. The soil used in this study (from Table 4) was classified according to the ASTM USCS as *SP* with a $D_{50} = 0.34$. Referring to the paper by Ashford, Rollins and Lane (2004) for pile experiments done at the NGES on blast-induced soil liquefaction, the soils at that location in San Francisco were also classified and indexed to have similar USCS designations.

In order to derive the Index Properties of the sand, the following data was taken on the sampling used during the sieve analysis:

$$W_T = 2.05 \text{ lbs, } W_S = 1.80 \text{ lbs.}$$

From standard index property relationships (by McCarthy and others), the following can be ascertained:

$$W_W = W_T - W_S \Rightarrow 2.05 - 1.80 = 0.25 \text{ lbs} \quad (6.4)$$

$$W_T = (V_T)(G_T)(\gamma_W) \Rightarrow V_T = 2.05 / (2.65)(62.4) = 0.012 \text{ cu. ft.} \quad (6.5)$$

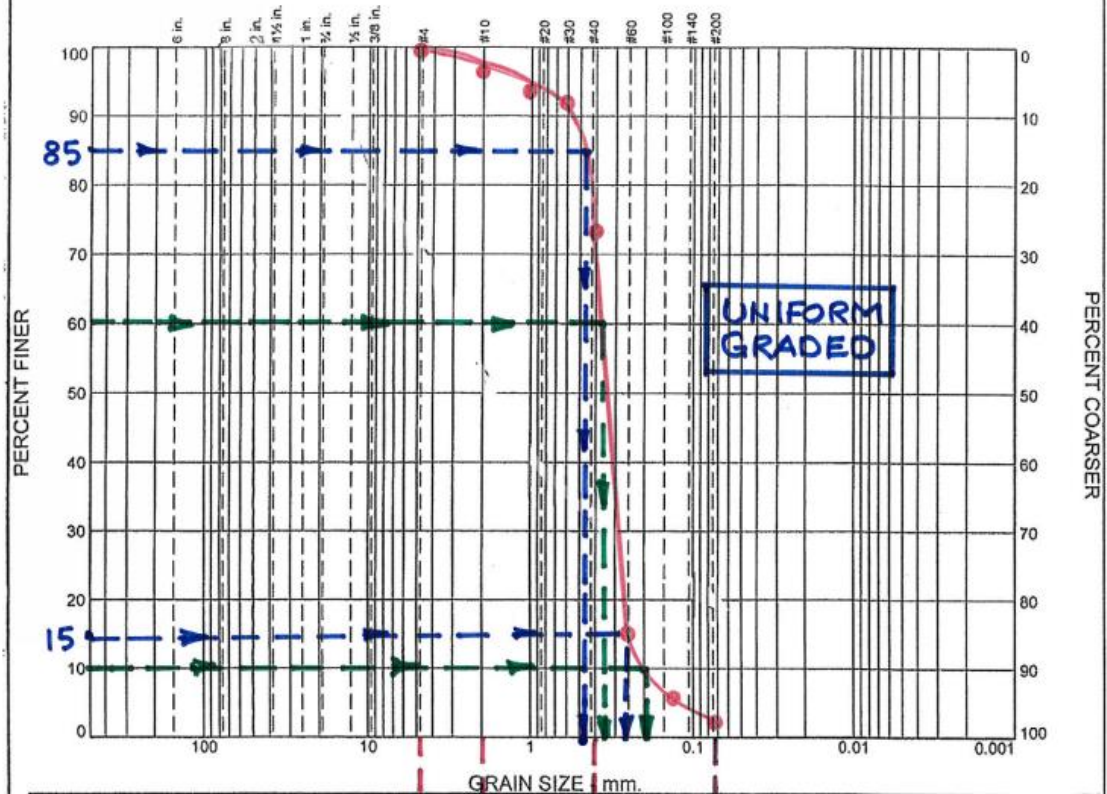
$$W_S = (V_S)(G_S)(\gamma_W) \Rightarrow V_S = 1.8 / (2.65)(62.4) = 0.0108 \text{ cu. ft.} \quad (6.6)$$

$$V_V = V_T - V_S = 0.012 - 0.0108 = .0012 \text{ cu.ft.} \quad (6.7)$$

$$e = V_V / V_S = 0.0012 / 0.0108 = 0.11 \quad (6.8)$$

$$n = V_V / V_T = 0.0012 / 0.012 \times 100\% = 1 \% \text{ or } .001 \quad (6.9)$$

Particle Size Distribution Report



	% +3"	% Gravel		% Sand			% Fines	
		Coarse	Fine	Coarse	Medium	Fine	Silt	Clay
○	0.0	0	0	1.2	48.8	47.5	0	0
×	LL	PL	D ₈₅	D ₆₀	D ₅₀	D ₃₀	D ₁₅	D ₁₀
○	NP	NP	0.52	0.38	0.34	0.31	0.27	0.17

MATERIAL DESCRIPTION		TEST DATE	USCS	NM
○ Uniform, Poorly Graded Sand; Non-Cohesive; M _z = 0.39		08/05/13	SP	-----

Project No. PH.d Disert. Client: UMCP - Dept of Civil Engineering
 Project: J. Cerquetti - Tank Sand Test for Freeing of Grounded Ships by BIL
 ○ Source of Sample: Model Tank Depth: +/- 2.5 ft. Sample Number: 1

Remarks:
 Sieve procedure per ASTM D422
 Classification per ASTM D2487

Soil Gradation Curve for Model Tank Sand

Figure

Table 4 – Model Sand Gradation Curve

The Mean Grain Size of the experimental sand used was calculated to be 0.39 mm, in Table 4, which is similar to those of the Ottawa sands in Table 2 ($M_z = (\phi_{16} + \phi_{50} + \phi_{84}) / 3$). See McHendrie (1988). The gradation curve of the sand used in this study, shown in Table 3, exhibits soil properties closely following those of Fig. 13 identified as soils susceptible to liquefaction.

6.7 Measurement and Recordings

In this section, the signal acquisition equipment is described. The major pieces of the test equipment include a *Tascam DA-88* Eight-Channel Recorder, in-house manufactured hydrophones (5 hydrophones), the in-house manufactured Air Cannon and, lastly, a mechanical tensiometer. In the following paragraph, the function of each of these items is described.



Fig. 36 – Tascam DA-88 Recorders (Left) and Input Soundboard (Right)

Four independent channels of the DA-88 were used to record the pressure signals and the corresponding spectra for each blast condition. The pre-blast pressure in the Air Cannon was both set and monitored by a pressure gauge attached between an air compressor and the Air Cannon. See the discussion of the Air Cannon in Section 6.3. Prior to a blast test, the weight of the dry, ballasted model was determined. This weight value was used to pretense the overhead support line to achieve a neutrally buoyant condition. Again, before conducting a blast test, a brute-force pull-test was performed. That is, the tension in the overhead support line was increased until the soil released the model. It was noted that for all of the models, the release tension was much greater than the measure dry weight. See the results in Table 5.

PULL TEST RESULTS				
AVERAGE PULLOUT FORCE P.O. [LB]	MODEL NO.	RELEASE TENSION RT [LB.]	TARE WEIGHT TW [LB.]	TRIAL NO.
<div>SS1</div> P.O. = 107.75 $\text{P.O. \%} = \frac{\text{RT}}{\text{TW}}$ $= \frac{107.75}{45.3}$ P.O. \% = 2.38	SS1	108	45.3	1
	SS1	107	45.3	2
	↓	107	↓	3
		106.5		4
		109		5
		108		6
		107		7
		108		8
		108		9
		109		10
	↓		↓	
<div>SS2</div> P.O. = 140.92 $\text{P.O. \%} = \frac{\text{RT}}{\text{TW}}$ $= \frac{104.92}{70.4}$ P.O. \% = 2.00	SS2	>110	70.4	1
	SS2	127	70.4	2
	↓	132	↓	3
		139		4
		141.2		5
		150		6
		156		7
		146		8
		159		9
		149		10
	↓		↓	
<div>SS3</div> P.O. = 115.2 $\text{P.O. \%} = \frac{\text{RT}}{\text{TW}}$ $= \frac{115.2}{65.0}$ P.O. \% = 1.77	SS3	110	65.0	1
	SS3	108	65.0	2
	↓	118	↓	3
		121		4
		115		5
		112		6
		116		7
		115		8
		108		9
		129		10
	↓		↓	

Table 5 – Model Pull-Out Baseline Test Results

These results are plotted graphically in the following figure:

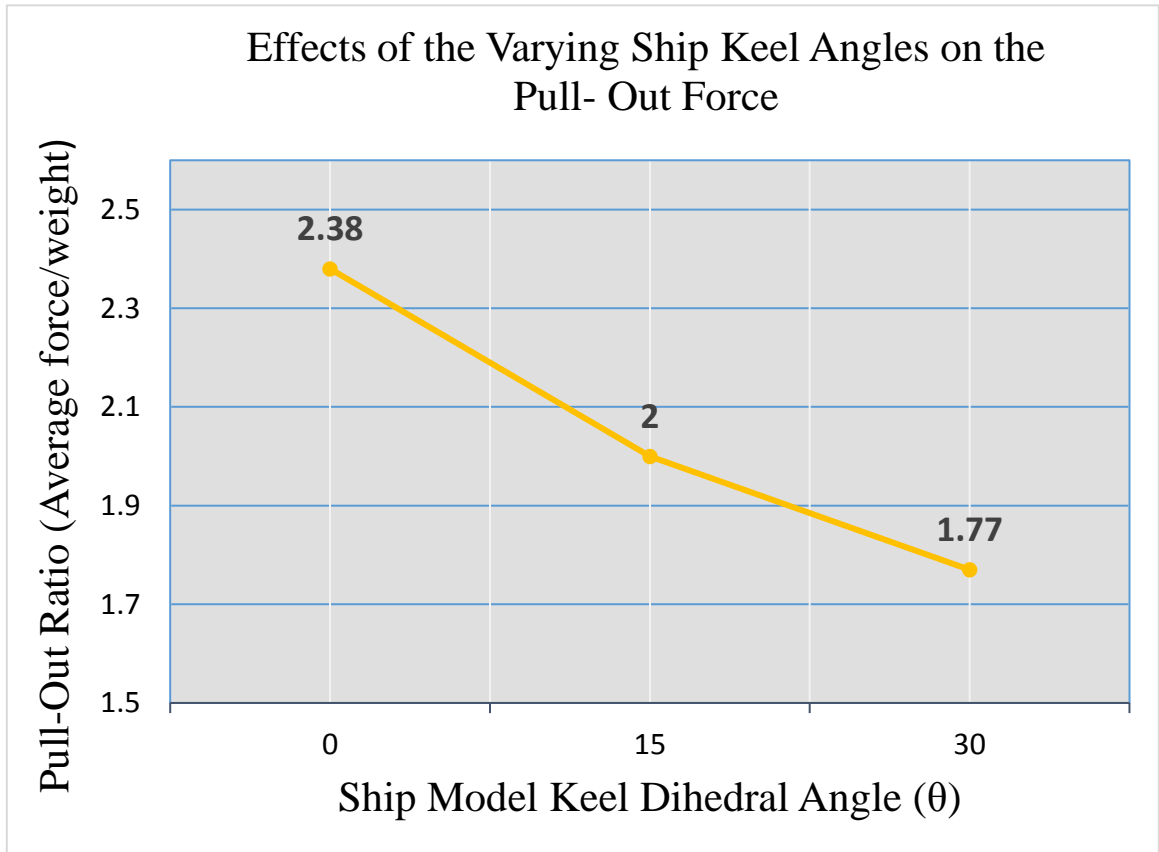


Fig. 37 – Plotted Results of the Effects of Pull-Out Force on each of the Three Ship Models

The difference in the measured line tension and the tare weight is actually the holding force of the soil on the model. See Appendix E for detailed information on the recording device.

6.7A Blast Pressure and Spectra

As previously stated, the blast pressure wave was generated by the Air Cannon coupled to an air compressor. The pre-blast pressure was between 80 psi and 110 psi, and was controlled at the Air Cannon. Following the blast, pressure signatures were measured

at four points in the soil adjacent to the model. The scheme is sketched in Fig. 32. Again, an example of a blast is shown in Fig. 35. That figure is used in the following paragraphs to help explain the various phenomena dealt with in the study. The model used in this example was the SS1.

Blast Pressure: In Fig. 35, the passage of a concussive wave at hydrophone-1 is shown. That is, the pressure signal in the top line of the figure, as measured, is shown in the time-domain. The experimental scenario was to have at least three blasts, where the blast intensity was increased from the first to the last blast. The number of blasts depended on the ship section model under study. The first cannon blast is seen on the left-hand side of the trace. The second cannon blast, which was of higher intensity, is shown to the right of the first. Here, we note that the intensity of the pressure signal is reduced. The reason for this is that the soil was partially liquefied by the first blast. To further explain, consider the sequence of events in previously discussed for the Soil Liquefaction Mechanism. In Fig. 14A, one sees the sand particles touching with water-filled voids. The interparticle contact force directions are sketched vectorially in Fig. 14B. In Fig. 14C, the contact forces are diminished as the pore-water pressure increases. This occurs as the blast wave passes. When the second blast wave arrives, the initial condition of the soil is where

Fig. 14C replaces Fig. 14A and the processes are repeated. Finally, the last trace in Fig. 35C is for the highest blast intensity with the highest degree of liquefaction. This can be explained mathematically by taking the pressure-celerity expression from linear acoustics. From Kinsler and Frey (1982), that expression is as follows:

$$p = K c^2 \quad (6.10)$$

Here, K is a proportionality constant that depends on the mass-density of the soil. We note that the celerity (c) decreases as the bulk-modulus of elasticity (soil strength) decreases, as is done in soil liquefaction. Similar signal analyses are applied to the remaining three hydrophone recordings.

Pressure Spectra: The pressure spectrum of the example in question is presented in Fig. 35 (Bottom). Referring to this figure, we see the period distribution from the signals in the above in that same figure. The spectra for the second and third blasts appear to be Gaussian. Hence, the probability densities are approximately Rayleigh in nature. When a typical spectra for the second and third blasts are normalized, the normalized spectra would appear as two truncated peaks having their half-period bandwidth, ω_0 , lower for the second signal than for the third. This means that the damping for the third blast is higher than that of the second. This results in the signal traveling at a reduced rate which, in turn, causes a lower pressure and frequency. The damping in the acoustic system can be inversely proportional to the Quality (or Q -) factor, which is defined as follows:

$$Q = \omega_0 / (\omega_2 - \omega_1) \quad (6.11)$$

Where ω_0 is the center-band frequency of the signal, and ω_1 and ω_2 are the respective upper and lower frequencies defining the half-power bandwidth. From Kinsler and Frey (1982), and others, the damping coefficient for the acoustic system is the following:

$$R = C \omega_0 / Q \quad (6.12)$$

Here C is a proportionality constant depending on the mass-density.

The behaviors shown in the example of this sub-section is similar to those from all of the blast tests. The signals for hydrophones-2, -3 and -4 for this example are presented

later and discussed. All of the pressure trace and some spectral plots are presented in Appendix H. The results of all of the studies are described further in chapters 8 and 9.

6.7B Blast-Pressure Effects on Pull-Out Loads

During the blast tests described in the last sub-section, simultaneous loading measurements were conducted to determine the reduction in the soil loading corresponding to the blast intensities for the three models. A sketch of the test setup for the load measurements is presented in Fig. 38. For the pre-blast condition, the line-tension was equal to the tare value. Hence, any change in this load must be due to decreasing soil resistance. Recall as previously seen in Table 4 that the ship model tare weight equals the pre-tense for the blast trials subtracted at the outset of the trial as: SS1 = 45.3 lbs, SS2 = 70.4 lbs and SS3 = 65.0 lbs. When, a blast occurred, the line-tension was reduced. When the second and third blasts occurred, the line-tension was reduced until the model was approaching the state of being positively buoyant. When this occurred, the line-tension lessened considerably in all cases and zeroed in others. With the pressure signal in the example in the last section, the load-signal as determined by the tensiometer is shown in the results in Column 5 of Table 5. It can be seen that the load is dramatically reduced at the trial outset and sequentially along the way from field notes with each blast. Results for the three models are presented in Table 5. In that table, the load values at the outset of all the blast pressures to which each trial was subjected, are presented.

The values in Table 6 are extremely important as to the efficiency of the blast-liquefaction mechanism and can be seen from the record data there.

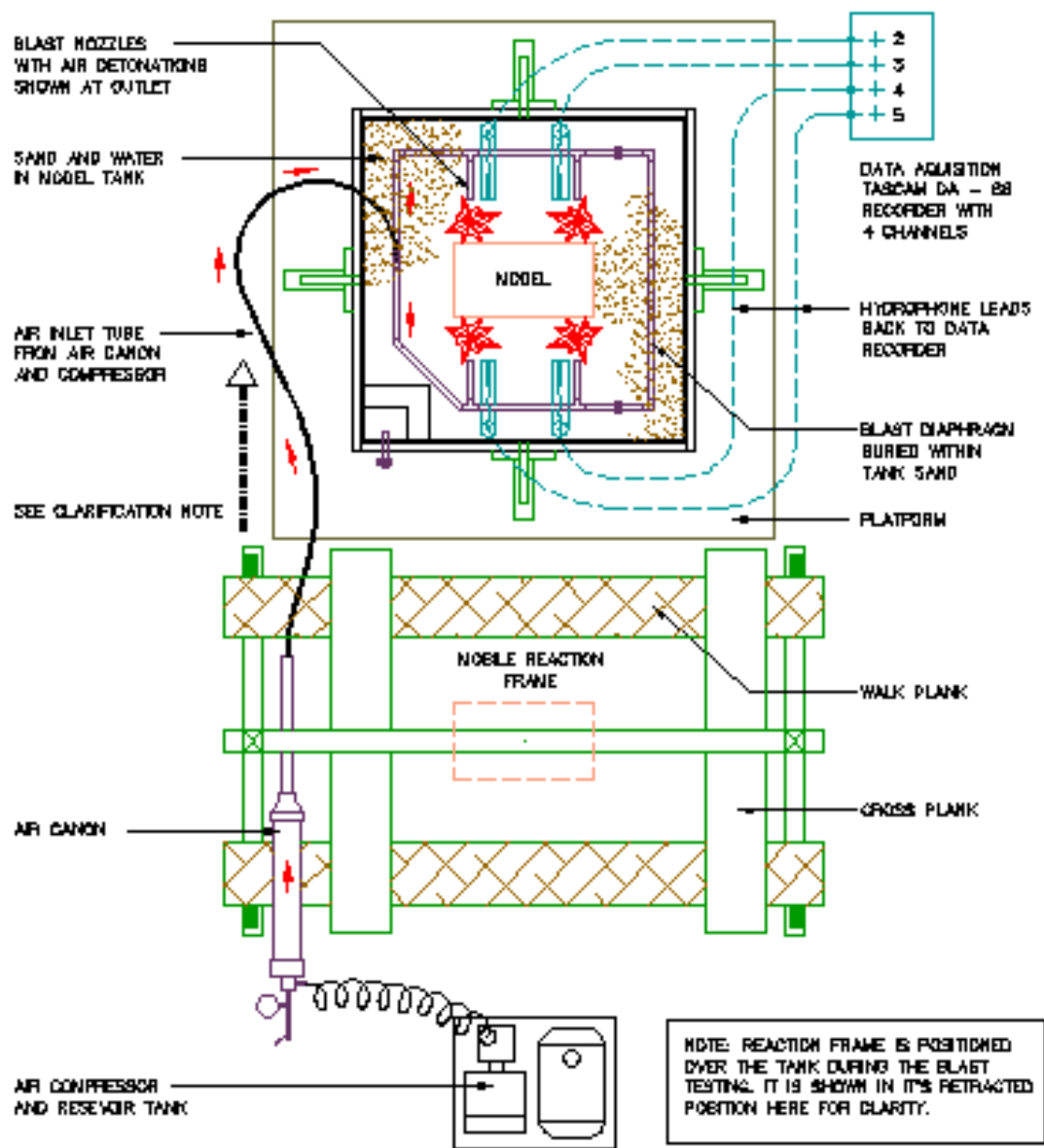


Fig. 38– Setup and Arrangement for Blast Tests

Model No.	Tape No.	Blast No.	Pressure from Air Cannon (psi)	Reading at Tensiometer To Pullout (lb)	Approx. Elapsed Time (min)	Date of Test
SS1	1	1	80	No Record	1.5	3/8/2014
SS1	2	1	80		3	3/15/2104
		2	90			
		3	92	$\pm 5^*$		
SS1	3	1	90	$\pm 16^*$	10	3/29/2014
SS1	4	1	90			3/29/2014
		2	92			
		3	95	$\pm 15^*$	5	
SS1	5	1	90			4/6/2014
		2	90			
		3	90	26	3	
SS2	6	1	90			4/12/2014
		2	92			
		3	94			
		6	85	37	6	
SS2	7	1	90			4/26/2014
		2	95			
		3	99			
		4	90			
		5	95	± 5	16	
SS2	8	1	95			5/3/2014
		2	95			
		3	95	± 15	6	
SS2	9	1	90			6/14/2014
		2	95			
		3	100	No record	6	
SS2	10	1	90			6/21/2014
		2	95			
		3	95	± 5	4	

* Tare weights subtracted from the field recorded readings for comparative use in this table

Table 6 – Blast Test Results from Written Logs for SS1 and SS2 (Partial)

Model No.	Tape No.	Blast No.	Pressure from Air Cannon (psi)	Reading at Tensiometer To Pullout (lb)	Approx. Elapsed Time (min)	Date of Test
SS2	11	1	92			7/13/2014
		2	95			
		3	100			
		4	100	±5	4.5	
SS2	12	1	93			7/13/2014
		2	95			
		3	105	53	5	
SS3	13	1	92			7/20/2014
		2	95			
		3	100			
		4	105	< 40	5.5	
SS3	14	1	95			7/26/2014
		2	100			
		3	105			
		4	NR	< 70	5.2	
SS3	15	1	80			8/2/2014
		2	95			
		3	97			
		4	100			
		5	100	40	20	
SS3	16	1	60			8/17/2014
		2	90			
		3	100			
		4	100	40	8	
SS3	17	1	90			8/21/2016
		2	100			
		3	100			
		4	80	43	15.5	
SS3	18	1	92			8/30/2014
		2	100			
		3	100			
		4	NR	29	12	

Table 6 (Con't) – Blast Test Results from Written Logs for SS2 (Balance) and SS3

7. RESULTS

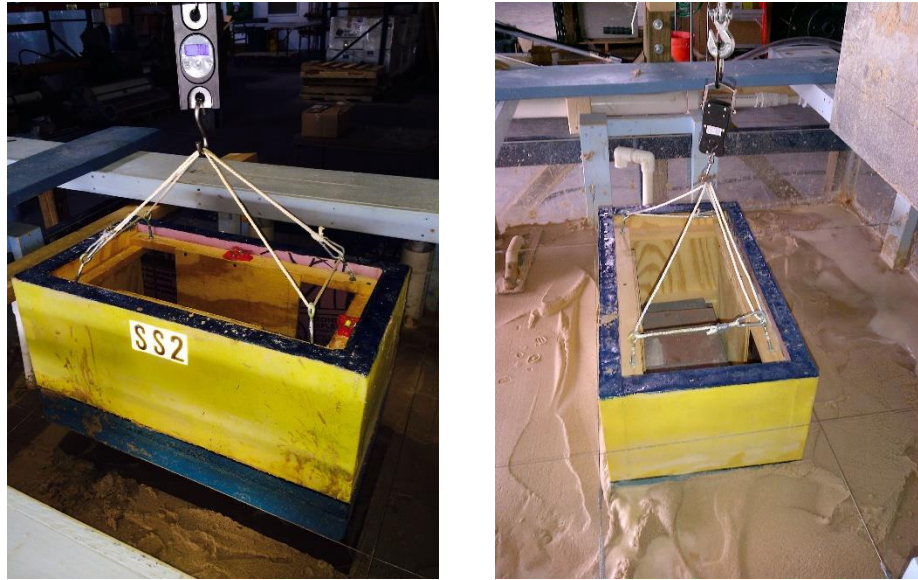


Fig. 39 – Baseline (Brute Force) Pull-Out Test

In Table 5, the pre-test pull-out force is presented for the various models and trial numbers. For the lowest trial number, one can see that there is a small difference between each model results. As the trial number increases, the pull-out force changes little over the trial sequence for the flat-bottom model (SS1). For SS2, the model having a dihedral angle of 15-degree, the pull-out force increases dramatically for trials 1 through 6. For trials 7 through 10, however, the values are approximately equal. For SS3 (30-degree dihedral angle), the force data are seen to gradually increase from trials 1 through 3, remain approximately constant from trials 4 through 8 and, then, drop and rise. Also presented in below the figure are the values of the ratios of the average pull-out force to the dry (or tare) weight. For models SS1, SS2 and SS3, the respective values of the ratio is seen to decrease. Those respective values are 2.38, 2.00 and 1.77. (from Table 4) and plotted in Fig. 37.

The results seen plotted in Figure 37 directly relate to the model geometries and their dihedral bottom angles. The flat bottom model (SS1 with 0-degree dihedral angle) has the greatest suction force potential when buried as indicated by its P.O. % = 2.38 while also having the lowest tare weight and associated tension forces needed to pull it from the sand mass during this brute force trial session of the experiment.

The SS2 (with a 15-degree dihedral angle) is less influenced by surface tension type forces within the sand mass than SS1 because of the moderate slope of the bottom when buried. It has a P.O. % = 2.00 but exhibits the highest of the models pull out forces required. The larger ballast needed to insure positive buoyancy made this model have the heaviest tare weight in combination with the moderately sloping bottom. Although meniscus forces are somewhat mitigated by the dihedral angle of the model bottom, the results show that this still influences the resistance.

The largest model, SS3 (with a 30-degree dihedral angle and a P.O. % = 1.77) is affected the least by capillary forces. Even though its weight is comparable to SS2 (65 lbs vs. 70.4 lbs.) and requires the deepest burial into the sand of the tank (see Fig. 20), it has less retraction force needed (as seen in the plot of Fig. 40) than SS2. This can be explained by the more “pointed” shape of the hull and its ability to be influenced by the granular nature of the sand which lacks cohesion and as indicated by its index properties shown in Section 6.6B. This is further discussed in Section 8. Figure 40 is a plot of each of the three models as a function of their differences from the average pull-out values.

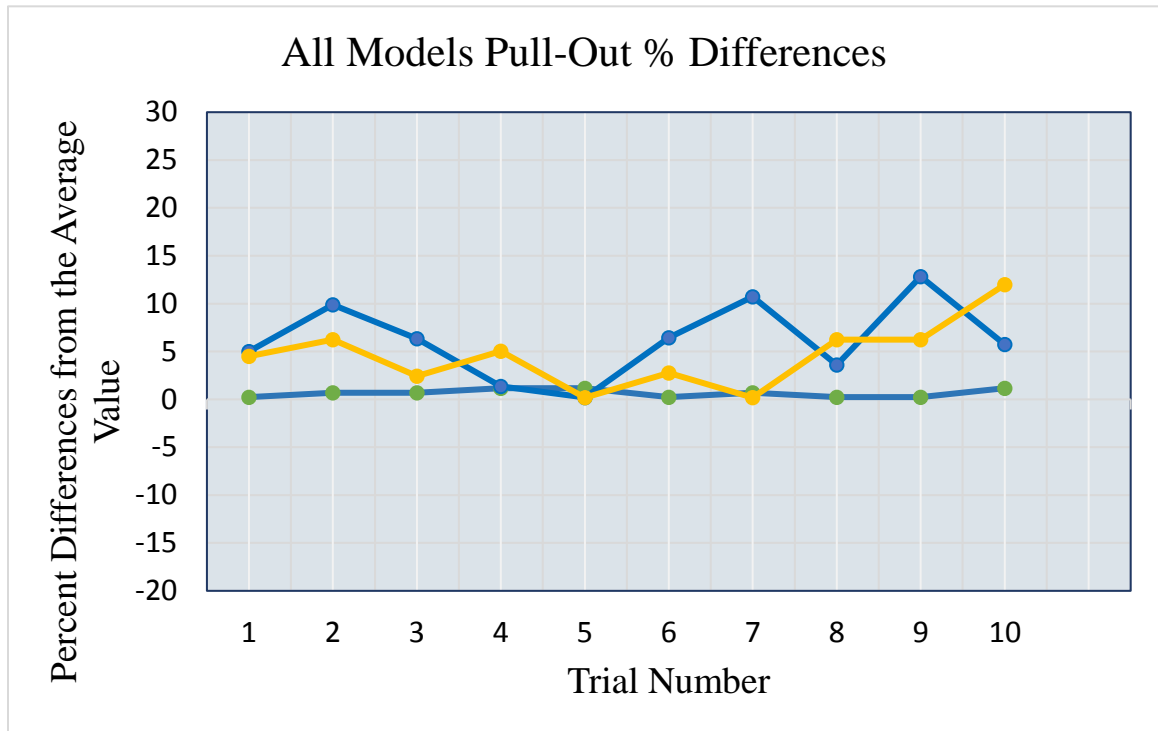


Fig. 40 – Pull-Out Differences from Average Variation

Moving now to the liquefaction segment of the testing, it can be seen that the top time trace (in Fig. 35) is the pressure signature. Signature A is associated with the first blast, B with the second blast and C with the third blast. Comparing the signatures of the three models (SS1, SS2 and SS3), the reader can see that about the same time lapse occurred between signal-pairs. What is evident is that the intensity of the pressure wave (maximum peak-to-peak) decreases from A to C. We note that the actual blast pressure increase from A to C. The reason for this is presented in the next section, Section 8.

We are essentially producing a catalyst that results in a spread of pore water buildup from a point of application to the ambient field. This is actually the release mechanism that was observed during the experiments. The phenomenon can be seen in the following three plot figures showing the progressive effect of the Air-Cannon blasts averaged over all three models:

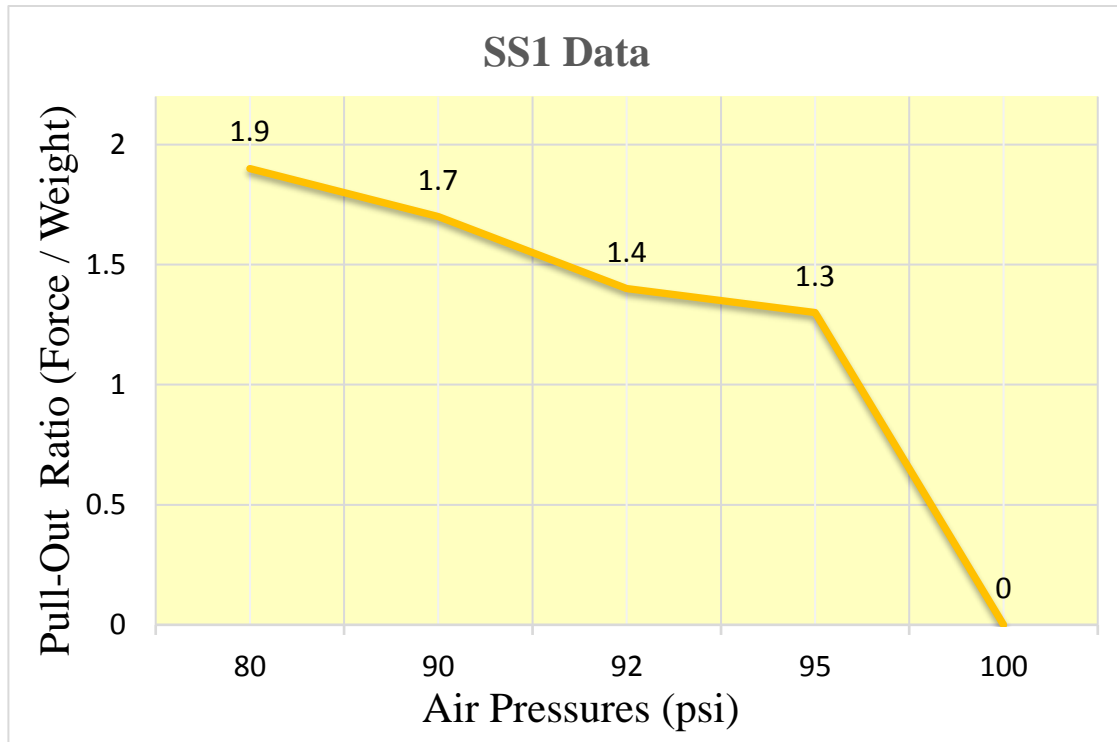


Fig. 41a – Effect of Air Pressure Variations on the Pull-Out Ratio (SS1) during Liquefaction Segment

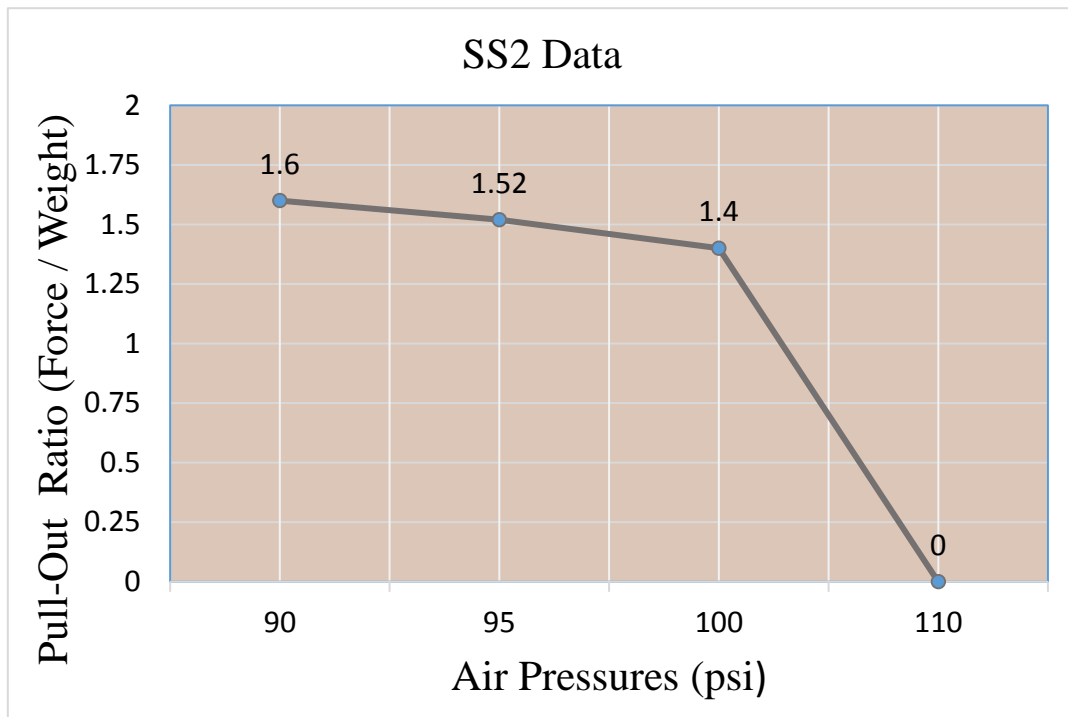


Fig. 41b – Effect of Air Pressure Variations on the Pull-Out Ratio (SS2) during Liquefaction Segment

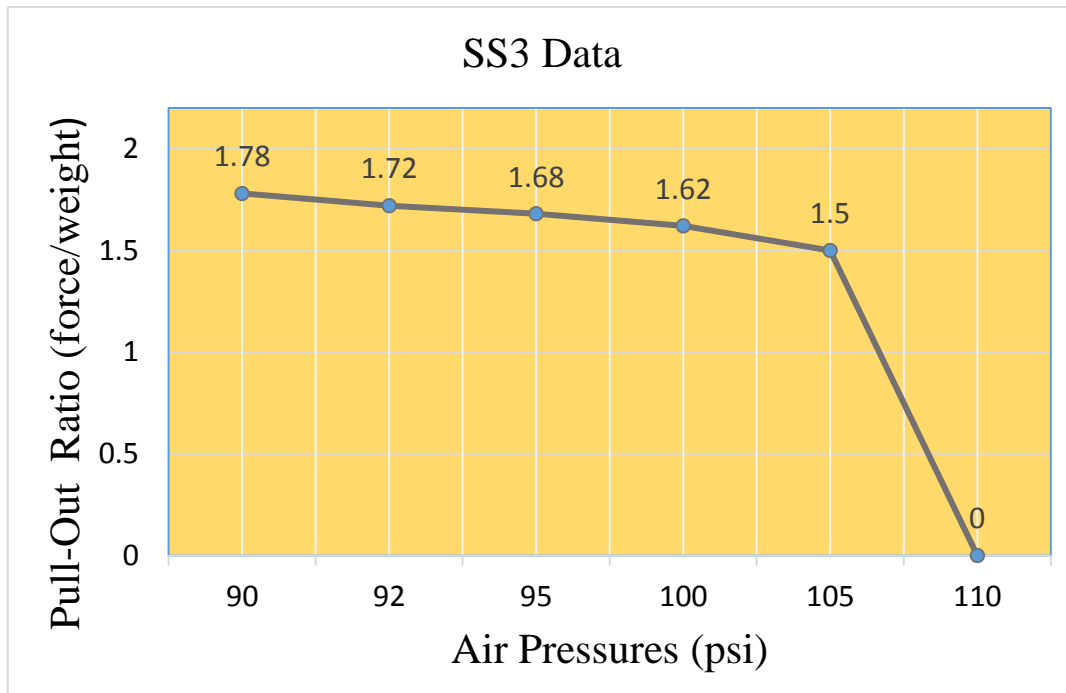


Fig. 41c – Effect of Air Pressure Variations on the Pull-Out Ratio (SS3) during Liquefaction Segment

Concerning the DA-88 multi-channel sound recorder: We saw the relationship between the release of the pressure-wave from the Air-Cannon and the recording of the event on the DA-88. From the standpoint of the observer, it was nearly instantaneous. After a time delay of approximately one minute between each blast, the tensiometer began a delayed response, as illustrated in the previous three figures. In those figures, the reader can see the scenario of the event with each successive air blast.

8. DISCUSSION

The study has several implications for naval ships and in the maritime industry. Naval vessel salvage operations could be enhanced once a grounding situation was assessed as to location and type. Depending on the nature and size of the cargo, it may be possible to aid in the regaining of the ship's buoyancy by making use of blast – induced soil liquefaction techniques. Instead of exerting efforts directed at removing the ships contents (of particular importance when carrying certain types of liquids) in order to re-float the ship or pulling on the hull during low – tide towing which could compromise the structure and jeopardize a bio – hazard incident as described in the events surrounding the TK Bremen previously mentioned (See Section 4.4 and Appendix B).

As the depth of the sea bed increases, the hydrostatic pressure and the overburden pressure increase. The method of liquefaction becomes more difficult as the water depth increases since these pressures must be overcome in order to have the soil liquefy. In a grounded-ship situation, the embedment is relatively small, and the condition to be overcome is a near sea-bed surface condition.

The results in Fig 37 are based on the value of the average pull-out force to the dry (or tare) weight. For models SS1, SS2 and SS3, the respective values of the ratio is seen to decrease. Those respective values are 2.38, 2.00 and 1.77 (From Table 4). This result is logical, since the flat surface has the highest suction force and relatively little side-wall friction. As the angles increase, the suction decreases and the side-wall friction increases. It must be noted that the side-wall friction is of second-order when compared to the suction force.

Another metric that can be ascertained from the baseline data is the relationship between the pull-out force and the soil contact surface areas for each of the models. This establishes the average pull-out pressures. Using the geometries and measurements from Table 1, Fig. 20 and the same P.O. % values from Table 4, the following are the pull-out pressures using the contact surface areas:

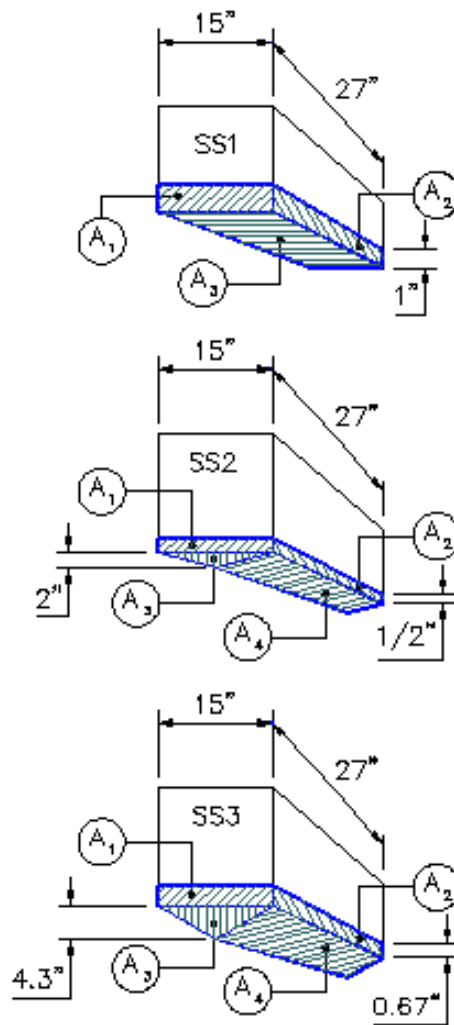


Fig. 42 – Model Surface Contact Areas

Model	A₁ [in ²]	A₂ [in ²]	A₃ [in ²]	A₄ [in ²]	Avg. Ten. [lb]	SA [in ²]	Pull-Out Press. [psf]
SS1 0 ⁰ Angle	15	27	405	-	107.8	489	31.7
SS2 15 ⁰ Angle	7.5	13.5	15	209+	140.9	491	41.5
SS3 30 ⁰ Angle	10.1	18.1	32.5	233.8	115.2	589	28.2

Table 7 – Results for Model Surface Area Pull-Out Pressures

There is a relationship among the pressure response signature, release mechanism and soil material. This is based on the fact that the soil particles move apart reducing the contact pressure, local liquefaction occurs and the model buoyancy is regained for the given section (cross-sectional) shape.

There is a time limit to the altered liquefied state. That is, it returns to its' pre-blast condition after a finite time. The response to a blast differs as the time between blasts occurs. As described in Section 6, this is due to the successive separation of the sand.

There is a threshold pressure of about 80 psi. That is, no substantial change was noticed if the pressure was below this value. The reader believes that this threshold value is a function of both the void ratio and the particle size.

As the number of blasts increase, the sand itself became segregated. There was the phenomenon of dilatancy. This was demonstrated by the presence of fines on the water surface. These were either removed or mixed back into the sand.

The experiment, although of small scale, is readily scalable to the prototype. The reason for this is that the grain size in the experiment is the same as that in full-scale. Hence, the liquefaction of the soil at the pressures-wave intensities studied herein are those that will liquefy the soil in full-scale.

9. PROJECTION FORWARD: CONCEPT-to-IMPLEMENTATION

With the findings of this study, a path forward to implementation of the BIL technique on full-scale ships can be conceptualized. In order to go from model to prototype, a two-part process follows. First, to “scale-up” the findings presented herein, a dimensional analysis of the phenomenon is performed. This is followed by a recommended practical implementation.

9.1 Dimensional Analysis

In the areas of fluid mechanics, soil mechanics and acoustics, there are a number of dimensionless parameters that are available. In viscous fluid mechanics, the Reynolds number (the ratio of the inertial force to the viscous force) is used as an independent parameter. In this study, the viscous effects are extremely small. As a result, the Reynolds number is not considered to be relevant. When water waves are of consequence, the Froude number (from the ratio of the inertial force and the gravitational force) should be used. The surface waves produced by the blasting in this study are present, but extremely small. Hence, the Froude effects can be neglected. Since acoustics and vibrations are involved in the present study, a logical choice is the *Strouhal* number. Physically, this is a dimensionless frequency ratio (the ratio of unsteady inertial force to the convective inertial force). Here, the Strouhal number is defined as follows:

$$S_t = f D / c \quad (9.1)$$

In this expression are the excitation frequency (f), the mean sand particle diameter (D) and the acoustic speed or celerity (c) in the soil. The Strouhal number represents a measure of the ratio of the inertial forces (due to the unsteadiness of the flow) to the inertial forces due

to the changes in velocity from one point to another in the flow field. We require that the Strouhal numbers for the model and prototype be equal. That is, we can write

$$S_{tm} = S_{tp} \quad (9.2)$$

Following the normal process of dimensional analysis, divide eq. (9.2) by the prototype Strouhal number, and write the result in terms of scale factors. The result is as follows:

$$S_{tm}/S_{tp} = (f_m D_m / c_m) / (f_p D_p / c_p) = n_f n_L / n_c = n_L / n_t n_c = 1 \quad (9.3)$$

Where $n_f = f_m / f_p = n_t^{-1}$, $n_L = L_m / L_p$ etc. Next, consider the ratio of the mass-densities of the model and prototype soils. The ratio is as follows:

$$\rho_m / \rho_p = n_\rho = n_p (n_t / n_c)^2 = n_p (1 / n_t n_c)^2 \quad (9.4)$$

In this equation, the scale factors (model/prototype) subscripts identify those of the pressures (p), Time (t) and acoustic wave speed (c). The length-scale factor (n_L) is defined by the investigator, depending on the facilities available. Equations (9.3) and (9.4) provide the engineer with what is needed to scale-up the experimental results. In Equation (9.3), the frequency and time scale-factors are determined, since the length scale-factor is known and the phase-velocity scale-factor is determined by the soils in question. Finally, the pressure scale-factor in eq. (9.4) is determined. Physically, from our model-scale measurements, we can determine the required air-cannon pressure. In addition, any time-lapse in the model experiments can be scaled to the prototype time-lapse since the time scale-factor is known. To converge on a more direct resolution of the dimensionless scaling parameters, the *Buckingham Pi Theorem* was used (see Appendix I for further explanation). To illustrate, consider the following example which is based on the model results in Fig. 35.

Example: Scaling-Up to Prototype

In order to show how scaling is represented from model to prototype, the example selected and used is the recent ship grounding (2017) of the Panama flagged *ARCA 1* Bunkering Tanker which ran aground off Cape Breton in Nova Scotia which was on a course to sail from Mexico to Montreal. (www.cbc.ca/news/canada/nova-scotia/canadian-coast-guard-tanker-arca-1-1.3928688). The *ARCA 1* is 174 feet in length with a 36-foot beam and average draught of 12 feet with a DWT of 1,317 tons.



Fig.43 – Bunkering Tanker ARCA 1 grounded off Cape Breton beach. Nova Scotia, Canada (from *Fisheries and Oceans Canada: On-Line*, 2017)

Using the information from both the model geometry, testing records of the experiment and the *ARCA 1* (*example prototype*) ship data we have:

$$L_m = 2.25 \text{ ft}; L_p = 174 \text{ ft} \rightarrow n_L = 2.25 / 174 = 0.013 \text{ or a } \pm 1/75 \text{ length scale factor}$$

$D_m = D_p = 3.5 \times 10^{-4} \text{ m} = 1.1 \times 10^{-4} \text{ ft}$ (from sieve analysis; assumption that the particle diameters are nearly of same size between the soil modeling soil and those encountered at a grounding site)

$\rho_m = \rho_p = (100 \text{ lb/ft}^3) / g = 3.1 \text{ slugs}$ (assumption, again, is that the soil mass density of the model sand and those encountered at the grounding site are nearly the same)

$f_m = 200 \text{ Hz}$ (predominant frequency from spectrums shown in Appendix H)

$c_m = 762 \text{ m/sec} = 2,500 \text{ ft/sec}$ (acoustic soil celerity, text reference by Urlick)

$St_m = St_p = f_m D_m / c_m = (200)(1.1 \times 10^{-4})/2,500 = 9.186 \times 10^{-5} = \text{Strouhal Number}$

$P_{o_m} = 100 \text{ psi} = 0.7 \text{ psf}$ (experiment average air cannon pressure for induced liquefaction)

$t_{o_m} = 2 \text{ sec}$ (air delivery average time from air cannon to buried diaphragm in the experiment)

A second integral formula for use with the scaling from model to prototype is the

Energy Flux Density of the soil which is again defined by Urlick as:

$$E_b = P_o^2 t_o / 2 \rho c \quad (9.5)$$

Substituting for the celerity defined in Eq. 9.5 into Eq. 9.1 we now have:

$$St = \left[f D P_o^2 t_o / 2 \rho E_b \right]_m = \left[f D P_o^2 t_o / 2 \rho E_b \right]_p \quad (9.6)$$

All of the variables listed in Eq. 9.6 on the left hand side (subscript: *m*)

Re-writing Eq. 9.6 in terms of E_b from the left side yields :

$$E_{b_m} = \left[f D P_o^2 t_o / 2 \rho St \right]_m \quad (9.7)$$

Which is now a known value using the parameters defined above.

Using the Strouhal relationship defined in Eq. 9.3 and Eq. 9.4 further defines:

$$1 = n_L (n_p)^2 (E_{b_p}/E_{b_m}) (\rho_p/\rho_m) = n_L (n_p)^2 (E_{b_p}/E_{b_m}) \quad (9.8)$$

Where $(\rho_p/\rho_m) = 1$, again because of the assumption that the sand of the model and the sand found at the grounding site are nearly the same.

Thus Eqs. 9.6 and 9.8 can now be written in terms of the prototype frequency that would be experienced at the grounding site and could be recorded as:

$$f_p = 2 \text{ St } \rho (E_{bm} / [n_L P_m^2]) / D_p t_p \quad (9.9)$$

which resolves to $f_p = 15,979 \text{ Hz}$ with all substitute values into Eq. 9.9

Likewise using the other model parameters for other air cannon pressures and frequency:

$$f_{p90} = 14,896 \text{ Hz with } f_m = 200 \text{ Hz and } P_m = 90 \text{ psi}$$

$$f_{p110} = 18,351 \text{ Hz with } f_m = 200 \text{ Hz and } P_m = 110 \text{ psi}$$

Another equality that can be used given Froude scaling for the dimensionless relationships is:

$$P_m / P_p = n_p = n_L \longrightarrow P_p = P_m / n_L \quad (9.10)$$

Which yields:

$$P_m = 90 \text{ psi} \longrightarrow P_p = 6,923 \text{ psi}$$

$$P_m = 100 \text{ psi} \longrightarrow P_p = 7,692 \text{ psi}$$

$$P_m = 110 \text{ psi} \longrightarrow P_p = 8,462 \text{ psi}$$

Using the values derived from Eq. 9.10 and plotting them graphically with similar values assumed for a smaller and a larger prototype gives:

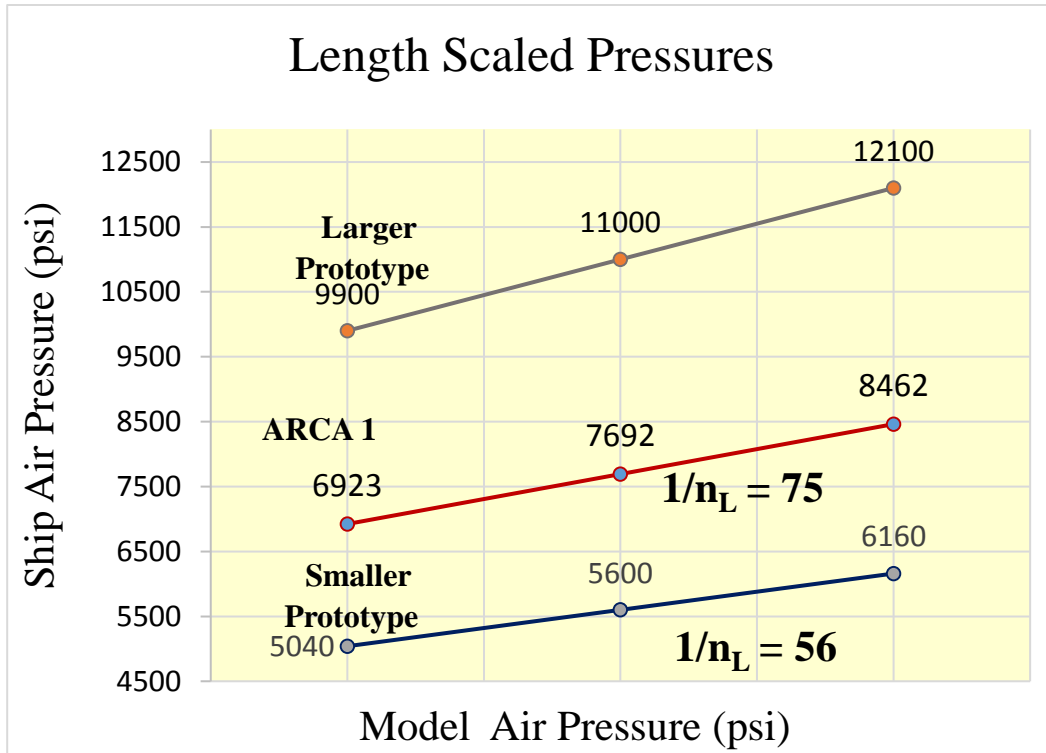


Fig. 44 – Values for Field Scaled Pressures compared to the ARCA 1 Ship Example

Another comparative metric for the scaling from model to prototype involves examining the vessel draft; T . The draft is reflective of the weight i.e. the amount of cargo, fuel, ballast etc. it is carrying since it is either floating shallower or deeper based on its' weight. Fig. 45 shows the midship sectional draft of a typical ship as described by *Rawson and Tupper; Basic Ship Theory*.

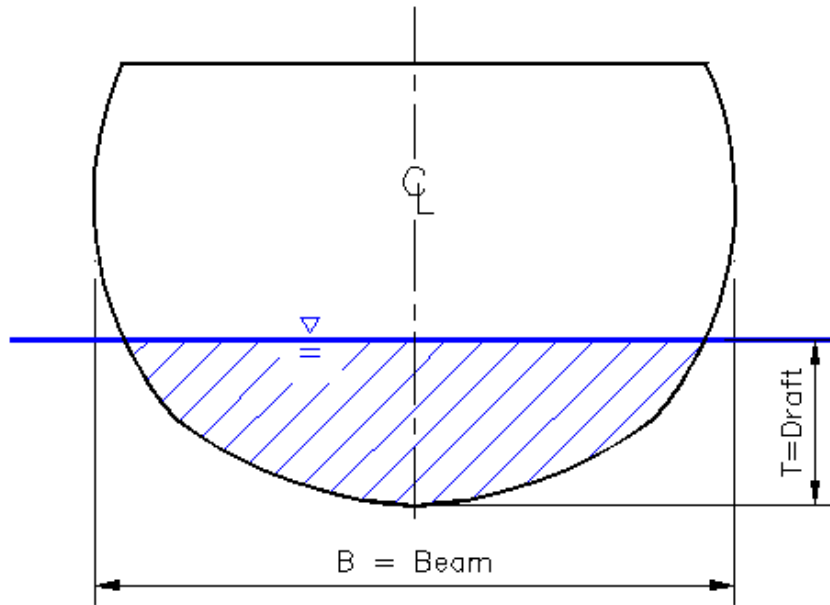


Fig. 45 – Draft Definition of Midship Section

Embedment potential can then be compared between the model and the prototype in a similar manner to the length scaling procedure described previously. We will once again use the ARCA 1 example parameters as the prototype vessel.

$$T_m = 2.5 \text{ in}; T_p = (11.5)(12) \text{ in} \rightarrow n_T = T_m / T_p = 2.5 / 138 = 0.018$$

or a $\pm 1/55.2$ draft scale factor

According to the naval geometric properties for the ARCA 1 (and with all actual ships), there are three given depths for draft defined as: *Minimum Draft* / *Average Draft* / *Maximum Draft*. These are (6.6 ft / 11.5 ft / 15.7 ft.). Once again, a dimensionless relationship can be scaled between the model and the prototype establishing blast air pressures required to induce liquefaction from the model data as follows in Fig. 46:

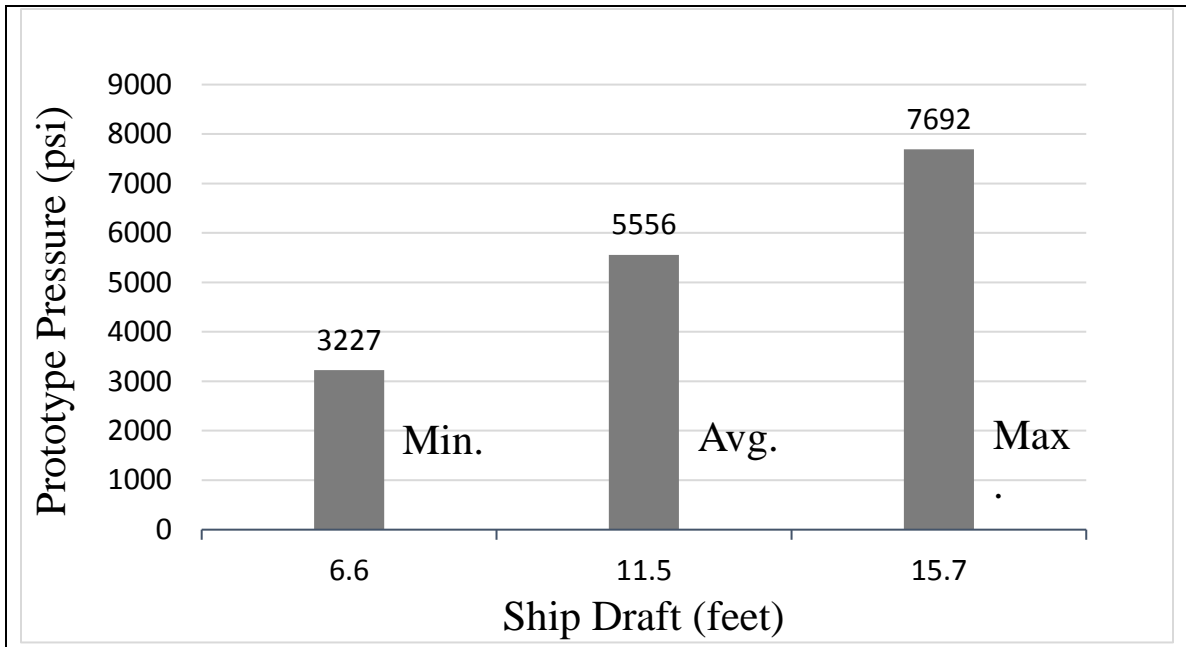


Fig. 46 – Ship Draft (depth) vs. Blast Pressure at the Site

This draft metric is also in the same order as the length scaling derivation used earlier.

9.2 Implementation

The technique makes use of a peripheral array of blast locations around a ship. This “planting” process of the blast/compression nozzles could be done by deploying a pre-equipped vessel or vessel towing a pre-fitted barge (typical size) arrangement to the ship grounding location. The rescue vessel would have a shallow draft in order to be able to maneuver on the leeward side of the grounded ship between itself and the shoreline. Time response availability of these release measures is a key factor in the ship grounding scenario as stated previously in this study. *“Time is of the essence you have to move fast. The longer that boat stays idle on the shoreline, the more precarious the situation becomes”*- N.S. Municipal Regional District 8 Councilor – Amanda McDougall (Reference to the ARCA 1 grounding in Nova Scotia). The concept would be to have the required

equipment onboard and be deployment-ready in order to be able to have a quick response to the ship grounding event.

The vessel would have the following equipment in ready supply:

1. Several high horsepower compressor(s); redundancy preferable.
2. High pressure receiver tanks; minimum of three.
3. Generator / independent power supply using onboard fuel supply.
4. Reel or rack storage of flexible high-pressure hose or flexible/ductile pipe.
5. Supply of submersible (rigid) nozzles that attach to the hose/pipe at various locations and frequencies.
6. Several mounted air cannons that are connected to the compressor on the barge.
7. A vibratory pile driving type hammer with an articulating head (such as a MoVax) to insert the nozzles several meters into the sand/soil matrix around the perimeter.
8. Intermediate hose weights or tie-down (clump) anchors to keep the hose between the nozzles in position as the high pressure air blasts are administered from the air cannon to the planted nozzles around the perimeter of the grounded ship.
9. General duty deck jib crane for various lifting and deployment activities.

Fig. 47 shows a conceptualized representation of a grounded ship rescue operation with a Panamax class ISO container vessel. The distance between nozzles along the perimeter is shown as the beam (B) of the grounded ship at a distance of $\frac{1}{3}$ to $\frac{1}{2}$ the beam as the length away in order to induce the soil to liquefy in a suitable perimeter. Full scale tests performed at NGES (see Ashford, Rollins and Lane, 2004) indicate that a radius of influence for subsurface detonations (as indicated earlier) is site specific but corresponds to the range

around each blast nozzle conceptualized here. The magnitude of the blast does affect soil liquefaction which increases with multiple detonations as is viable with the technique used in this study. Further field tests would need to be carried out to verify these dimensions empirically.

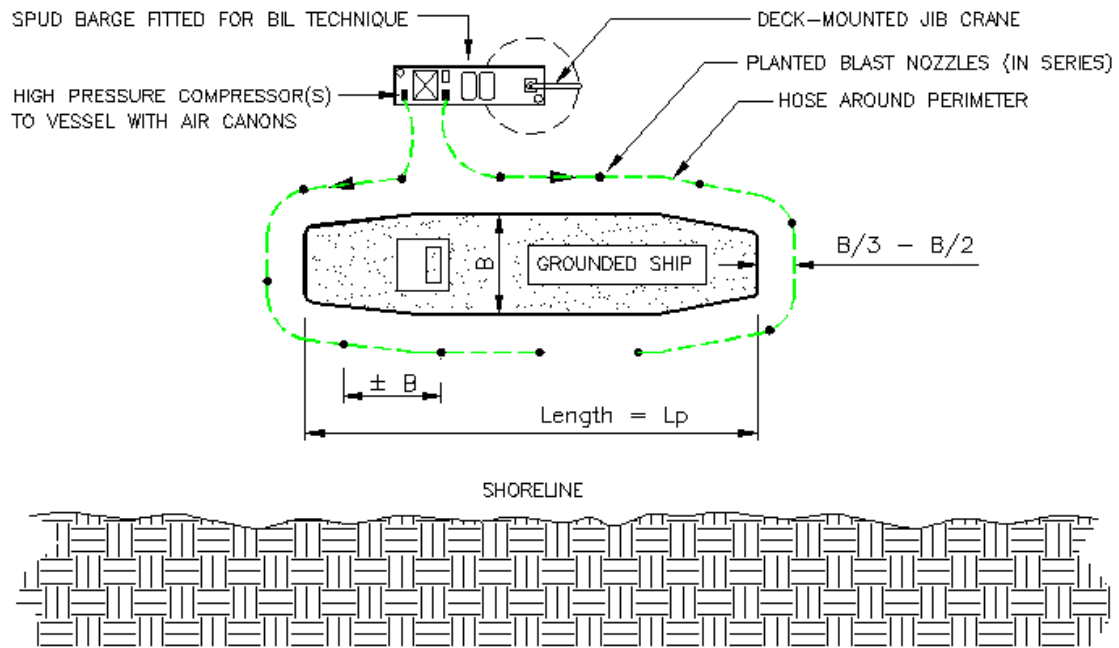


Fig. 47 - BIL Equipped Rescue Barge in Position Around a Grounded Ship

The barge itself would be well suited to have the capacity to be self-anchored, such as a spud-barge or jack-up barge, in order to resist the lateral air blast force administered by the air-cannon / compressors through the hose(s). A jack-up type barge may prove to be better suited considering that the wave climate on the seaward side of the stranded vessel could still be quite energetic following a storm event during the time attempted for the ship rescue. Multiple hose and compressors would be synchronized in at least two lines of the nozzles in order to better distribute the air pressure along the length. The air compressors and the air cannon(s) would have to be scaled up considerably because of the hose fill air

volume required and the related blast needed through each nozzle in order to induce liquefaction. The distance from the ship hull to the blast nozzles would have to be field-determined based on the soil conditions and as guided from the positions used in the model tank relative to the ship models. Blast pressure and depth of the embedment could be scaled from ratios of those used in this experiment and from similarities in the soil properties of those surrounding the grounded ship.

The cost to fit out and subsequently deploy a rapid-response vessel suited to administering the Blast Induced Liquefaction technique is far outweighed by the costs associated with grounded ship damages and environmental cleanup. The lack of a Grounded Ship response plan for marine cargo freight insurance is a costly part of doing business for vessels. On a marine cargo insurance company's marquee page it states:

“Over the last couple of years, ocean cargo insurance has become more important because more ships are experiencing casualties ...such as...

- ***Being stranded***
- ***Some cargo has to be off loaded*** “

Information obtained during this research has shown that an average container ship pays as much as \$1,000,000.00/yr/vessel for the lack of a grounded ship mitigation plan. The success of the method proposed by this work could seriously defray these costs throughout the marine industry and provide a great benefit.

The usefulness, as well as cost effectiveness, of this technique as applied to real world applications is considerable given that ship groundings present many negative impacts in the marine environment. It is the author's belief that furthering this BIL research

work into an applicable means to more effectively aide in the release of grounded ships can be of true benefit in the future to the marine and nautical spheres.

10. CONCLUSIONS and RECOMMENDATIONS

The purpose of the present study is to test the hypothesis that air-blasts can liquefy the sea-bed material beneath a grounded ship, thereby restoring the lost buoyancy of the ship. The lost buoyancy has been shown to be time-dependent – gradually disappearing over period of about 15 minutes. As discussed in Section 8, this time period would be the same on the prototype scale, since the grain size used in the present study is the same for the prototype. Furthermore, a method of introducing such an air blast is presented.

The method of proving the hypothesis is experimental – the experiment being of relatively small-scale. In the experimental study, small-scale models of three ship sections are embedded and subsequently released by the air-blast method. The models are of flat-bottom and two dihedral angles, 15-degrees and 30-degrees. The experiments are essentially two-dimensional and, therefore, simulate mid-ship sections of the ship. A method to scale experimental model results (which is performed on a prototype vessel of actual size) has been demonstrated within scaling limitations.

In addition, the technique is somewhat “green” in that there are little or no environmental consequences and its’ use can prevent hazardous spills because of the relatively quick response availability. The effects of the air cannon blasts are localized around the grounded ship and their respective pressures are deterministic based on the scaling parameters demonstrated in this study. They are minimally invasive and the soil returns to its’ original condition after liquefaction in relatively short order. The blast technique prior to that introduced in this study was to use explosives. These do alter the ambient environment for a period of time and are much more detrimental to the vessel.

From the results presented previously, it has been shown that the blast technique is experimentally feasible for releasing grounded ships. This conclusion is made based on the typical force signal record presented and in the pressure trace plots in the Appendix. These results are then depicted graphically where it can be seen that the buoyancy increases corresponding to the pull-out force with each successive air blast. When the pull-out force is zeroed, liquefaction is achieved and the model in question is totally buoyant and free to sail.

Additional future work related to this study should be a larger implementation of this BIL technique utilizing a larger tank and bigger models. This would further assist in defining the parameters used to scale the results in this experiment.

It is further recommended to perform the proposed BIL release method on a full size grounded ship using the scaling parameters derived during this present study.

APPENDIX

Appendix A: Experimental Photograph Record

The sequence of events in the construction and utilization of the experimental tank and ancillary equipment are presented in this appendix. The reason for doing so is that the reader can gain some idea of the processes and how these produced the experimental results. The photographs were taken over a two-year span: from 2012 through 2014. The photographs are presented in their chronological order. The P in the photographic number simply means “picture”. The photographic record follows:

2012



P12-01



P12-02



P12-03



P12-04



P12-05



P12-06



P12-07



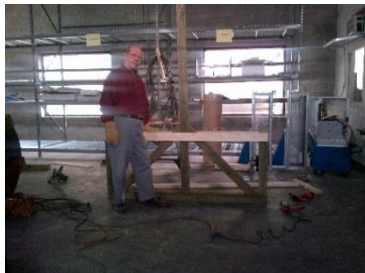
P12-08



P12-09



P12-10



P12-11



P12-12



P12-13



P12-14



P12-15



P12-16



P12-17



P12-18



P12-19



P12-20



P12-21



P12-22



P12-23



P12-24



P12-25



P12-26



P12-27



P-12-28



P12-29



P12-30



P12-31



P12-32



P12-33



P12-34



P12-35



P12-36



P12-37



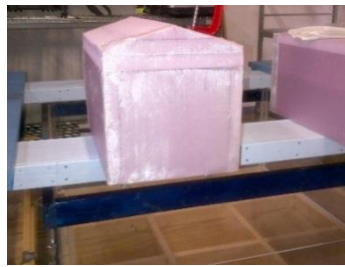
P12-38



P12-39



P12-40



P12-41



P12-42



P12-43



P12-44



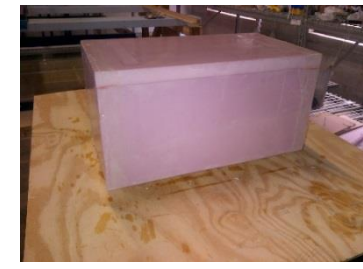
P12-45



P12-46



P12-47



P12-48



P12-49



P12-50



P12-51



P12-52



P12-53



P12-54



P12-55



P12-56



P12-57



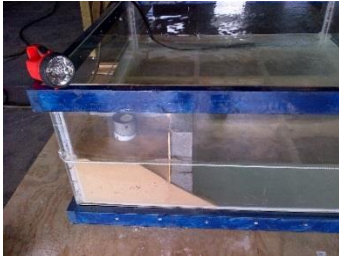
P12-58



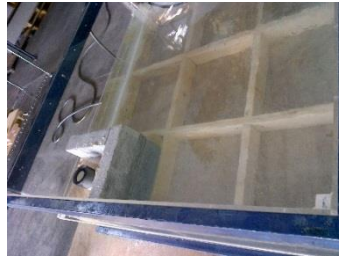
P12-59



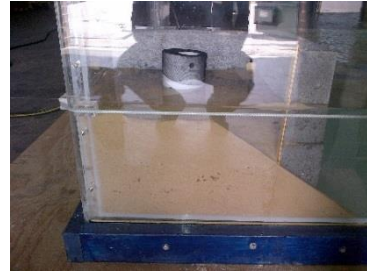
P12-60



P12-61



P12-62



P12-63



P12-64



P12-65



P12-66



P12-67



P12-68



P12-69



P12-70



P12-71



P12-72



P12-73



P12-74



P12-75



P12-76



P12-77



P12-78



P12-79



P12-80



P12-81



P12-82



P12-83



P12-84



P12-85



P12-86



P12-87



P12-88



P12-89



P12-90



P12-91



P12-92



P12-93



P12-94



P12-95



P12-96

2013



P13-01



P13-02



P13-03



P13-04



P13-05



P13-06



P13-07



P13-08



P13-09



P13-10



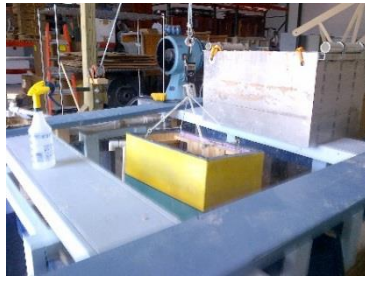
P13-11



P13-12



P13-13



P13-14



P13-15



P13-16



P13-17



P13-18



P13-19



P13-20



P13-21



P13-22



P13-23



P13-24



P13-25



P13-26



P13-27



P13-28



P13-29



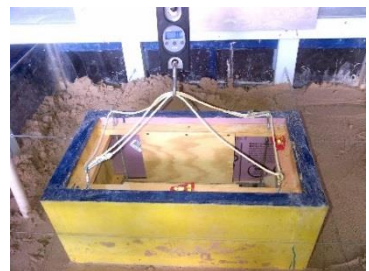
P13-30



P13-31



P13-32



P13-33



P13-34



P13-35



P13-36



P13-37



P13-38



P13-39



P13-40



P13-41



P13-42



P13-43



P13-44



P13-45



P13-46



P13-47

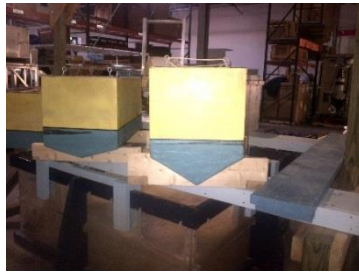


P13-48

2014



P14-01



P14-02



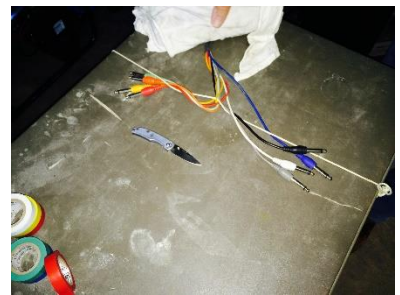
P14-03



P14-04



P14-05



P14-06



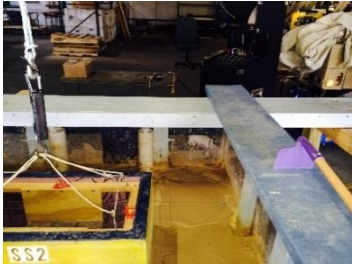
P14-07



P14-08



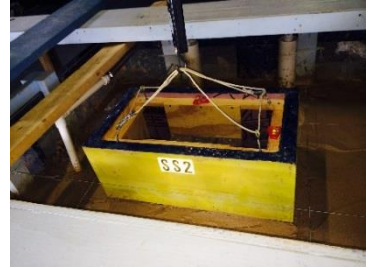
P14-09



P14-10



P14-11



P14-12



P14-13



P14-14



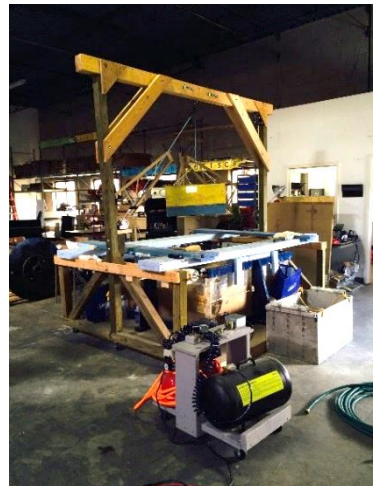
P14-15



P14-16



P14-17



P14-18

Appendix B: Sample Case Studies

In the following case studies of ship groundings, considerable financial losses were incurred, as well as delays in delivering and unloading the cargo that remained undamaged. The financial repercussions were substantial and amounted to many times the value of the vessels themselves. Fortunately, several of the referenced ships did not end up releasing any hazardous materials to the environment, although the risk was certainly present. Other ship grounding incidents have not been as environmentally fortunate and have been proven to be detrimental in terms of oil or hazmat spills. See, for example, the discussion and analysis by Hudson (2001) in the case of the M/V New Carissa (see ref.) off the coast of Oregon and the previously mentioned case of the T.K. Bremen detailed below.

Case 1 – M/V Pasha Bulker: Another similar case grounding is that of the *M/V Pasha Bulker*, a Panamax bulk carrier off the coal port of Newcastle Harbor, South Wales, Australia. The *Pasha Bulker* was a 738' L, 76,741 DWT commodities carrier that was driven aground under power with anchorage complications in heavy seas of four meter storm waves. Within hours of the grounding, the outer shell of the ship's double hull was breached and taking on water. Once fully aground and driven alongshore, the 23 man crew has to be rescued by Westpac Rescue Helicopter - seen here in Fig. B1 while air lifting a crew member from the deck in an emergency response rescue.



Fig. B1 - M/V Pasha Bulker Taking on Heavy Seas (from *1233 ABC Newcastle News*, “M/V Pasha Bulker Grounding”, On-Line, 2012)

The ship underwent three attempts to dislodge it from the shore over the next month after unloading and salvage operations. It was finally refloated during a seasonal high-tide event and had temporary repairs done off Australia in order to make it transportable.



Fig. B2 - M/V Pasha Bulker Grounded off the coast of Nobbys Beach, Australia, (from *1233 ABC Newcastle News*, “M/V Pasha Bulker Grounding”, On-Line, 2012)

It was eventually towed back to Japan where it had extensive structural repairs done at great cost and down time. The *Pasha Bulker* was sold by the former owners for undisclosed reasons the following year.

Case 2 – TK Bremen: As previously referenced in Chapter 1, the bulk commodities and cargo carrier *TK Bremen* grounding in Lorient, France in 2011 caused French coastal authorities to enact offloading and salvaging procedures for the crew and subsequently for the cargo. Part of the cargo was liquid fuel oil that began immediately leaking with the grounding of the ship.

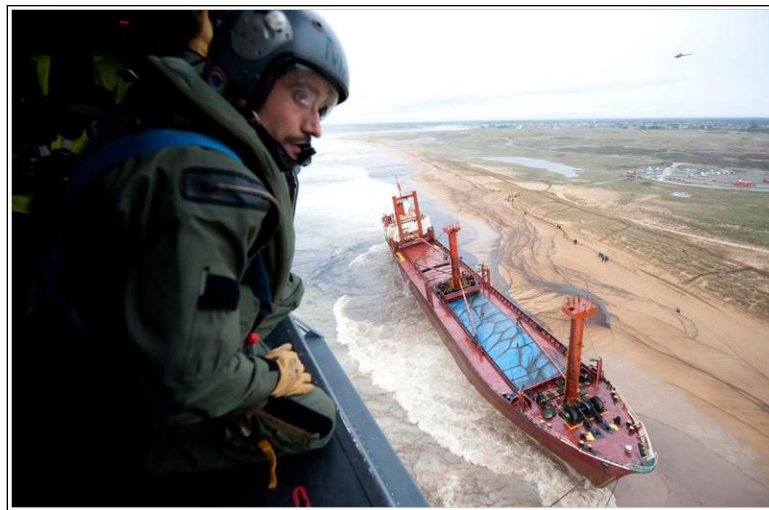


Fig. B3 – TK Bremen is Stranded on Kerminihy beach. Rescue Measures begun. (from *Marine Nationale*: “T. K. Bremen Grounding”, On-Line, 2011)

Breaking waves in the nearshore and at the beach drove the *TK Bremen* to a fully stranded alongshore position causing dune and backshore environmental contamination with the spilled fuel oil which triggered weeks of beach cleanup by workers and firefighters. The vessel was deemed impossible to refloat in its’ completely stranded final condition on the Kerminity beach and was broken apart for removal three weeks later.



Fig. B4 – TK Bremen is Broken Apart on January 7, 2012 at Erdeven, France (from *Marine Nationale*: “T. K. Bremen Grounding”, On-Line, 2011)

The *TK Bremen* was a total loss for its’ owners and posed hazards in many ways to the French authorities.

Case 3 – M/V Victoria: In July of 2016, the Liberian-flagged bulk carrier, the 46,000 DWT *M/V Victoria* ran aground at Fladen, some 15 nautical miles from the Swedish coast at Varberg. The vessel was loaded with wheat and was on route from Rostock in Germany to Guinea.



Fig. B5 – Liberian Flagged M/V Victoria Grounded at Fladen (from *World Maritime News: M/V Victoria Grounding*,” On-Line, 2016)

The Coast Guard suspected that there was a possibility of structural hull damage and so divers were dispatched to examine the vessel's bottom and found a 19 foot tear. There were no oil spills recorded but prior to salvage maneuvers were to begin, it was decided to remove the fuel oil in order to stabilize the bulker. Two emergency vessels were standing by to help in case there was a need to respond to a potential oil or environmental emergency.



F

Fig. B6 - Tug Towing / Fuel Unloading following to Night-Time Salvage Attempts (from *World Maritime News: M/V Victoria Grounding,*” On-Line, 2016)

Attempts to pull the ship free prior to unloading were deemed hazardous. At last report the ship remained grounded for 5 days until weather allowed the fuel to be unloaded.

Appendix C: Design and Construction of the Experimental Equipment

Model Tank Construction: The support structure of the tank is a wood-base frame and top rail. The base of the tank is a frame with intermediate members in both the horizontal coordinate directions to distribute the water and sand loads on the impermeable Lexan bottom. The tank perimeter is composed of wood members (nominal 2" x 4" lumber) that are placed on the inside and outside of the tank wall to form the outer sides.



Fig. C1 – Tank During Construction and Water Leak Testing

Each sidewall base frame member is through-bolted along the edges using $\frac{1}{4}$ " diameter bolts with nuts/washers. This system forms a stiffened horizontal tank sidewall support at the base along the entire perimeter. The top rail is similar, but runs along the outside and is attached to the Lexan wall with wood screws. The corners of the tank are attached with square acrylic bar-stock members that are vertically bolted in opposing directions through the adjacent Lexan sidewalls along the tank height. All fasteners used are stainless steel.

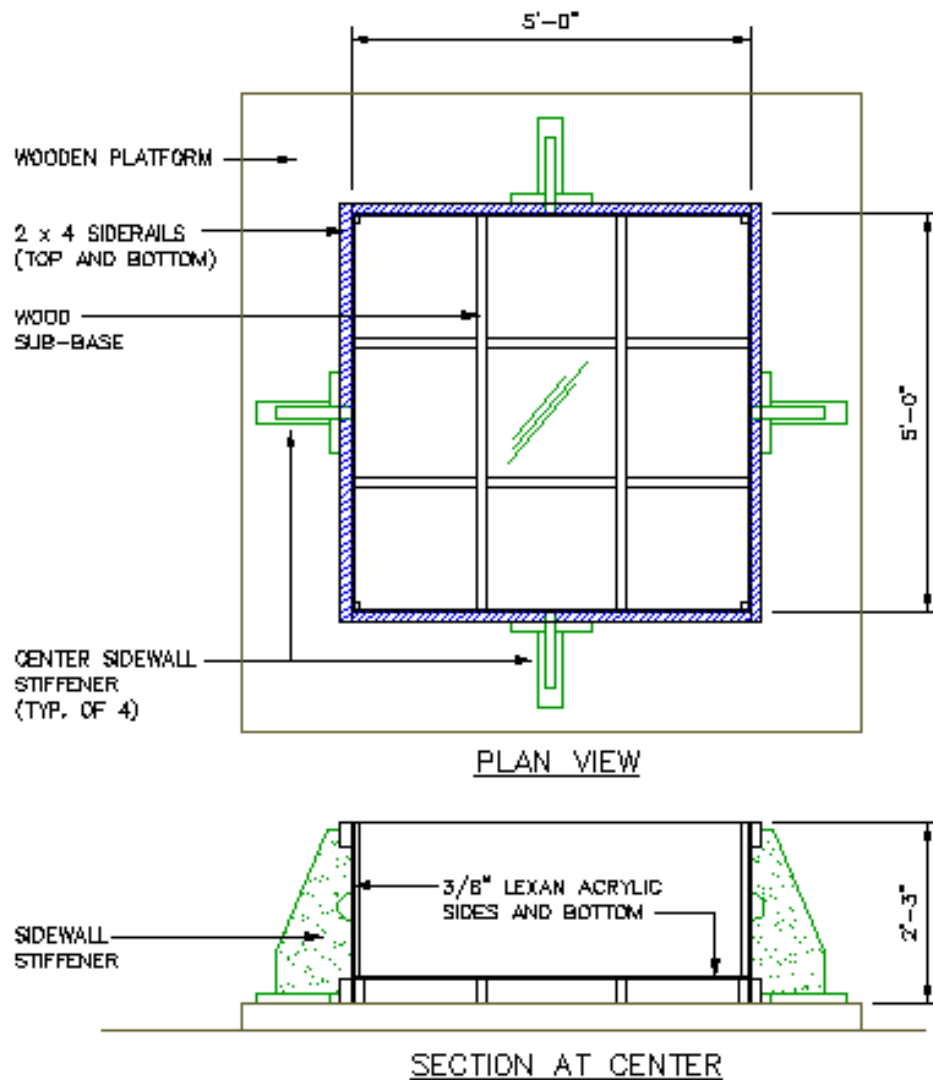


Fig. C2 – Model Tank Schematic with Sidewall Stiffeners

The assembly of the tank was done by, first, gluing all adjoining Lexan parts together and, then, caulking all the wetted perimeter corners. The glue used was *Weld-On #16* Plexiglas Low VOC fabrication adhesive in tube form for acrylics. A 100% pure

silicone adhesive caulk was used at all locations where a watertight seal was required. This included all bolt hole and screw penetrations.

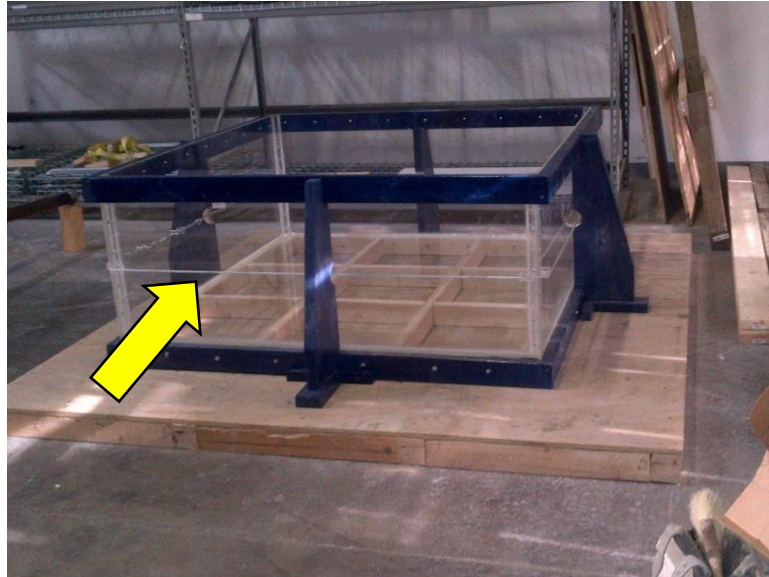


Fig. C3 – Completed Model Tank with Lexan Sides, Stiffeners and Tension Cable

There is a mid-height cable assembly attached around the perimeter of the tank walls. This is to provide an inward hoop confinement force on the tank, since the latter stages of the experiment involve the use of compressed air blasts within the soil mass. This (multi-strand) cable assembly has thimbles at each end with clamps joined by an adjustable tension turnbuckle. The tank has exterior sidewall Lexan block mounts for the cable, designed to place equal distributed inward pressure forces at the corners of the tank, as the turnbuckle is tightened.

Four wooden vertical stiffener units were placed on the outside of the tank walls at the midpoints. These stiffeners transfer internal water and sand induced pressures that are strongest at the middle of the long sides of the tank, back to the lower platform in order to relieve long-axis bending stress. The units account for the anticipated forces during

repeated model trials, and allow the cable assembly to pass through while supporting the sidewalls. Each of these stiffeners is mechanically fastened to the tank and the platform.



Fig. C4 – Ship Models showing Geometry and Embedment Lines

Ship Models: The models were each constructed with an inside wooden frame. This frame was the structural interior portion of the model onto which the outside rigid foam exterior and the various ballast were attached and set on. The size of the wooden frame in each case

was 12”H x 24”L x 12”D. The addition of the 1-1/2” rigid exterior skin (Owens-Corning Foamular rigid board insulation) to these frames made up the final sizes of the models as described earlier in Fig. 19. The frames were assembled from 1 x 2 top and bottom rails connected by 1/2” plywood ends and center panels. These plywood connector panels, glued with construction adhesive (Liquid Nails) and joined with wood screws, made the whole assembly rigid in all directions.



Fig. C5 – Ship Model Wooden Subframe Construction

Attachment of the rigid foam skin to the frame needed to be done without puncturing the surfaces in order to keep the models ultimately as watertight as possible. This was done by attaching the insulation to the wood frame using a glue that would not damage nor react chemically with the insulation. A glue specially made for this purpose was identified and used which was: Loctite PL 300 foam-friendly adhesive. This gluing/attachment process of the foam to the frame had to be done accurately and securely and so nylon strap-chains

were used to pull the foam tightly against the subframe while the glue set up. See Fig. C6 (seen additionally in more detail in Photo Record images P12-22 through P12-39)



Fig. C6 – Model Foam Gluing Procedure with Nylon Strap-Chains

In order to provide long-term lifting capabilities, each model was assembled with four lifting eyebolts at the corners. These eyebolts attach to threaded rods with couplers extending down through the top and bottom rails of the frame. These can be seen in Fig C4 for each of the models as well as in Fig. 33. The bottom connections had to engage not only the frame but also the bottom layer of rigid insulation through more than just glue attachment. This was accomplished by placing flat aluminum straps into the foam which the threaded rods were connected through as seen in the diagram of Fig. C7. These (two) straps distribute the tensile loads transmitted through the eyebolt/threaded rod/coupler assemblies during lifting and pull-testing. The eyebolt/rod assemblies were equidistant from the centers of gravity for achieving equal tension on the lanyard through each lift/pull exercise.

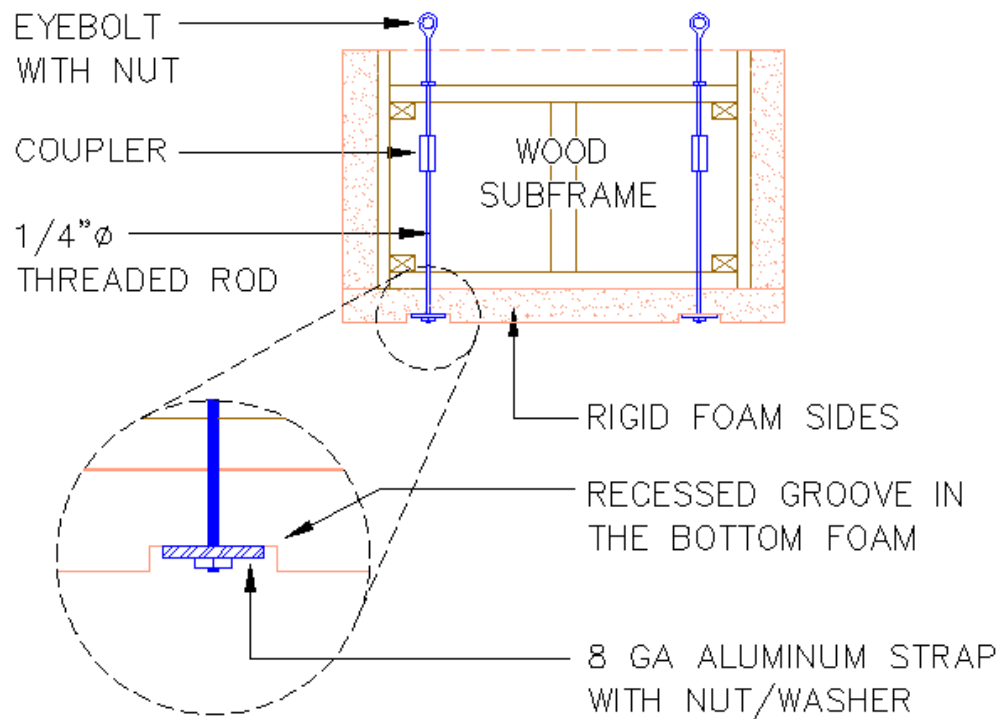


Fig. C7 – Section of Model Subframe with Aluminum Straps and Eyebolt Rod Assembly

The bottom of the models needed to be planar with no irregularities caused by the installation of these pull straps. To account for this, fitted pieces of foam were glued over the sections where the grooves were cut for the aluminum straps. These were sanded and eventually covered over with fiberglassing mesh in the final stages of their construction. The end result was that there was no indication of the recesses for the strap pulls in any of the bottoms.

Cofferdam and Vibrator System: The force required to insert the bottom edges of the cofferdam into the sand during model burial and pull trials was significant and proved to be difficult as well as intrusive to the setup. A vibrator and PVC side-slide mount assembly was added for use in assisting with this effort. Seen below in Fig. C8 is the vibrator and PVC side mounts on either side of the cofferdam as an insertion operation is carried out:



Fig. C8 – Vibrator Used with Sideslide Mounts for Insertion of Cofferdam into Tank Sand

There were many model trials to be done as the main body of work with a multitude of burials in the tank sand. To facilitate these many ongoing operations, a means to quickly and easily excavate the wet and saturated sand from the inside of the cofferdam was needed. A device was built for this purpose that incorporated a 2-1/2" diameter screw that was inserted into a 3" diameter PVC pipe and able to be operated with a drill from the top. The screw base was dropped deep into the cofferdam and the wet sand was drawn up the wide threads spaces to a side exit port. This enabled the sand to be mechanically evacuated during the many model burials that were done in both the Baseline and Blast Test phases of the experiment.



Fig. C9 – Screw Dredge for Sand Removal during Model Trials

The screw was made of several garden variety earth bulb cutter screws that had to be cut and re-welded to accommodate the length and screw line for sand withdrawal needed to fit the cofferdam depth and model(s) draft requirements.

Reaction Frame: The reaction frame was built as a roll-over assembly integral to the size of the tank and the maneuverability of the ship models. It was essential for this to be able to be retracted and re-situated over the tank and base for operational setup as well as access during the procedures.

The design of the frame is such that it accommodates all the vertical space requirements of the deepest-draft ship model while being able to be placed over the tank. The entire reaction frame is constructed of timber members with the exception of some structural steel corner attachment angles. It is designed with locking casters for ease in positioning and to be stationary during operation. This makes the frame somewhat portable for use in rigging the models over the floor area when setting up each trial. The frame has a structural 6" overhead (double 2" x 6" with plywood flitch plate) beam attached to two side (4" x 4") columns. Lumber used was Southern Pine No. 2. A pulley and locking rope

winch assembly were attached to the beam center and onto the left column respectively. The sides of the reaction frame were attached with spanning walk-planks from side to side. These planks bridge the tank when in position, and are designed to support a two-man load at any location. To provide an access over the water areas of the tank, there are two mobile crosswalk planks that are maneuverable between the primary walk-planks. The reaction frame also served as a staging and mount for the compressed air cannon during the model blast testing phase of the experiment.

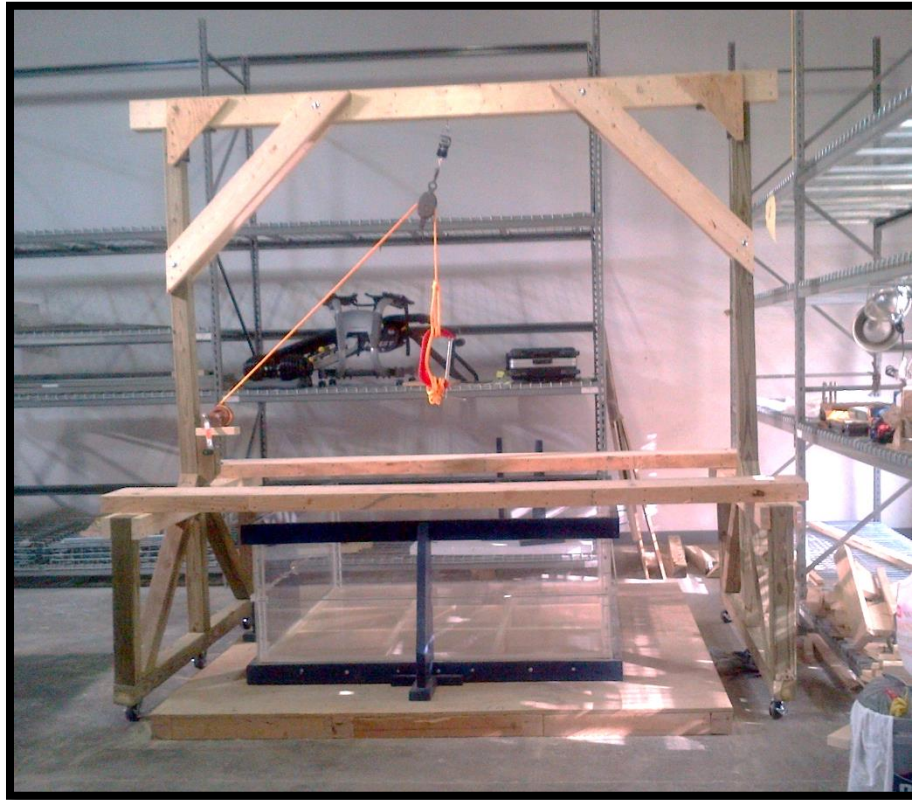


Fig. C10 – Reaction Frame in Mobile Position Over Model Tank

Appendix D: Additional Equipment Listing

All the ancillary equipment listed in the table in this appendix was essential to the work needed to be done and were either built specifically in combination with other standard equipment or directly during the course of the experiment. Many other pieces were built along the way which proved to be less effective for specific needs and were abandoned and replaced by others that better fit the needs at that point. One such item was a sand scoop for use in the cofferdam to evacuate the sand during model embedment operations. It is seen in the photo record images P12-84, 85 and 86. Once this was completed and tested for use, it was found to not work as well as planned and another tool for the purpose of sand evacuation had to be devised. This lead to the design and building of the sand dredge shown in the following table which proved to be quicker and able to be used with greater ease.

In general, pieces of ancillary equipment were added along the course of the experiment out of necessity in order to carry out successive steps. Certain things like the rope winch and pulley were anticipated but the specific way they needed to be attached and placed for repeated operations was not known until the reaction frame was fully built and able to integrate with the model tank setup. Several versions of the compressor / tank were tried before the moveable station (gray painted) cart was built as seen in the table. In fact, this is actually the second compressor we used since the first one (shown in P12-94 image) was not powerful enough to supply the air pressure needed once the blast tests were underway.

Another example was the way of inserting the cofferdam into the sand of the tank which proved to be more difficult than expected. Even when standing on the top of the







edges with full body weight while the cofferdam was to be inserted, it was not able to be sunk into the wet sand to the required depth for use with the ship models. Additional striking with a sledge hammer on a wooden block was also not enough to get it into position. It was then researched and found out that a vibratory means of sinking it into position could work. A handheld flexible shaft mechanical concrete vibrator was acquired that fit the constraints of the tank and frame. We then added side PVC mounts to the cofferdam for use with the vibrator (see P13-10,11). This proved to work well once it was tested and was then used throughout.

A lanyard was made using $\frac{1}{4}$ " nylon rope for use in hoisting all the models from the tank. It has woven rope ends that have a swivel eye and snap spring with cinch knots (www.fishinglakes.com/knots.htm) at each end. This was used on all the models (seen, for example, in P13-33) and had sufficient tensile strength to be used repeatedly over the duration of all testing.

In the 2012 timeframe, a series of trials were done using low capacity explosives in saturated sand. This involved waterproofing the charges and the fuses and a way to ignite them remotely. After several weeks of variations on this, the concept of using compressed air and the air cannon in-lieu of explosive charges (like the method employed in the papers by *Fragaszy* et al in the ref. section) was arrived at and ultimately used in this study.

In the setup of the model tests in the tank for both the baseline and the blast testing, the consistency of the sand/water mix had to be maintained. Several types of paddles were used in conjunction with an electric drill to facilitate this. The mixing process was necessary since the tank sand tended to dry out during the times between testing (normally a week) and water was added at the outset of each reset on the weekends during which

operations commenced. This was modulated by measuring and adjusting the tank water level with the hose and spigot in the corner viewport area (seen in P12-91, P13-08 and in Fig.32).

Item	Description	Photo
Compressor/Tank	For pressurizing the Air Cannon during the blast phase of the experiment.	
Tensiometer	Placed at the base of the rope pull assembly for reading of weighs and tension on the models in the tank.	
Rope Winch/Crank	Attached to the left side off the reaction frame for lifting and pulling.	
Pulley	Placed at top of reaction frame for rope tension transfer from winch.	
Vibrator	Used in embedding the cofferdam into the sand to place all models in tank.	
Sand Screw Dredge	Used to excavate sand during model burial operations.	

TASCAM

TEAC Professional Division

DA-88

Digital Multitrack Recorder



OWNER'S MANUAL

5700141001

Specifications

Transport

Recording Format : 4-rotary head digital recording
Tape : Hi8 video tape
Number of Channels : Eight plus subcode area
Recording Time : 108 minutes using P6/E6-120 tape/113 minutes using P5/E5-90 tape
Tape Speed : 15.9 mm per second
Fast Forward/Rewind Time : Approximately 80 seconds using P6/E6-120 tape/85 seconds using P5/E5-90 tape (100 times play speed)
Shuttle Speed : 1/4 to 8 times play speed

Inputs and Outputs

Digital I/O : TDIF (TEAC Digital Interface Format), 25 pin D-sub x1
Analog Input : 25 pin D-sub connector x1, +4 dBm, 10k ohms (balanced)
 RCA jack x8, -10 dBV, 50k ohms (unbalanced)
Output : 25 pin D-sub connector x1, +4 dBm, 75 ohms (balanced)
 RCA jack x8, -10 dBV, 250 ohms (unbalanced)
Sync Input : 15 pin D-sub connector x1
Output : 15 pin D-sub connector x1
Word Sync Input : BNC connector x1
Output : BNC connector x1
Remote Input : 8 pin DIN connector x1
Remote Punch In/Out : 1/4" phone jack x1

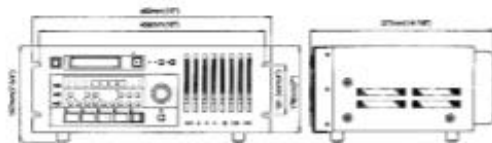
Typical Performance

Sampling Rate : 44.1/48 kHz
Quantization : 16 bit linear
Pitch Control : +/-6% in 0.1% increments
Frequency Response (Record and Play) : 20 Hz to 20 kHz, +/-0.5 dB
Dynamic Range : Better than 92 dB
Wow and Flutter : Less than measurable limits
Total Harmonic Distortion : 0.007%

General

Power Requirements :
 USA/Canada : 120 V AC, 60 Hz
 Europe : 230 V AC, 50 Hz
 U.K./Australia : 240 V AC, 50 Hz
Consumption : 74 Watts
Dimensions (WxHxD) : 482 mm x 176 mm x 377 mm
Weight : 14 kg

Changes in specifications and features may be made without notice or obligation.



Optional Accessories

RC-848 Full-function Remote Control Unit

- 99-point autolocator functions
- ACCESSORY 1 and 2 connectors for controlling TASCAM (or other) audio machines
- RS-422 connector for controlling VT machines
- Jog/shuttle wheel for locating a specific point at variable speeds
- Keypad-entered time locations
- Menu-selectable controls of the optional SY-88 synchronizer

RC-808 Basic Transport Remote Control Unit

Has duplicates of REC FUNCTION, ALL INPUT, AUTO INPUT, REHEARSAL, AUTO IN/OUT, CLEAR, REPEAT, MEMO and LOC in addition to the transport controls.

SY-88 Sync Board

- All SMPTE/EBU time codes supported : Drop 29.97 fps, Non Drop 29.97 fps, 30 fps, 25 fps (EBU), and 24 fps (Film).
- Offset sync with sub-frame accuracy
- Automatic offset entry

PW-88S Sync Cable

For connecting multiple DA-88s in series when one serves as the master and others as slaves. One cable establishes connection between two DA-88s.

PW-88D (1 m)/PW-88DL (5 m) Dubbing Cable

For connecting two DA-88s through their digital I/O port when one serves as the source machine and the other as the target.

MU-8824 24-channel Meter Unit

Allows metering three DA-88s.

PW-88M Meter Cable

For connecting the MU-8824 meter unit to the DA-88.

IF-88AE Interface Unit

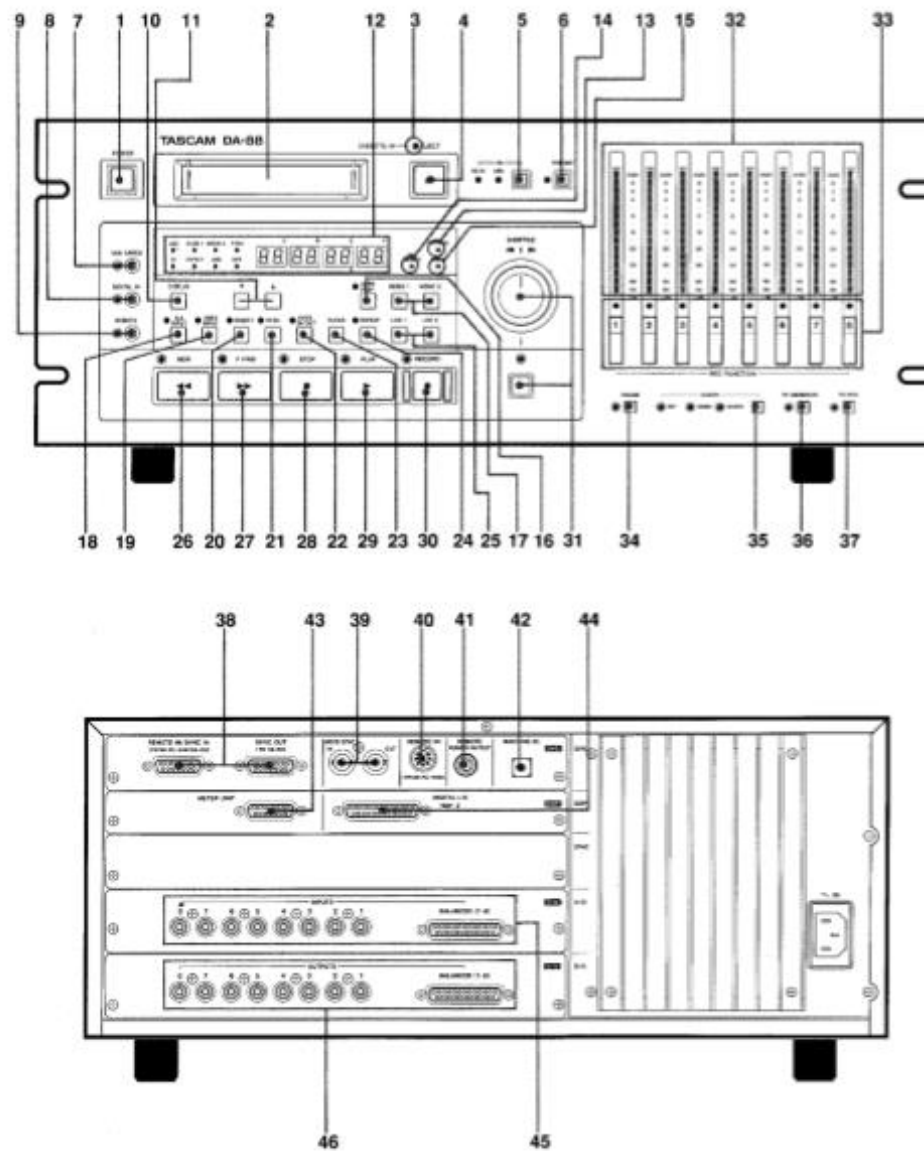
For data communication between the DA-88 and other digital machines with AES/EBU digital I/O or SPDIF.

IF-88SD Interface Unit

For data communication between the DA-88 and other digital machines with SDIF-2.

RC-30P Punch-In Footswitch

Features and Controls



DA – 88 Front and Rear Panels

Skim through this section of the manual to get a bird's-eye-view of the DA-88, that way you will be able to locate information whenever you need. It is not necessary to memorize all what is here nor to try to build up details into a systematic whole to get started.

Functions available only when the optional SY-88 Sync Board is installed are not explained here. Information on them is provided in the SY-88's manual.

FRONT PANEL

1. POWER switch

Controls the power to the DA-88. See also page 4, "Backup Feature."

2. Tape loading window

NOTE

Don't use any Hi8 tape which was once used for video recording. No audio recording can correctly be made on such tapes.

3. CASSETTE IN LED

Lights when a cassette is inside the deck.

4. EJECT key

When pressed, the cassette is ejected.

EJECT can operate during stop only.

5. Fs (sampling frequency) switch

Toggles two sampling frequencies (or rates) for your choice. When formatting a tape you have to select 48 kHz or 44.1 kHz depending on the applications. During play the deck will automatically switch to the rate at which the recording was made, and either of the two LEDs will light accordingly.

NOTE

If you attempt to record additional material to augment the original one, and the incoming sampling rate is not the same as that is previously recorded on the tape, one of the Fs indicators will flash, warning you that recording cannot correctly be done.

6. FORMAT key

To format a tape is to record it with subcode data, of which ABS (absolute) time is one. This ABS data express the elapsed time from the beginning of the tape, not from any optionally selectable intermediate point : hence the name "absolute."

Formatting a tape erases whatever is previously recorded on it. To prevent formatting from starting accidentally, the FORMAT key is not actually activated unless you press it twice.

IMPORTANT

Audio can be recorded while formatting. But it's wise of you to format the tape from the beginning all the way to the end before recording audio. This insures against noise and discontinuity of absolute time data. If you want to record audio and format a tape at one time, don't stop recording by stopping the tape with STOP or PLAY. Press REC FUNCTION instead, which allows the tape to be continuously formatted up to the end.

7. VARI SPEED switch

When pressed, "PITCH" will show in the display and you can use the ▼ and ▲ keys to change the play (or the record) speed up to +/-6.0 % in 0.1 % steps.

CAUTION

The pitch change affects the record speed also. Check to see that the VARI SPEED LED is turned off unless you are using the function intentionally.

8. DIGITAL IN switch

Selects either the analog or the digital input. Pressing this switch to turn on its LED activates the DIGITAL I/O port. Turning off the LED selects the analog inputs (RCA jacks or multipin connector) as the source of the deck.

9. REMOTE switch

When this switch is pressed, and the associated LED lights, the DA-88 is submitted to the optional RC-848 remote control unit, and all controls are locked out except DISPLAY (item 10), ▼ and ▲ (item 11), and STOP.

10. DISPLAY switch

Each time you press this switch, the following will show in the digital display window in sequence, as confirmed by the corresponding LEDs being lit next to the display :

- (1) ABS (absolute) time (elapsed time from the beginning of the tape up to the current position)

(2) MEMO 1 point

(3) MEMO 2 point

(4) % of pitch change

- To go back to ABS time display mode quickly, you can hold DISPLAY and press ▲.

11. ▼ and ▲ keys

Used to enter the following :

- Crossfade time (p. 17);
- Offset time (p. 24);
- Track delay time (p. 21);
- Pitch change (p. 21);
- Preroll time (p.17).

The following can be trimmed or fine tuned with the ▼ and ▲ keys :

- MEMO points (p.22) ;
- Punch-in and out points (p.17).

The keys are also used together with DISPLAY to get access to :

- ABS time indication — if you hold DISPLAY and press ▲.
- Track delay time setting mode — if you hold ▲ and press DISPLAY.
- Crossfade time setting mode — if you hold ▼ and press DISPLAY.

12. Digital display window

Shows the ABS time, MEMO 1 point, MEMO 2 point, or amount of pitch change (or SMPTE time code numbers when the optional sync board is installed), as selected by the DISPLAY switch.

The display will also show error messages. For details on them, see page 26.

- The display can quickly be switched back to show ABS time when you hold DISPLAY and press ▲ at any time (except when error messages show).
- The ABS time display can flicker when the tape is fast winding (while in F.FWD, REW or LOC).

13. WARNING LED

Flashes to warn you that trouble occurred. Error messages will also then show in the display, specifying what is wrong. See also page 26.

14. REC INHIBIT LED

Lights when the tape in use is write-protected. Check the write protect tab on the cassette.

15. ERROR LED

Lights when errors occurred at so constraint a rate in digital data, that they cannot be corrected, and are submitted to interpolation to arrive at an approximation to the correct data.

This indicator also lights to indicate that dirt accumulates on the heads or tape paths, or that the tape is damaged. If another tape is loaded and the indicator does not turn off, consult TASCAM or your nearest TASCAM dealer.

See also the 3rd paragraph under the heading, Recommended tapes, on page 5.

16. AUTO PLAY key

Automates play start at the end of each autolocation function.

17. MEMO 1 and MEMO 2 keys

Pressing MEMO 1 stores the current tape location into that register, to which the tape will be autolocated when pressing LOC 1. MEMO 2 is similar to MEMO 1, and is used to capture any point to which you can return by pressing LOC 2.

NOTE

"MEMO" points you recall into the display by pressing DISPLAY are the points to which the tape will be autolocated when pressing LOC, except when RHSL lights solid. When RHSL lights solid, "MEMO 1" shows the punch-in point, and "MEMO 2" the punch-out point, as established during Rehearsal Setting mode (during which RHSL should blink). This does not mean that punch-in and out points are stored into the MEMO registers. When they are recalled into the display, the "MEMO 1" LED only indicates the punch-in point, and the "MEMO 2" LED the punch-out point.

18. ALL INPUT switch

When pressed to turn on its LED, all the channels' outputs are switched to carry signals derived from the inputs, whatever the transport mode (primarily for alignment).

19. AUTO INPUT switch

When this switch and INSERT are both previously activated, the channel inputs selected by REC FUNCTION are automatically switched to directly feed the outputs whenever the transport goes into rewind, fast-forward, shuttle, or stop mode. This allows the talent in studio to talk to the engineer in control room without having to change any settings on the mixer.

20. INSERT switch

Lets you monitor tape during preroll and postroll for punch-in recording. See table below.

Relationships between the output signals, transport modes and switch settings

ALL INPUT	REC FUNCTION	INSERT	AUTO INPUT	PLAY	RECORD	SHUTTLE	STOP
ON				INPUT			
OFF	ON	ON	ON	TAPE	INPUT		
		OFF	OFF	TAPE	INPUT	TAPE	—
	OFF			INPUT			
				TAPE			

21. RHSL switch

Puts the deck into rehearsal mode which allows you to check the auto punch in and out points for accuracy.

22. AUTO IN/OUT switch

Automates the punch-in sequence (preroll, punch in, punch out, and postroll) as you have set during rehearsal.

23. CLEAR key

Defeats the RHSL and AUTO IN/OUT functions.

24. REPEAT 1-2 switch

Lets the tape play between two MEMO points.

25. LOC 1 and LOC 2 keys

LOC 1 locates the tape to the MEMO 1 point, and LOC 2 to the MEMO 2 point.

26. REW key

Winds the tape at high speed in reverse.

Pressing REW during recording punches out and the tape rewinds.

27. F.FWD key

Winds the tape at high speed in the forward direction.

Pressing F.FWD during recording punches out and the tape fast forwards.

- When you press F.FWD or REW for the first time after powering up or replacing the tape, this will run at an intermediate speed for a few seconds before starting running at the expected high speed. During this interval the transport is detecting the tape characteristics.

28. STOP key

Disables the current transport mode and stops any tape motion.

29. PLAY key

Enables play mode ; or, punches out of record if pressed during record.

30. RECORD key

Pressing PLAY while holding RECORD initiates record on any track whose REC FUNCTION indicator was blinking to show Record Ready mode.

Hitting RECORD during play lets any "Ready" track punch into record.

31. SHUTTLE switch and the knob

Pressing the switch to let its LED turn on allows you to use the knob to monitor the tape at variable speeds in search of a specific point. Turning the knob to the right of center rolls the tape in the forward direction, and turning it to the left of center provides reverse cueing. The further you turn it in either way, the higher the tape speed will be. The initial speed is 1/4 times normal play speed, and if you turn the knob all the way to the left or right, the tape will play at 8 times normal play speed.

Pressing the SHUTTLE switch during recording gets you out of record, allowing you to begin to "shuttle" the tape immediately.

SHUTTLE will automatically be disabled if you leave the knob at its center position for 10 seconds.

32. Peak level meters

Register the signal levels being fed to the outputs, the levels coming either from the inputs or the tape, as shown in the left column of this page.

33. REC FUNCTION switches

Put the corresponding tracks into Record Ready mode, or directly into Record if RECORD and PLAY are previously pressed.

The associated LEDs flash to indicate Record Ready, and turn on solid during Record.

34. CHASE key

Lets the slave DA-88(s) chase and lock to the same ABS time point as the master. Once locked up, they will play, record, or fast-wind in sync in response to the commands from the master.

The installation of the optional SY-88 sync board allows the DA-88 to run in sync with VTRs or other ATRs (digital or analog). For more details, refer to the SY-88 manual.

35. CLOCK switch

Selects the clock to which the deck will be referenced. If the DA-88 is used as a stand-alone deck, it has to be referenced to the **INT**(ernal) clock.

The **WORD** clock is used when making a digital copy between the DA-88 and other digital tape machines, or when letting them run in sync (the optional SY-88 Sync Board is required).

For the DA-88 to be slaved to VTRs, select **VIDEO** (the optional SY-88 sync board is required).

When one or more DA-88s are hooked up as the slaves, the **CLOCK** switch on them are locked out (all the associated LEDs turned off), and they are automatically referenced to the clock to which the master DA-88 is referenced.

The next two items can operate only when the optional SY-88 sync board is installed. For their functions, refer to the SY-88 manual.

36. TC GENERATE switch

37. TC REC key

REAR PANEL

38. REMOTE IN/SYNC IN and SYNC OUT jacks

When two or more DA-88s are hooked up, a sync signal and commands from the master's SYNC OUT jack are fed into the first slave's SYNC IN jack; and its SYNC OUT jack feeds the second slave's SYNC IN jack, and so on.

The optional RC-848 remote control unit may alternatively be connected to the SYNC IN jack. The remote can control a maximum of 6 DA-88s, separately.

Use only the optional PW-88S sync cable for establishing the sync in and out connection.

WARNING

Please use only TASCAM cables, as there are very specific cable requirements, these cables are specially configured for connection to REMOTE IN/SYNC IN, SYNC OUT, METER UNIT, TDIF-1 (DIGITAL I/O).
(Do Not use standard computer cables.)

It is possible to damage certain internal components by the use of non TASCAM cables. If the use of non TASCAM cables causes or results in damaged this will void the Warranty.

39. WORD SYNC IN and OUT jacks

The DA-88 can be referenced to the clock derived from the WORD SYNC IN for it to be slaved to other digital tape machines. Inversely, they can be slaved to the DA-88 by letting them be referenced to the clock the DA-88 transmits from its WORD SYNC OUT. (For the DA-88 and other digital machines to be synchronized, the optional SY-88 Sync Board is required.)

The clock the WORD SYNC jacks carries may also be used when making a digital copy between the DA-88 and other digital machines.

40. REMOTE IN jack

For connection to the optional RC-808 basic remote transport control unit.

41. REMOTE PUNCH IN/OUT jack

For connection to the optional RC-30P footswitch.

42. MACHINE ID rotary switch

For two or more DA-88s to be synchronized, they have to be given their own ID (identification) numbers. Allot "0" to the master, "1" to the first slave whose SYNC IN is directly fed with the master's SYNC OUT; and, in a similar

Bescheinigung des Herstellers/Importeurs
Hiermit wird bescheinigt, daß der/die/das
TASCAM DA-88 DAT-Recorder
(Gerät, Typ, Bezeichnung)
in Übereinstimmung mit den Bestimmungen der
AMTSBLATT 163/1984, VFG 1045/1984, VFG 1046/1984
(Anzeigegerätverfügung)
funk-entstört ist.
Der Deutschen Bundespost wurde das Inverkehrbringen dieses Gerätes angezeigt und die Berechtigung zur Überprüfung der Serie auf Einhaltung der Bestimmungen eingeräumt.
TEAC CORPORATION
Name des Herstellers/Importeurs

way, allot "2" and upper numbers to the remaining slaves in sequence, in their order of SYNC IN/OUT connections. "11" and upper numbers are represented by alphabets ; "11" by "A," "12" by "B," and so on.

⚠ *Don't assign the same ID number to two or more machines. This may cause incorrect functions to them.*

NOTE

When operating the MACHINE ID switch, make sure that the deck is turned off or it has no effect.

43. METER UNIT connector

Carries the output of eight channels and the power for driving eight of the twenty-four meters on the optional MU-8824 meter unit.

44. DIGITAL I/O TDIF-1 port

This serial interface carries all eight channel signals at one time, and allows digital dubbing between two DA-88s using the optional PW-88D dubbing cable.

For the DA-88 to be connected to other digital machines, the following optional accessories are available from TASCAM :

- IF-88AE : for connection to machines with AES/EBU digital I/O or SPDIF port.
- IF-88SD : for connection to machines with SDIF-2 port.

45. INPUTS

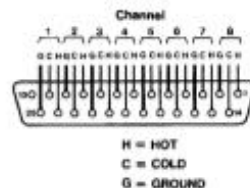
Jacks 1 to 8 : receive unbalanced -10 dBV analog sources.

Multipin connector : receives balanced +4 dBm analog sources.

46. OUTPUTS

Jacks 1 to 8 : for connection to the unbalanced analog inputs of external equipment.

Multipin connector : for connection to the balanced analog inputs of external equipment.



Note for U.K. Customers

DO NOT cut off the mains plug from this equipment. If the plug fitted is not suitable for the power points in your home or the cable is too short to reach a power point, then obtain an appropriate safety approved extension lead or consult your dealer.

If nonetheless the mains plug is cut off, remove the fuse and dispose of the plug immediately, to avoid a possible shock hazard by inadvertent connection to the mains supply.

If this product is not provided with a mains plug, or one has to be fitted, then follow the instructions given below:

IMPORTANT. The wires in this mains lead are coloured in accordance with the following code:

GREEN-AND-YELLOW:	EARTH
BLUE:	NEUTRAL
BROWN:	LIVE

WARNING: This apparatus must be earthed.

As the colours of the wires in the mains lead of this apparatus may not correspond with the coloured markings identifying the terminals in your plug proceed as follows.

The wire which is coloured GREEN-and-YELLOW must be connected to the terminal in the plug which is marked by the letter E or by the safety earth symbol \perp or coloured GREEN or GREEN-and-YELLOW.

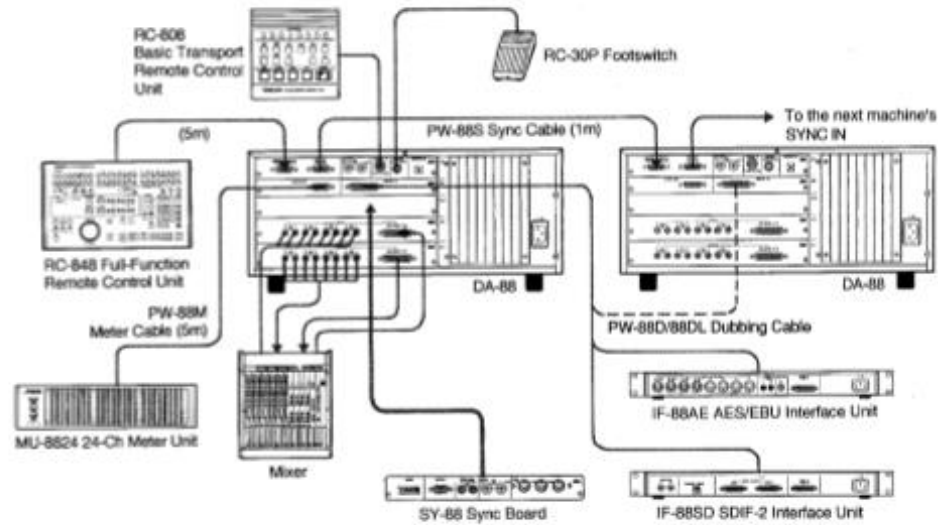
The wire which is coloured BLUE must be connected to the terminal which is marked with the letter N or coloured BLACK.

The wire which is coloured BROWN must be connected to the terminal which is marked with the letter L or coloured RED.

When replacing the fuse only a correctly rated approved type should be used and be sure to re-fit the fuse cover.

IF IN DOUBT — CONSULT A COMPETENT ELECTRICIAN.

Hookup



Formatting a Tape

Before starting to record any audio program on a new tape, it should be formatted, i.e. it should be time-indexed and given tracking and other subcode data.

NOTES

- Be sure to let formatting start from the very beginning of the tape.
- Once formatting starts, all transport control buttons except STOP are locked out. If you stop the tape before formatting is complete, reformat it from the beginning.
- Tapes once used for recording video cannot correctly be formatted. Don't try to format such tapes.

To format a new tape :

- Switch on power to the DA-88.
- Load a Hi8 tape into the DA-88.
- Press **FORMAT**. Its LED will start blinking.
- Press **FORMAT** again. Its LED will turn on solid showing that the deck is ready for formatting.
- Press the **Fs** switch to select either of the two sampling rates available. Select 44.1 kHz if the recording will be used as a digital master for CD production. Or, select the professional standard 48 kHz rate for other applications.




Appendix F: Hydrophone Construction Design

The hydrophones for this study were assembled and built from the parts of the guidelines and instructions referenced in this appendix. They were built over several weeks' time and as also seen in Fig. 30.

COSEE TEK ~ University of Connecticut
Simple Hydrophone Design

Mechanical Preparations of the Hydrophone Container:


Completed Hydrophone Container



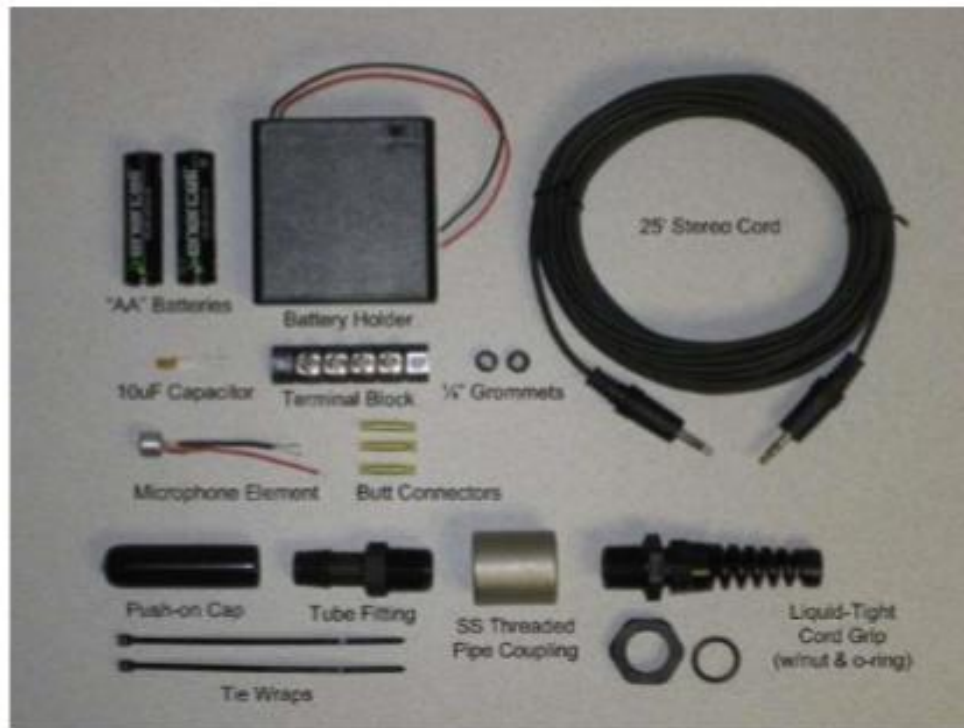
The hydrophone container is the underwater component of the system designed to provide a watertight enclosure in which to house the microphone element. In this design, the hydrophone container utilizes simple nylon and stainless steel parts that seal to one another by means of compression.

All threaded components utilize National Pipe Thread (NPT) tapered threads to form a compression seal between interlocking threads. When installing an NPT fitting, thread the two components together by hand until they are "hand tight". Next, using a suitable wrench, tighten the fittings another 1-1/2 to 3 turns past finger tight to complete the installation. Caution: never loosen an installed NPT fitting. Loosening installed NPT fittings may compromise the seal and contribute to leakage and/or failure.

1) Following the description above for installing NPT fittings, thread the tube fitting into the stainless steel (SS) threaded pipe coupling until the two units are properly secured. If available, vise-grip pliers are a useful tool for holding cylindrical objects like the SS pipe coupling.



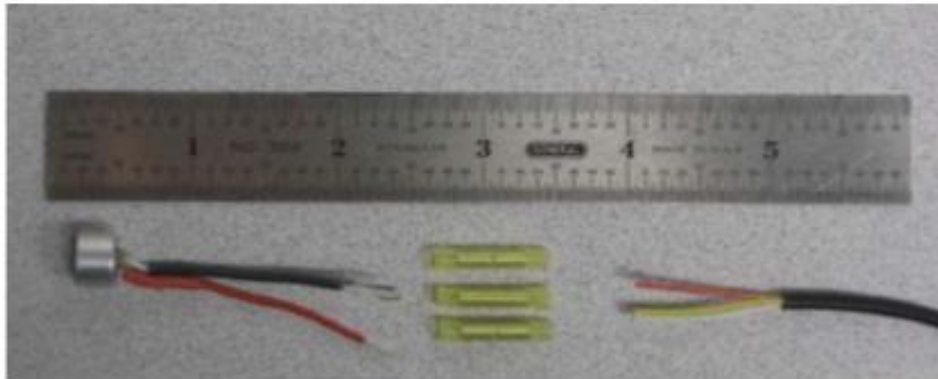
Hydrophone Build Instructions



Description	Vendor	Part Number
Condenser Microphone Element	Radio Shack	270-092
4 "AA" On/Off Battery Holder	Radio Shack	2700409
Vinyl Grommets	Radio Shack	6403025
Tantalum 10uF Capacitor	Radio Shack	272-1436
Telephone Butt Connectors (24pk)	Radio Shack	6403073
"AA" 4-Pack Alkaline Batteries	Radio Shack	2300849
Stereo Cord with 3.5mm Connectors (25')	McMaster-Carr	8317T15
Push-on Round Cap, 1/2" OD, 2" Height (25pk)	McMaster-Carr	40005K22
Nylon Single-Barbed Tube Fitting (10pk)	McMaster-Carr	5463K253
Stainless Steel Threaded Pipe Fitting, Coupling	McMaster-Carr	4464K353
Nylon Liquid-Tight Cord Grip (.08" - .24")	McMaster-Carr	69915K62
Space Saver Terminal Block, 4 Circuits	McMaster-Carr	8173T12
Standard Nylon Cable Tie 4" L, Black (100pk)	McMaster-Carr	7130K52

Note: McMaster-Carr is an online reseller of industrial supplies (see www.mcmaster.com). See Appendix 1 for the complete material list and alternative sources.

Parts List



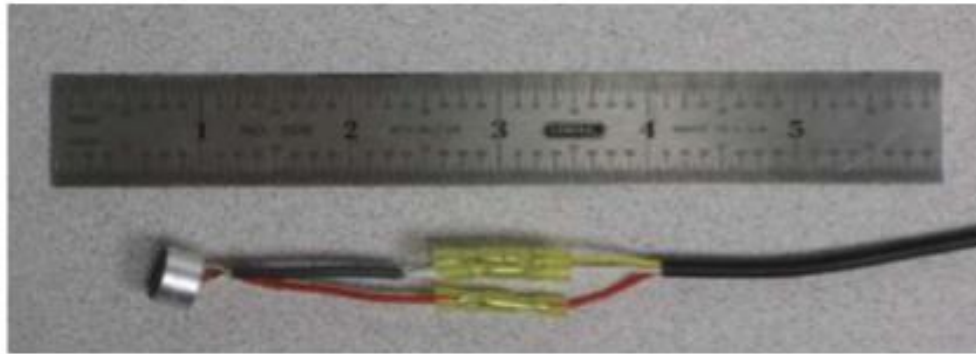
Hydrophone Cable Preparation: Complete steps 1 through 3 below for initial hydrophone cable preparations...

- 1) Measure the required distance from the male-plug end of the audio cable and cut the cable through. This will form the "output cable", connecting the hydrophone battery/terminal enclosure to the topside computer or audio device. The remaining length of cable will form the "hydrophone cable", connecting the hydrophone container to the battery/terminal enclosure. If the original cable assembly had two connectors, cut off the second connector from the hydrophone cable.
- 2) Working from one end of the hydrophone cable, strip back and remove approximately 1" of the outer cable jacket, exposing the individual wire leads within. Note, the #14 AWG wire stripper works well for this task. Be careful not to penetrate the insulation of the wires inside.
- 3) Using the #26 AWG wire stripper, strip approximately ¼" of insulation from the end of each wire. Set the hydrophone cable aside until step 8.

Microphone Preparation: Working with the microphone element, complete steps 4 through 6 below...

- 4) Cut the red wire so that all three wires are of equal length.
- 5) Strip and remove the gray insulation surrounding the white wire and un-insulated shield wire to expose approximately ¾" of each.
- 6) Using the #24 AWG wire stripper, strip approximately ¼" of insulation from the end of the white and red wires.

Wiring Preparations



- 7) Working with the microphone, slide one butt connector onto each of the individual wires until the exposed wire strands are completely contained within the centermost metal section of the connector. Use the crimp tool to crimp the metal section of the connector to the wire leads.
- 8) Matching wires from the hydrophone cable to those from the microphone (white to white, red to red, and yellow (or shield) to shield), slide each wire into the open ends of the three butt connectors. Use the crimp tool to crimp the connector to the wire leads.

Wiring Preparations

Mechanical Preparations of the Hydrophone Container:

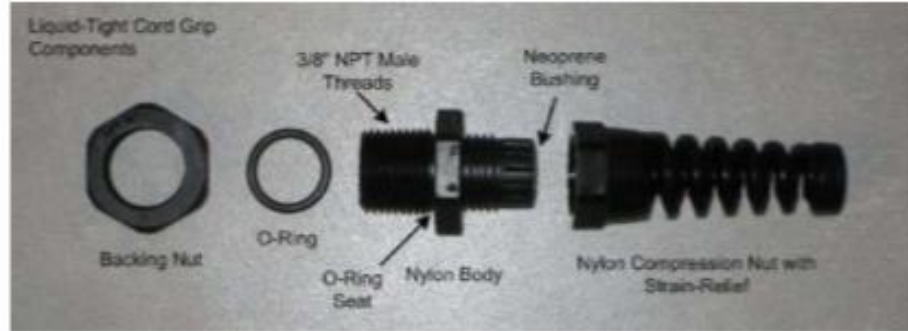


The hydrophone container is the underwater component of the system designed to provide a watertight enclosure in which to house the microphone element. In this design, the hydrophone container utilizes simple nylon and stainless steel parts that seal to one another by means of compression.

All threaded components utilize National Pipe Thread (NPT) tapered threads to form a compression seal between interlocking threads. When installing an NPT fitting, thread the two components together by hand until they are "hand tight". Next, using a suitable wrench, tighten the fittings another 1-1/2 to 3 turns past finger tight to complete the installation. Caution: never loosen an installed NPT fitting. Loosening installed NPT fittings may compromise the seal and contribute to leakage and/or failure.

- 1) Following the description above for installing NPT fittings, thread the tube fitting into the stainless steel (SS) threaded pipe coupling until the two units are properly secured. If available, vise-grip pliers are a useful tool for holding cylindrical objects like the SS pipe coupling.

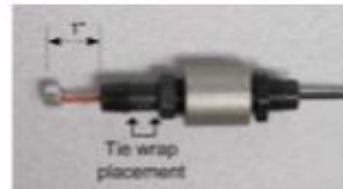




- 2) Working with the liquid-tight cord grip, remove the compression nut with strain-relief from the nylon body and set the compression nut aside for later use.
- 3) If the liquid-tight cord grip came assembled with the backing nut threaded to the nylon body, remove the backing nut and set aside. This nut will not be required for the hydrophone assembly.
- 4) Take the O-ring supplied with the cord grip assembly and feed it over the NPT male threaded end of the nylon body until it fits within the O-ring seat on the underside of the built-in nut (see diagram above)
- 5) Thread the nylon body of the cord grip into the open end of the stainless steel (SS) threaded pipe coupling until the two units are properly secured.



- 6) Working from the tube fitting end of the hydrophone container, feed the hydrophone cable through the container and out the end of the cord grip body. Continue feeding the remaining length of cable through the hydrophone container, until the cloth head of the microphone is approximately 1" from the end of the tube fitting.



- 7) Slide the push-on nylon cap over the microphone element and tube fitting end of the hydrophone container until it bottoms out against the built-in nut.



Hydrophone Assembly

- 8) Install each of the tie wraps over the push-on nylon cap and cinch down securely, compressing the cap against the outside of the tube fitting. These tie wraps should be positioned over the cap and within the tie-wrap channel of the tube fitting (see step 6 diagram above).



- 9) Holding the assembly in one hand, gently push the hydrophone cable into the hydrophone container until you feel a slight resistance. This should be the point at which the microphone element is touching the interior end of the nylon cap.



With the cable in place, view the point at which the hydrophone cable penetrates the nylon body of the cord grip. You will see a gray neoprene bushing around the hydrophone cable and within the cord grip body. When compressed, this bushing will form a watertight seal around the outer jacket of the hydrophone cable. This seal will be ineffective if the neoprene bushing is compressed against the individual conductors of the hydrophone cable rather than the outer jacket of this cable. You must therefore ensure that the outer jacket of the hydrophone cable is completely within the neoprene bushing before proceeding on to the next step.

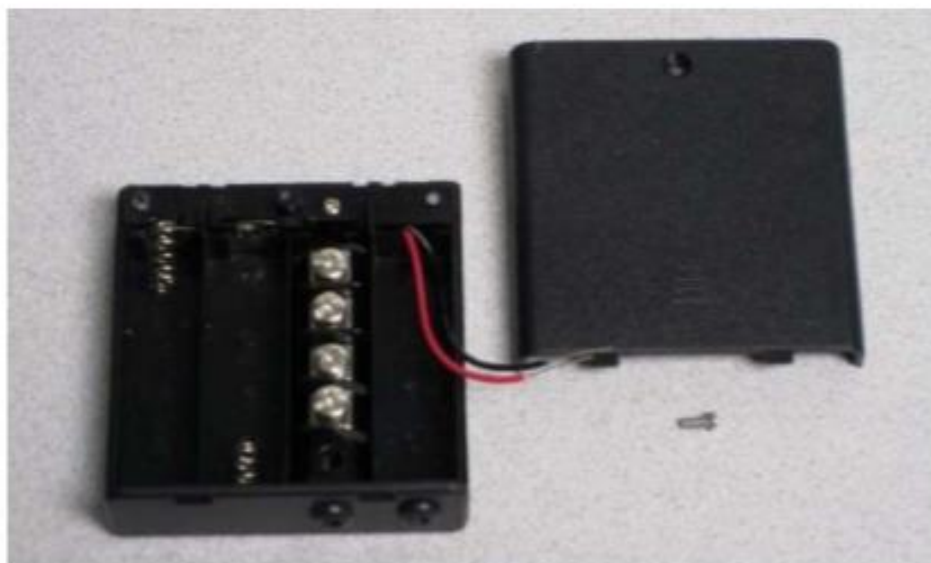
- 10) Slide the nylon compression nut with strain-relief over the length of hydrophone cable until you reach the hydrophone container assembly. With the outer jacket of the hydrophone cable positioned appropriately within the neoprene bushing, thread the compression nut onto the body of the cord grip, tightening it fully.



- 11) Ensure that an appropriate seal is made between the cord grip and the hydrophone cable by pulling on the cable with slight to moderate force as it exits the hydrophone container assembly. You should not feel any movement between the cable and the container if the seal is in place.

Hydrophone Assembly

Mechanical Preparations of the Battery/Terminal Enclosure:

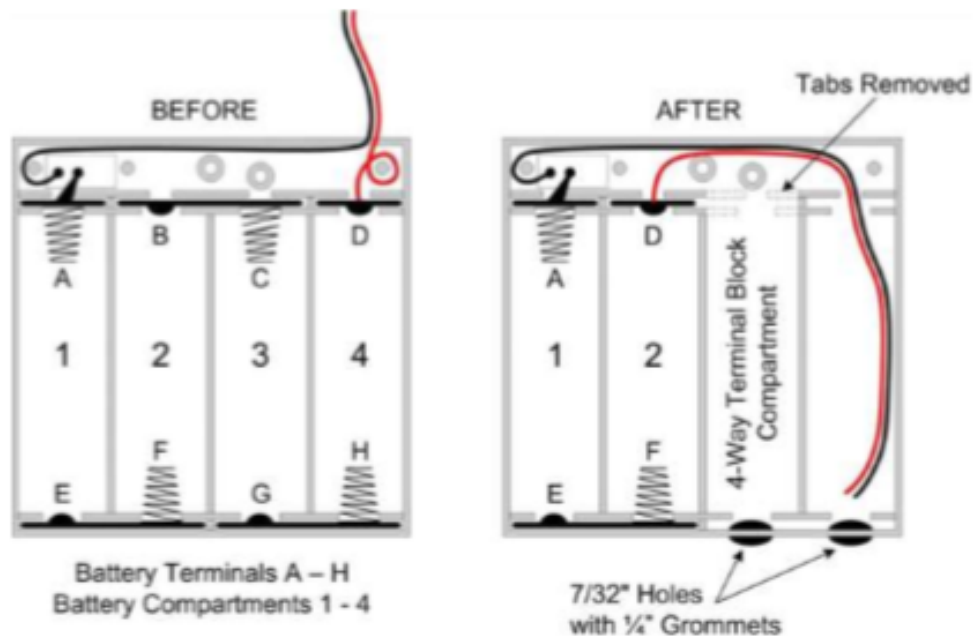


The battery/terminal enclosure provides a single, splash-proof environment for the provision of power to the hydrophone as well as for connections between the hydrophone cable and the output cable. The basis for this enclosure is a simple 4 "AA" on/off battery holder that you will modify to accommodate the required 2 "AA" batteries and terminal block, necessary to make the final connections.

- 1) Remove the Phillips head screw securing the outside cover of the "AA" battery holder and remove the cover. Set the cover and screw aside for later use.
- 2) Remove the Phillips head screw securing the plastic wire cover within the battery holder and pry off the cover with a small flathead screwdriver. Note: in addition to the Phillips head screw, there are three plastic melted grommets securing the wire cover to the battery holder base. In prying off the cover, the heads of these grommets will snap off releasing the cover for removal. Set the wire cover and screw aside for later use.



Battery Assembly



- 3) Using a small flathead screwdriver, pry out and remove battery terminals B-C, D, & G-H. Note the orientation of terminal D as it will be reused in a different terminal location. In removing terminal D, the red wire will need to be fed into the battery holder, through the exterior hole in the enclosure. Similarly, feed the black wire through the same hole and route this wire into battery compartment 4. Discard terminals B-C and G-H.
- 4) Insert terminal D into the slot previously occupied by terminal B and route the red wire into battery compartment 4 following the path of the black wire.
- 5) Using an electric drill or similar tool, center and drill two 7/32" holes through the sidewall of the battery holder centered on battery compartments 3 & 4.
- 6) Insert a 1/4" rubber grommet into each of the 7/32" holes drilled through the sidewall of the battery holder. You may find that a small flathead screwdriver is helpful with this task.

You will note that the 4-circuit terminal block, as delivered, is too long to fit within the "AA" battery compartments. Depending on available tools or individual preferences, two options are provided to address this challenge. Option A employs the use of a hack saw to shorten the length of the terminal block itself, while option B requires the use of a razor knife or similar tool to remove interior

partitions of the battery holder to accommodate the full length of the terminal block.

- 7) Option A: Using a hack saw, remove one end of the 4-circuit terminal block up to the outside edge of the first terminal divider. This removes an unnecessary portion of the terminal block while enabling it to fit comfortably within the battery compartment 3.



Option B: Using a razor knife, or similar tool, cut away and remove the four plastic tabs at the topmost end of battery compartment 3 (see the dashed lines on the diagram above depicting the tabs to be removed). This will form a compartment of sufficient size to fit the 4-way terminal strip.

- 8) Insert the 4-way terminal block into battery compartment 3.
- 9) Replace the wire cover removed previously and secure it with the Phillips head screw.
- 10) Cut each of the red and black battery wires approximately 2-1/2" from the point at which they enter battery compartment 4.
- 11) Using the #24 AWG wire stripper, strip approximately 1/2" of insulation from the end of each wire.

Battery Assembly (Con't)

Final Assembly and Wiring of the Battery/Terminal Enclosure:



In this final step, the hydrophone and output cables will be prepared and connected together along with the remaining components within the battery/terminal enclosure.

A screw-type terminal block will be utilized to enable all necessary topside connections for this hydrophone assembly. Screw terminals form an electrical bond between two or more conductors by joining and securing wires between the head of a screw and a conductive plate. When connecting multiple stranded wires under one terminal, it is recommended that these wires be twisted together before making the final connection. It is also recommended that all conductors be inserted under the left-hand side of the screw to ensure that they are pulled into the terminal as the screw is tightened.

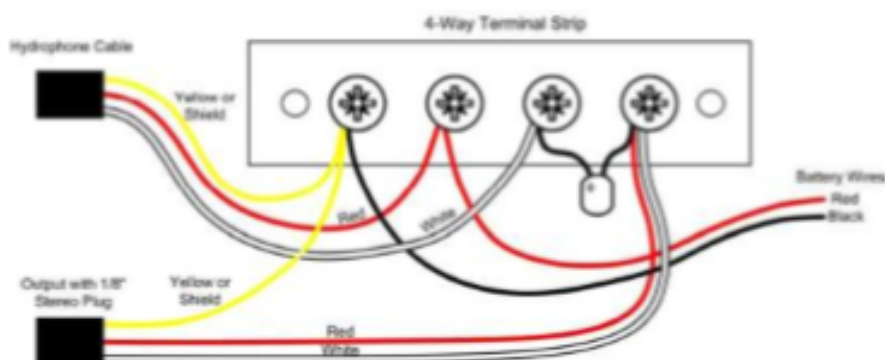


- 1) Working with both the hydrophone and output cables, strip back and remove approximately 3" of the outer cable jackets, exposing the

Final Hydrophone Assembly

individual wire leads within. Note, the #14 AWG wire stripper works well for this task. Be careful not to penetrate the insulation of the wires inside.

- 2) Using the #26 AWG wire stripper, strip approximately 1/2" of insulation from the end of each wire.
- 3) Working with the hydrophone battery/terminal enclosure, insert the un-terminated end of the hydrophone cable into the enclosure, routing it through the inner-most grommet. The outer jacket of the cable should be captured by the grommet and just penetrate the enclosure.
- 4) Insert the un-terminated end of the output cable into the hydrophone battery/terminal enclosure, routing it through the outer-most grommet.
- 5) Following the wiring diagram below, attach each of the wires and capacitor leads to the terminals of the 4-way terminal strip. Take note of the mark on the capacitor indicating the + lead on this component.



Note: if the hydrophone and output cables contain un-insulated shield wires, it is recommended to make them as short as possible to connect to the terminal while ensuring that no wire strands make contact with any other terminals.

- 6) With all wires connected accordingly, insert two AA batteries
- 7) Slide the cover onto the hydrophone battery/terminal enclosure and replace the Phillips head screw securing the cover in place.

You have just completed the fabrication and wiring of your hydrophone assembly.

Appendix G: Model Testing Log Sheets (Baseline and Blast Test)

The following two figures represent sample field logs for each of the two main parts of the experiment. One for the baseline (pull-out or brute force, designated as Part I) test in Fig. G1 and the other for the blast test (designated as Part II) in Fig. G2. These two are included only to show one example of each of the test results recorded at the times of each trail. There are many other sheets of similar data records that were taken each time any testing work was performed which were not included here. For the baseline tests, thirty trials were performed and for the blast tests, eighteen trails were carried out. The recaps of all these are shown for the baseline tests in Table 5. Similarly, for the blast tests, the data is recapped in Table 6.

Baseline tests were set up and carried out such that up to as many as three trials per working day could be successfully concluded. In the cases of the blast test phases, a maximum of one trail was set up and concluded in any working day. The timeframe for carrying out the baseline trails was between June 23, 2013 and November 3, 2013. The timeframe in which the blast tests were performed was between March 8, 2014 and August 3, 2014.

FIELD EXPERIMENTATION LOG		J. CERQUETTI		
<u>PARAMETERS</u>		DATE: 10/19/13 11/3/13 SS 3		
PART I	SHIP MODEL:			
	# OF BALLAST BRICKS USED:	5 + R		
	WEIGHT OF MODEL + BALLAST:	65#		
	WATER LEVEL IN TANK:	8 1/2"		
	HEIGHT OF SAND IN TANK:	11 1/2"		
<u>PULL-OUT TEST RESULTS</u>		TRIAL No.	FORCE TO RELEASE (#)	TIME
• HOLDS AT LENGTH AT 181# (PROLONGED)		8	115# 48 ^m	S: 11:37 AM F: 12:25 PM
11/3/13 ↓				
DIDN'T GET THIS BURIED TO AS FAR AS USUAL		9	108# 94 ^m	S: 11:01 AM F: 12:35 PM
• DEEPER BURIAL, PROLONGED HOLD AT 86# ON DECLINE PULLS		10	129# 57 ^m	S: 1:18 PM F: 2:15 PM

Fig. G1 – Typical Baseline (Pullout) Test Field Record

J. CERQUETTI

PART II

DATE : 4/12/14

SHIP MODEL: SS2

No. of BALLAST BRICKS USED: 13

WEIGHT OF MODEL + BALLAST: $\pm 70^{\#}$

WATER LEVEL IN TANK: 8' 6"

HEIGHT OF SAND IN TANK: $11\frac{1}{2}$ "

WATER
SIDE

PULL-OUT RESULTS

• STAYED HERE \rightarrow 37 psi TO FREE ON
UNTIL MORE 3rd PLAST
TENSION WAS APPLIED

1:05 PM

DATA
RECORDING
SIDE

TAPE ID:

TAPE 6

COMPRESSOR PRESSURE: 90psi 92 94
85psi
SETUP 4

SETUP

(i) L ON TAPE = 32

② 2:07

B

③ 4:00

W

④ 6:20

B

4 BLASTS

60R

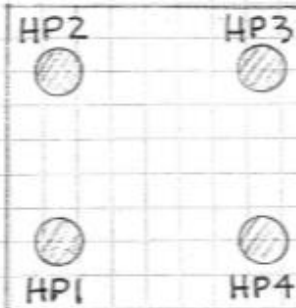
HP #	CHANNEL #
------	-----------

HP1	2
-----	---

HP2	3
-----	---

HP3	4
-----	---

HP4	5
-----	---



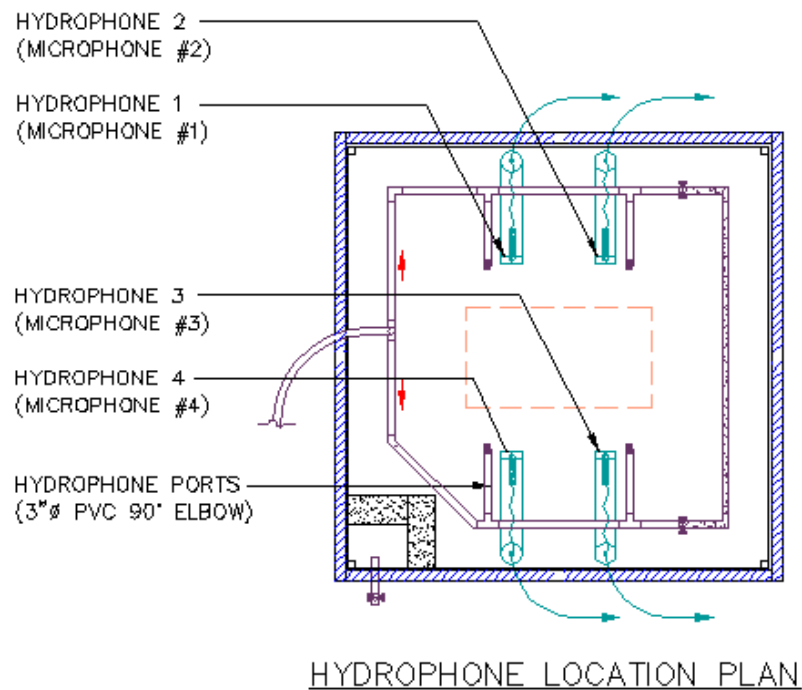
AIR
HOSE
←
←
IN

TANK ORIENTATION

Fig G2 – Typical Blast (Compressed Air) Test Field Record

Appendix H: Pressure Trace Plots and Spectrum Plots

The following images are the blast pressure traces recorded at each of the four hydrophones (microphones) within the tank at each blast. Their locations are labeled below:



There were various (longer) time lengths between each blast as originally recorded on the DA-88 raw tapes. In order to provide more comparative visualization of these record blasts, the non-essential time lags between each were edited out and the blast signatures were digitally aligned as now can be seen in the *MATHCAD Software* generated graphs of Figs H1- H18. The Time (horizontal axes) and pressure record Amplitude (vertical axes) are scaled relative to each other and to each microphone but do not correspond to actual time-length and pressure. These can be seen from the field notes recapped in Table 6.

The spectrum plots at the latter part of the appendix are showing frequency content of the blast signatures on a per-hydrophone (microphone) basis.

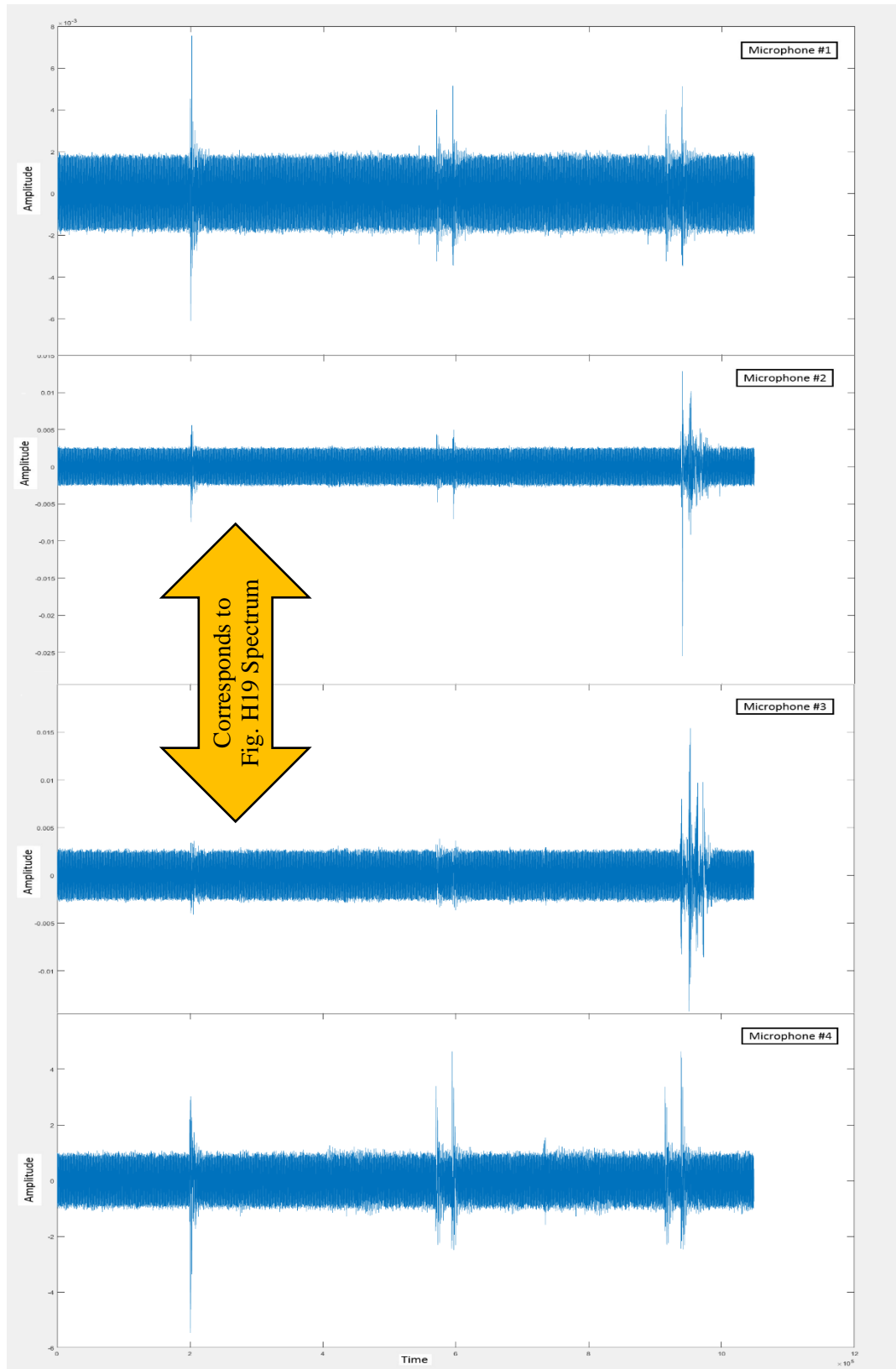


Fig. H1 - Tape No.1, Blasts 1, 2 and 3

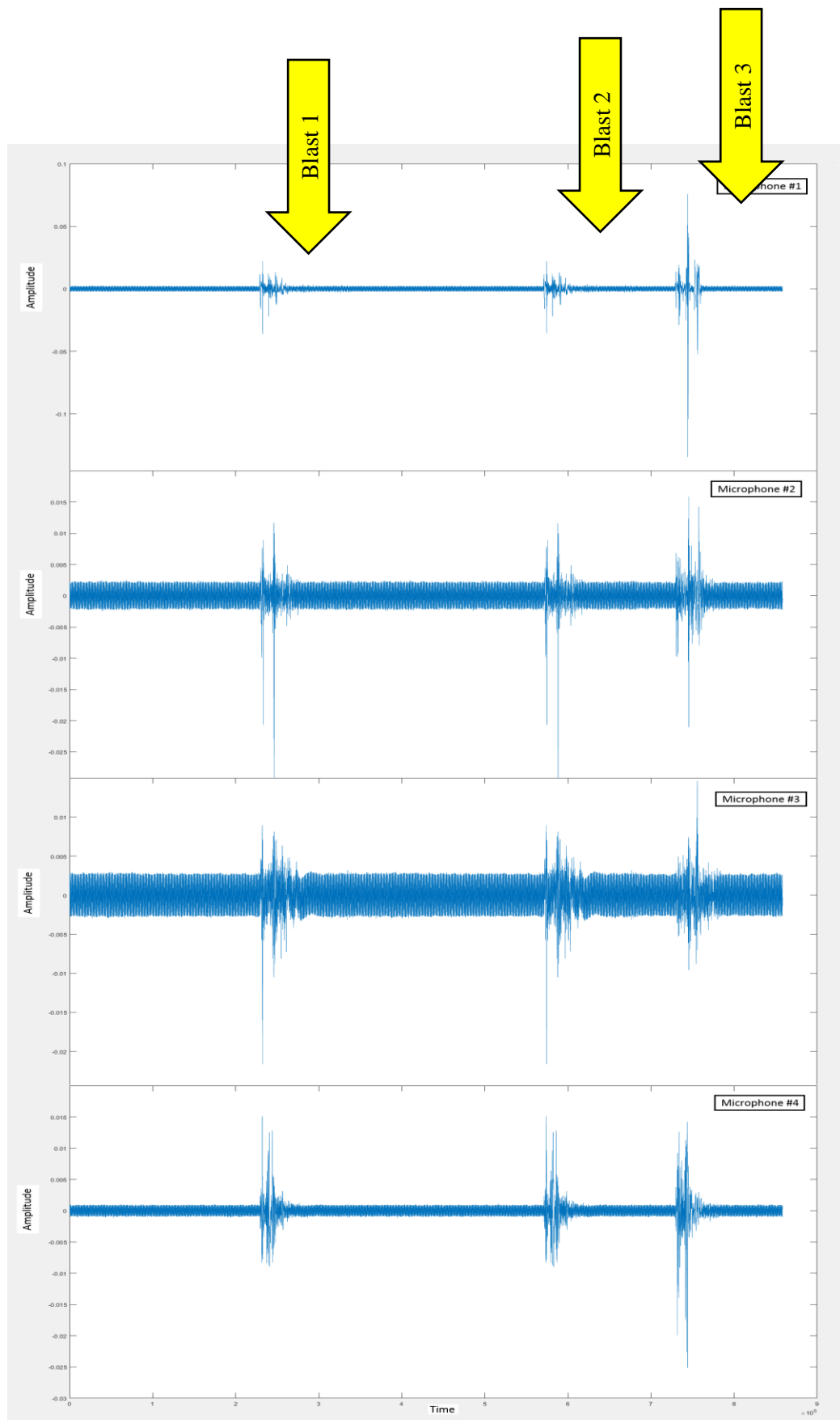


Fig. H2 - Tape No.2, Blasts 1, 2 and 3

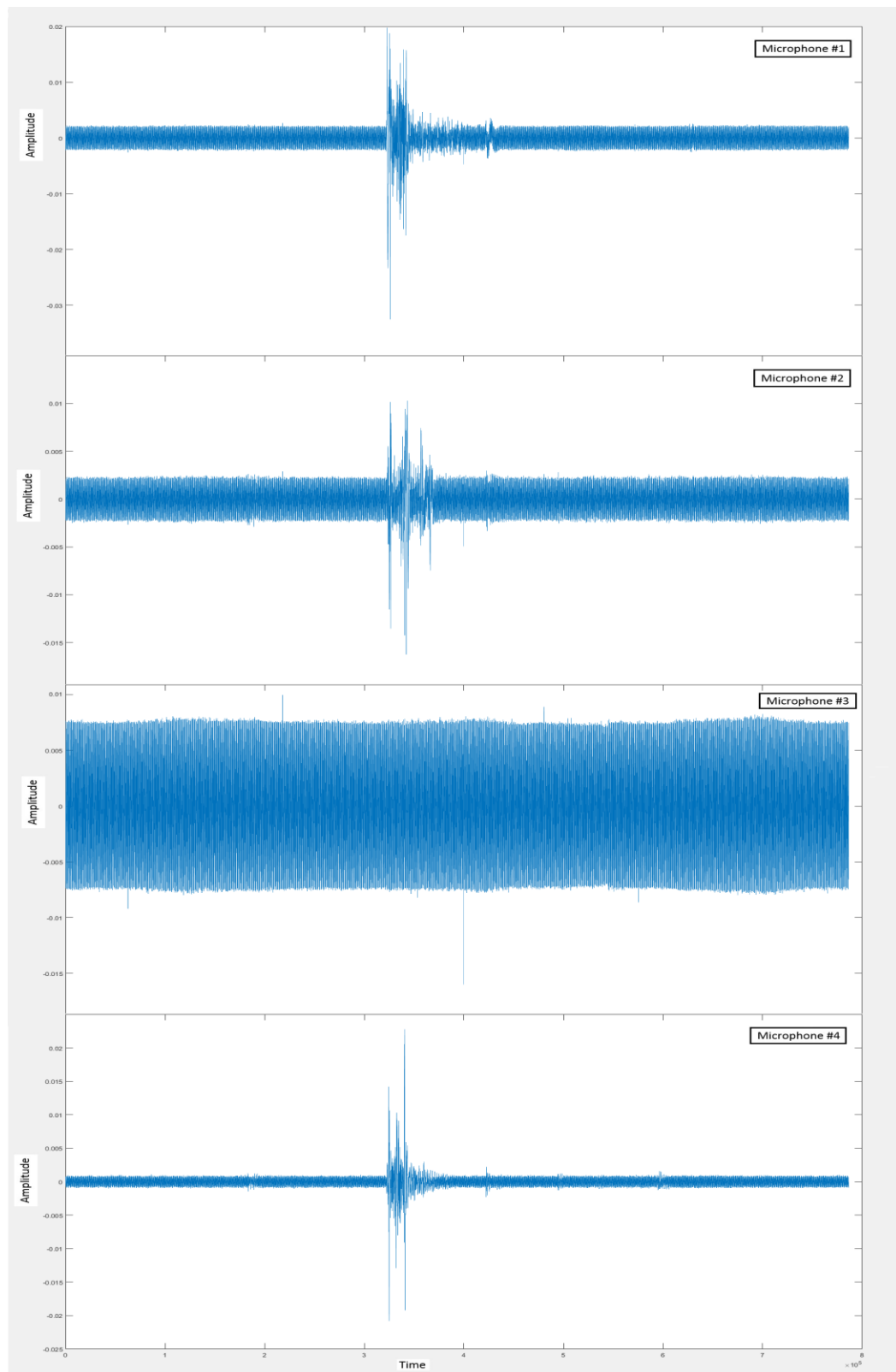


Fig. H3 - Tape No. 3, Blast 1

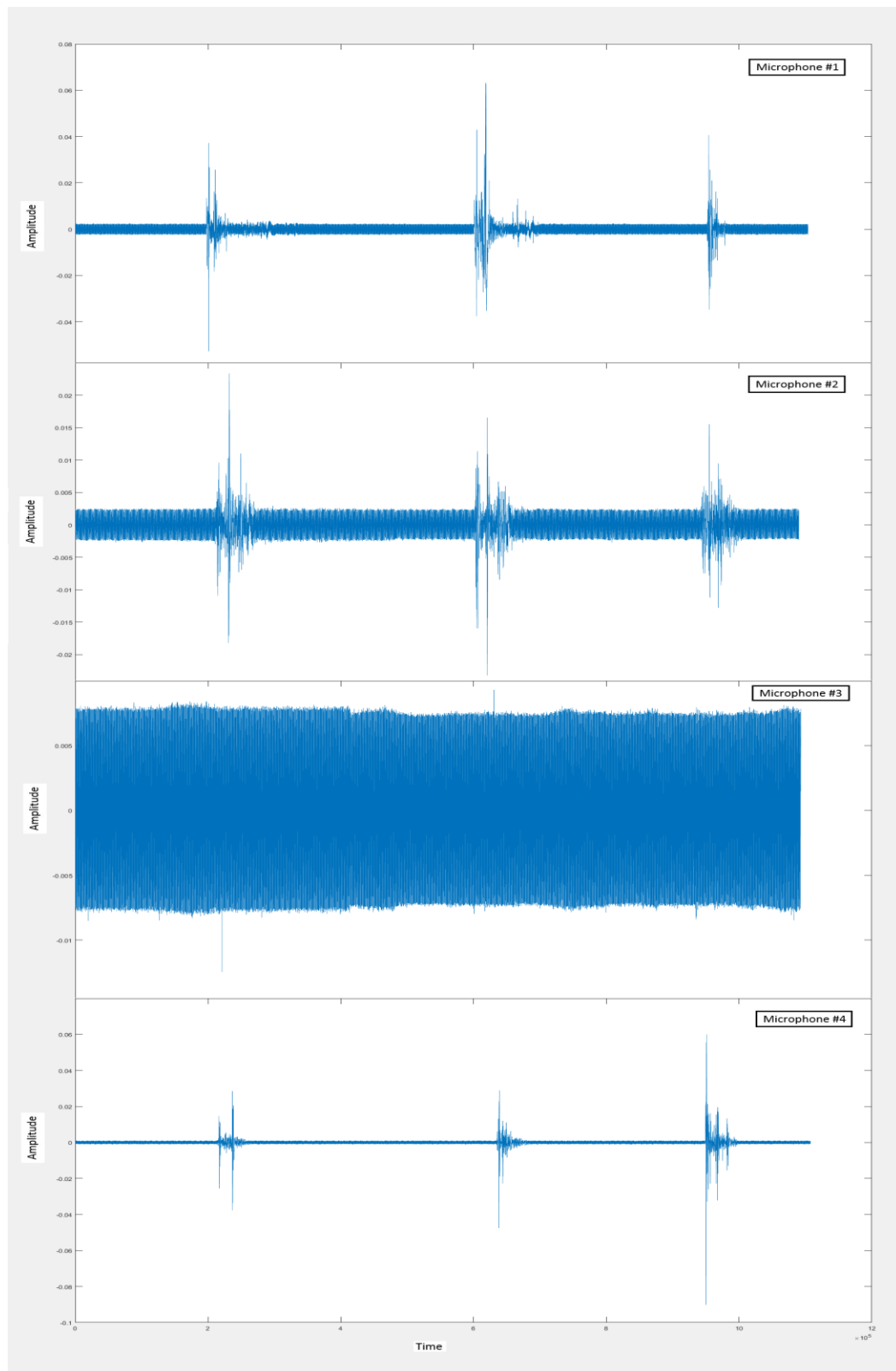


Fig. H4: Tape No. 4, Blasts 1, 2 and 3

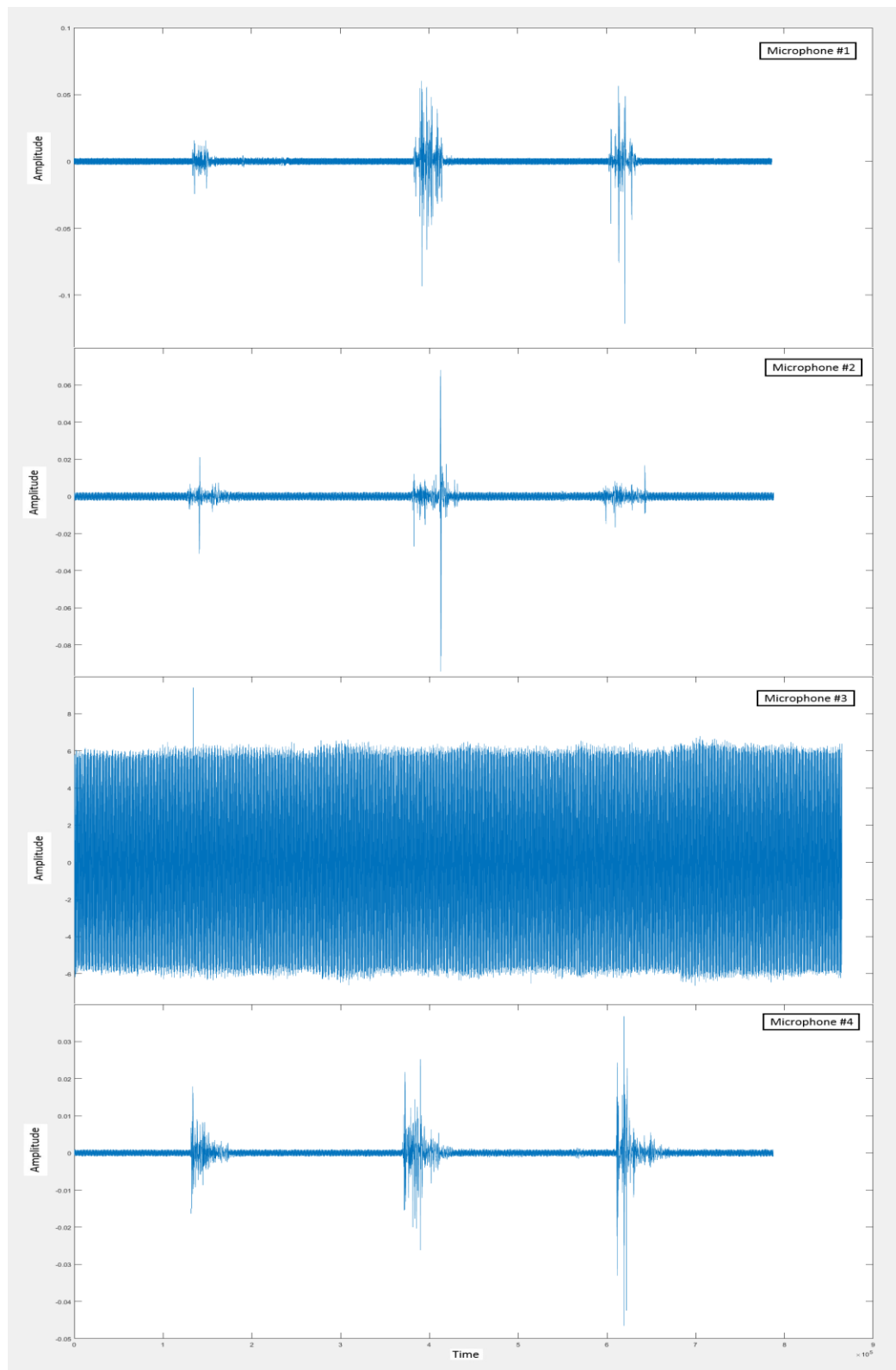


Fig. H5 - Tape No. 5, Blasts 1, 2 and 3

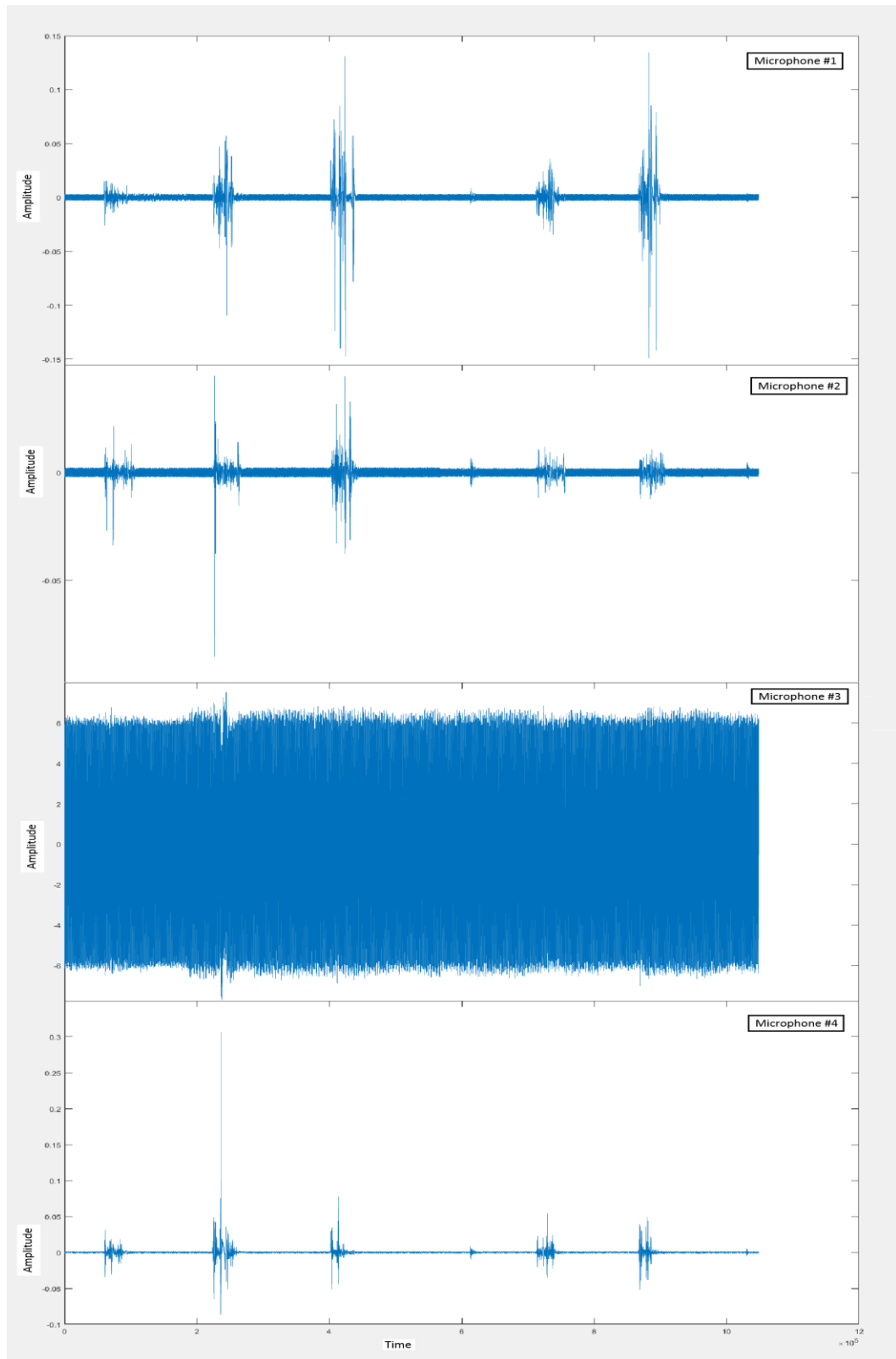


Fig. H6 - Tape No. 7, Blasts 1, 2, 3, 4 and 5

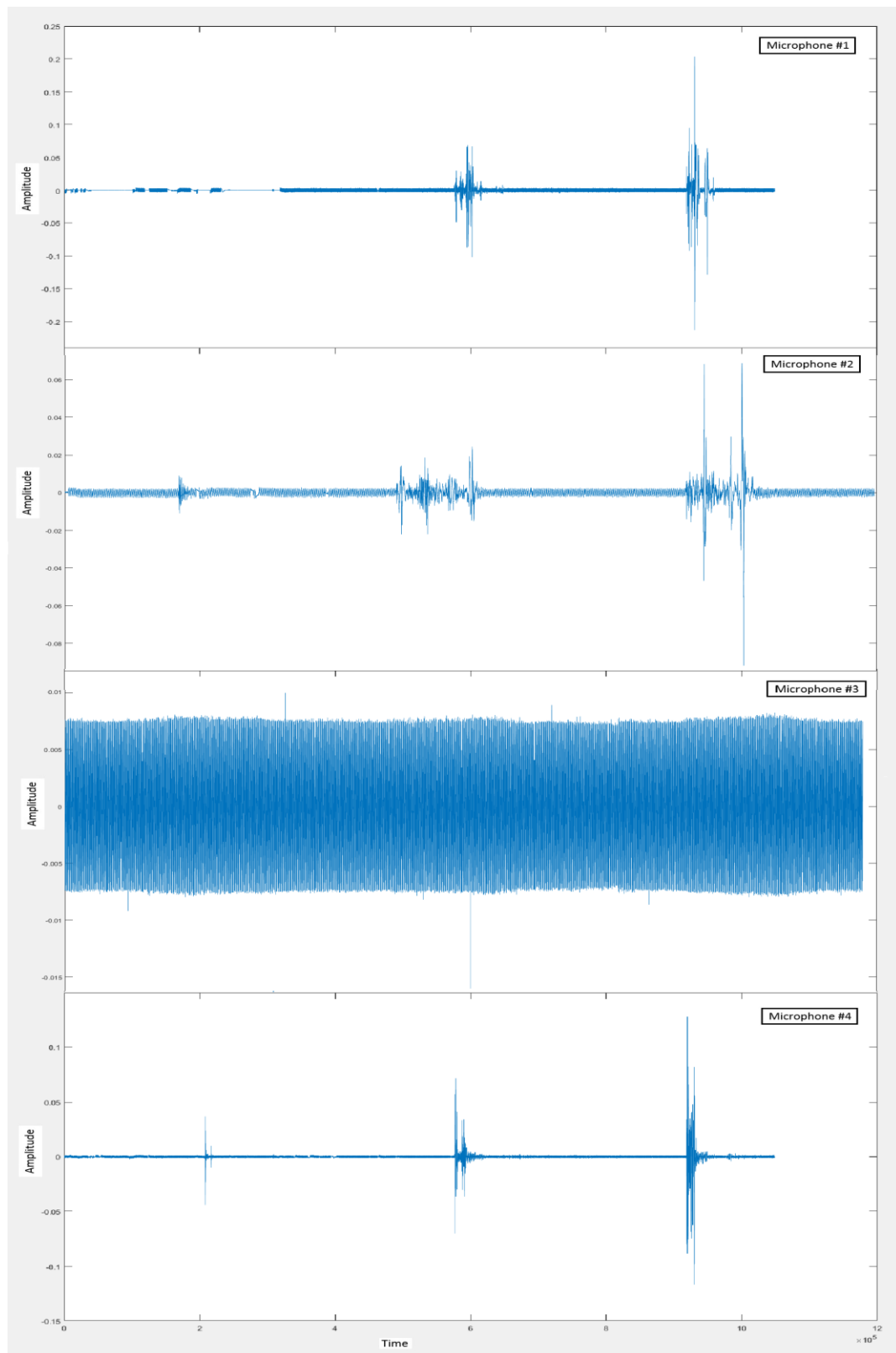


Fig. H7 - Tape No.8, Blasts 1, 2, and 3

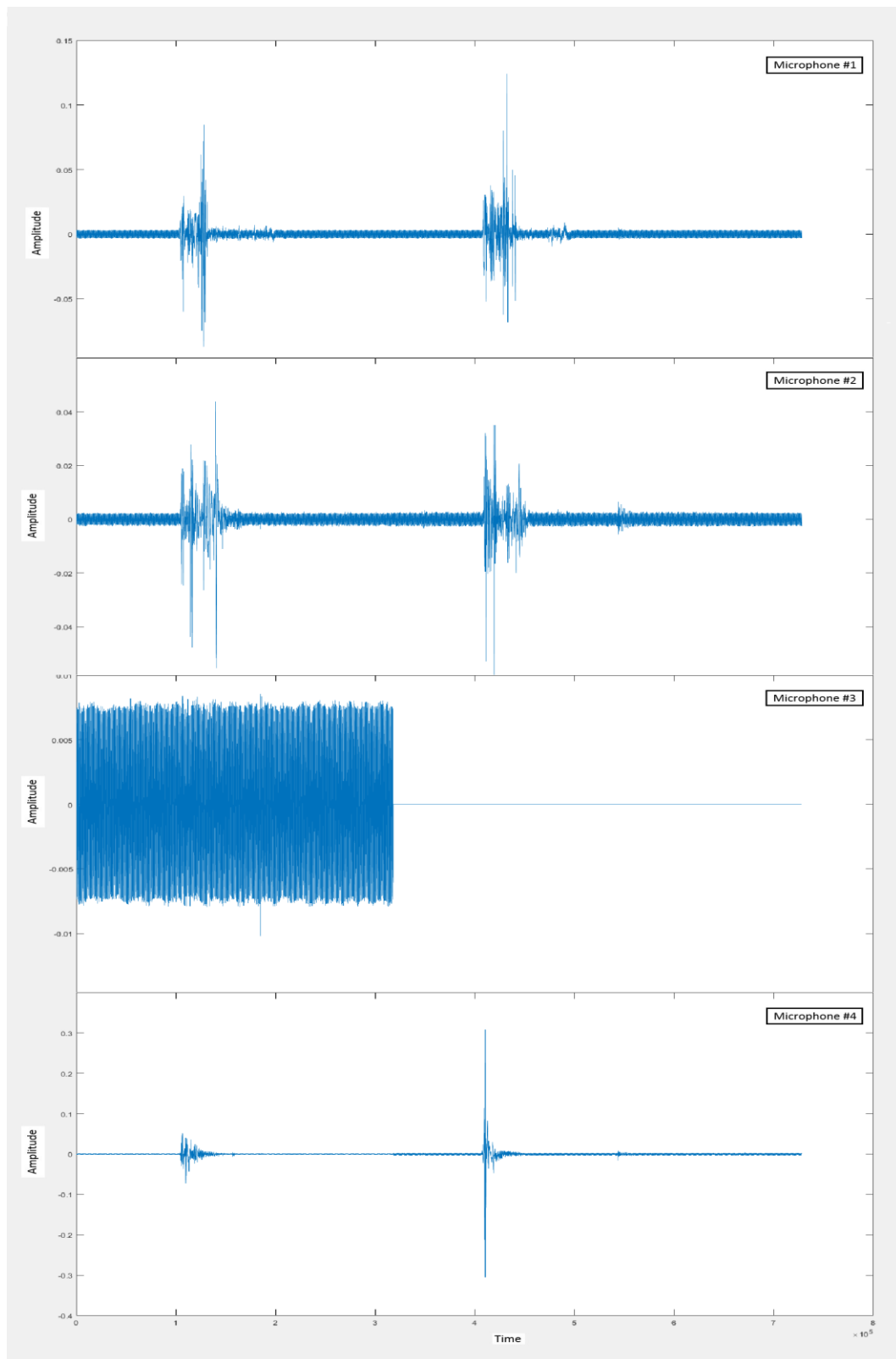


Figure H8 - Tape No. 9, Blasts 1 and 2

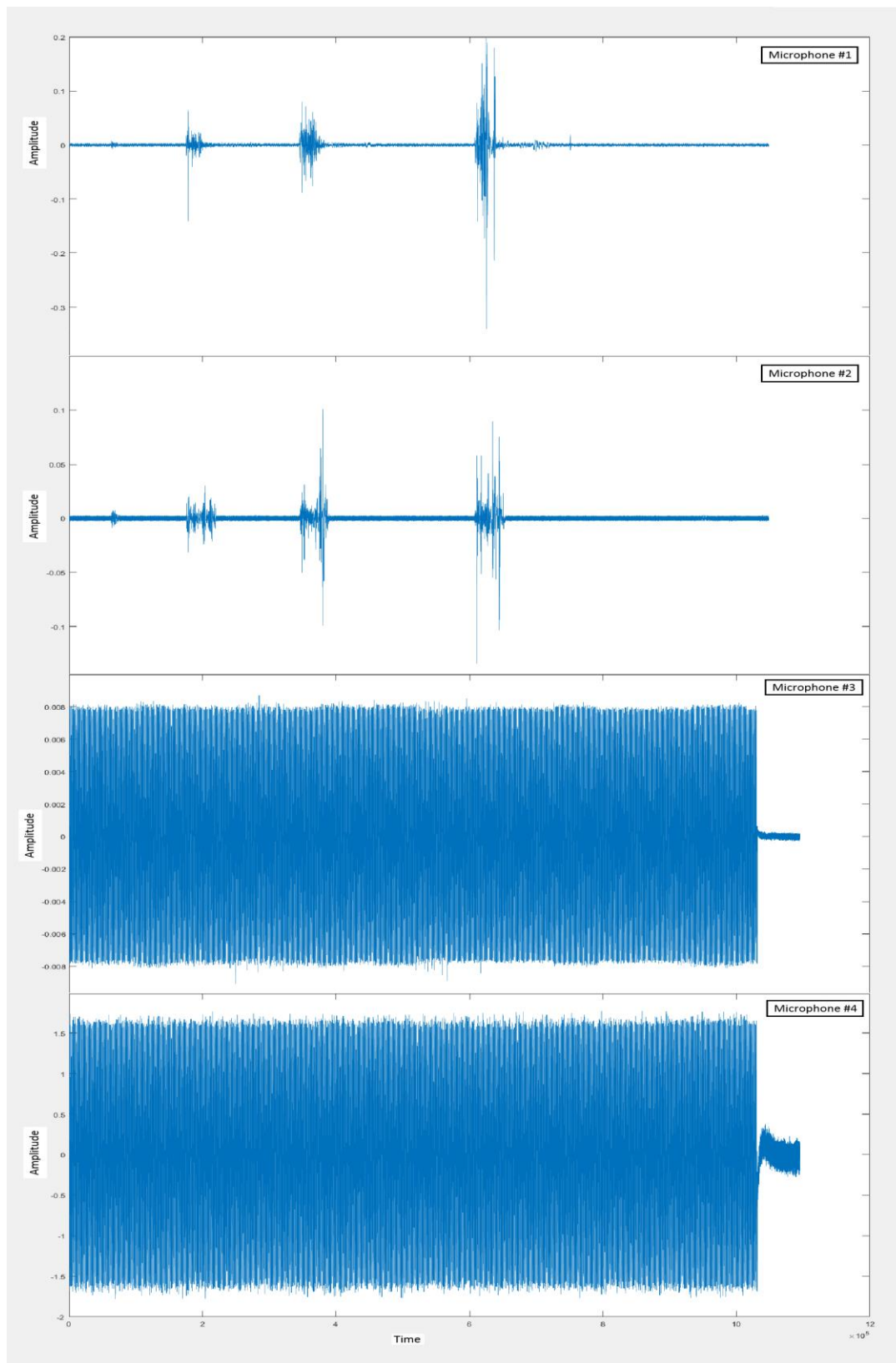


Fig. H9 - Tape No. 10, Blasts 1, 2, and 3

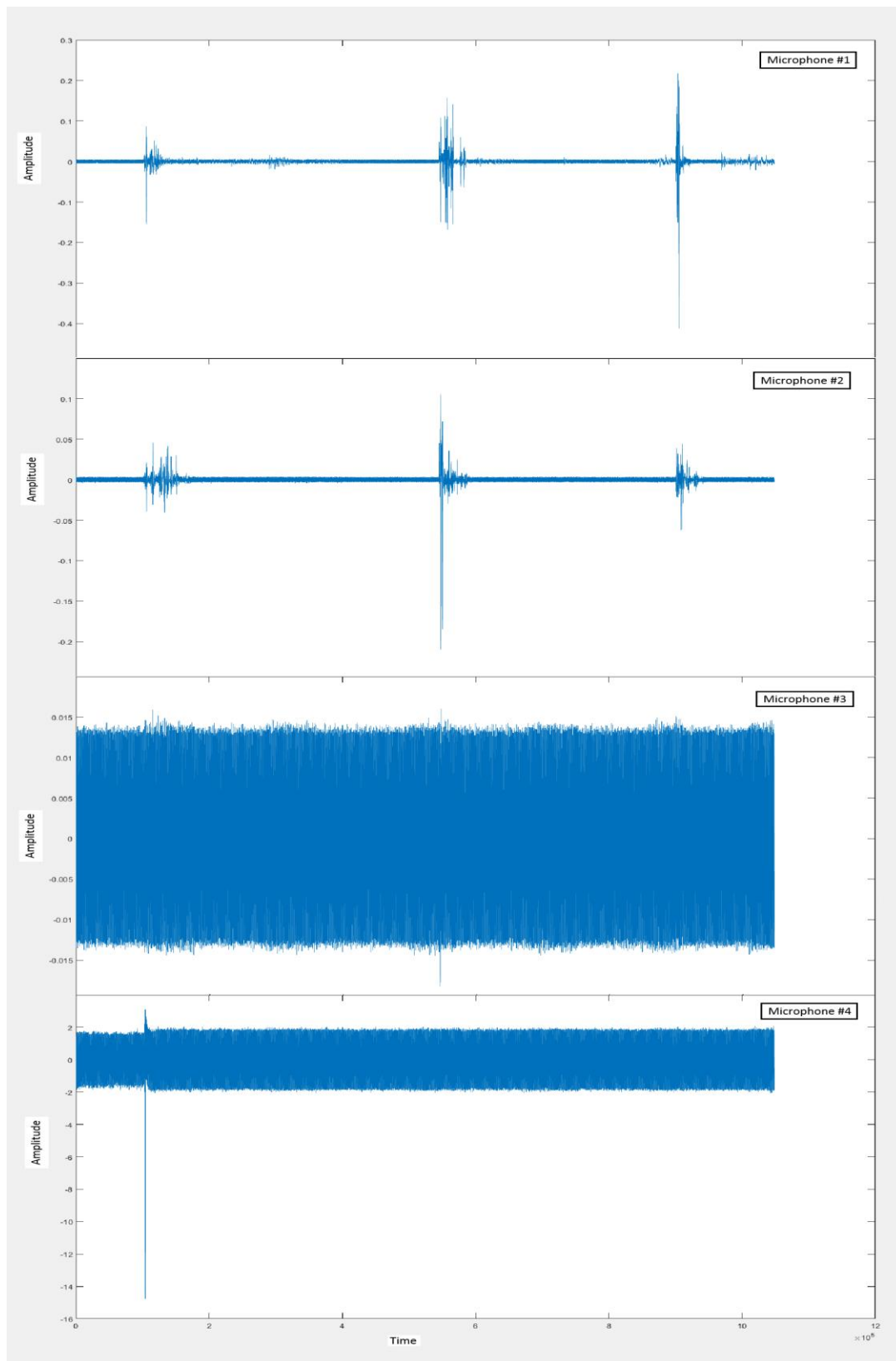


Fig. H10 - Tape No. 11, Blasts 1, 2, and 3

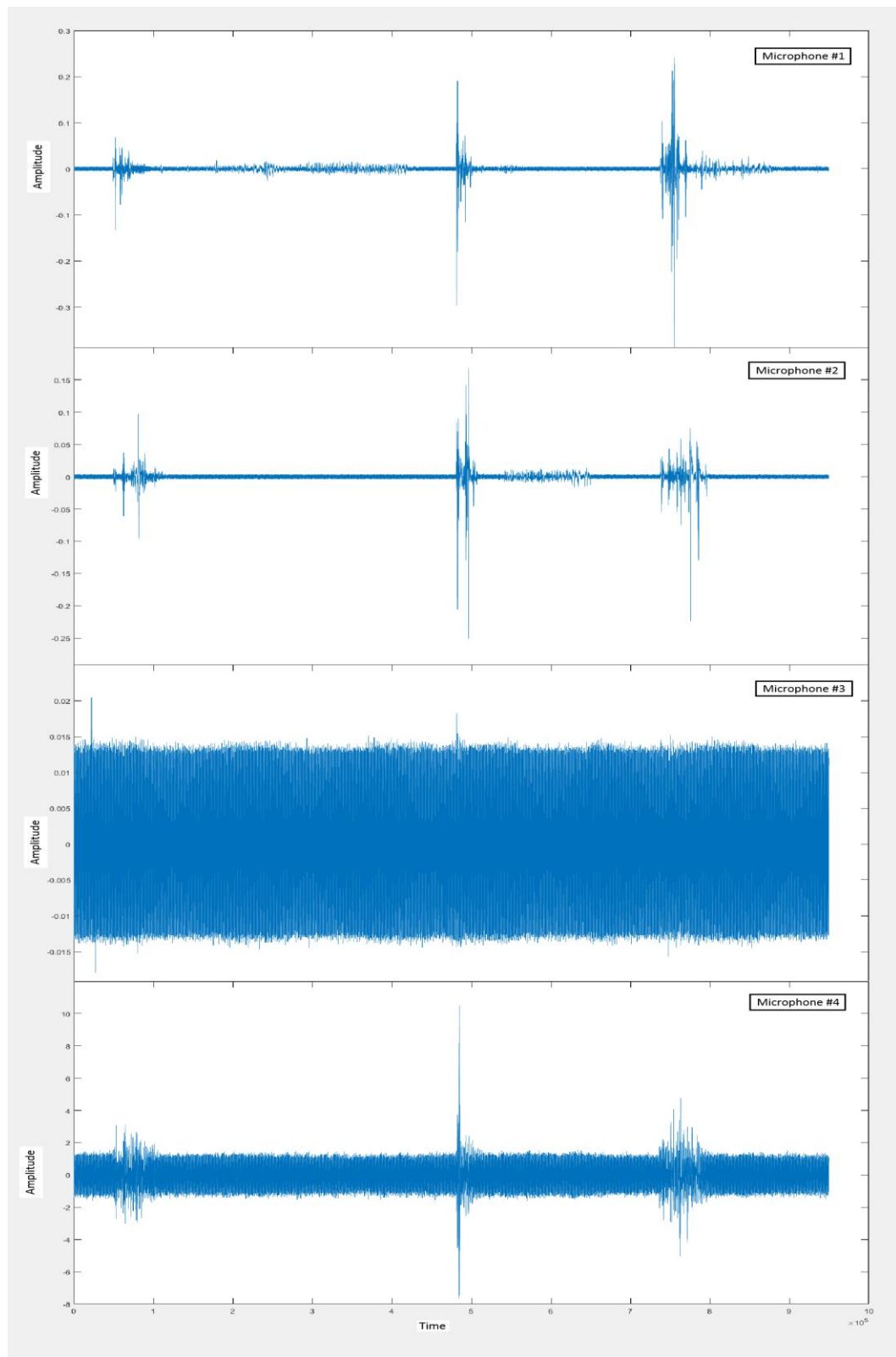


Fig. H11 - Tape No. 12, Blasts 1, 2, and 3

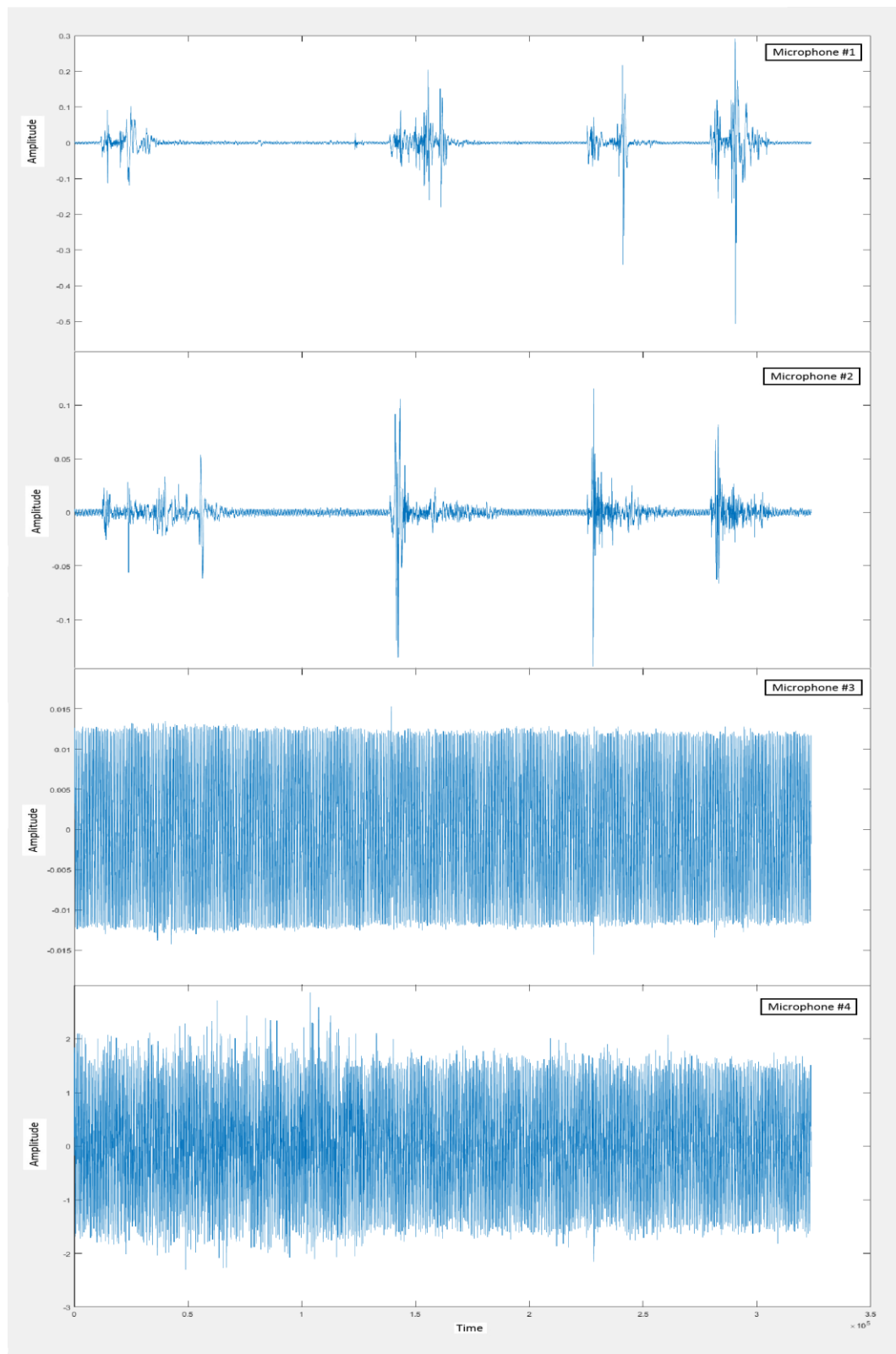


Fig. H12 - Tape No. 13, Blasts 1, 2, 3 and 4

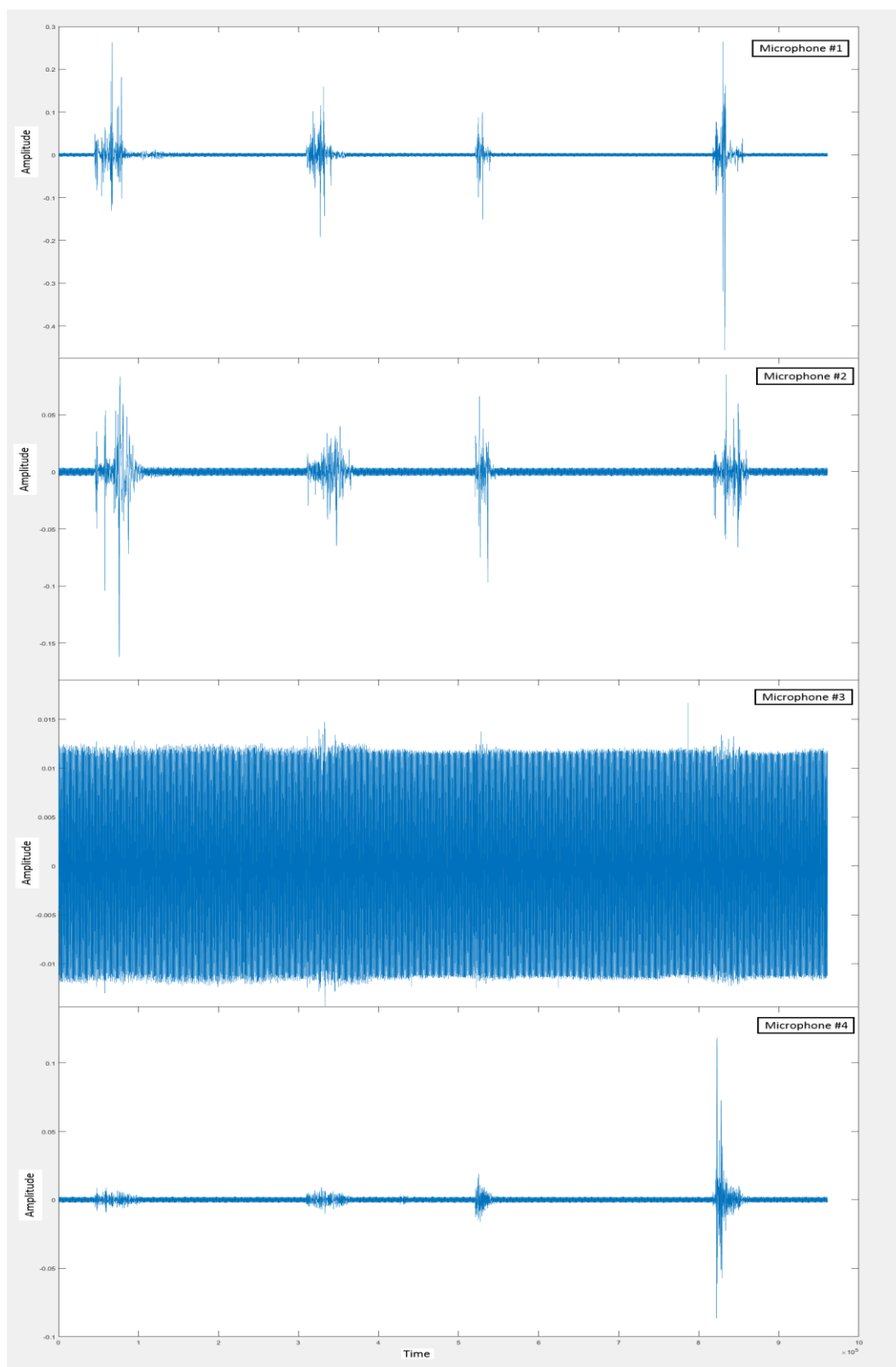


Fig. H13 - Tape No. 14, Blasts 1, 2, 3 and 4

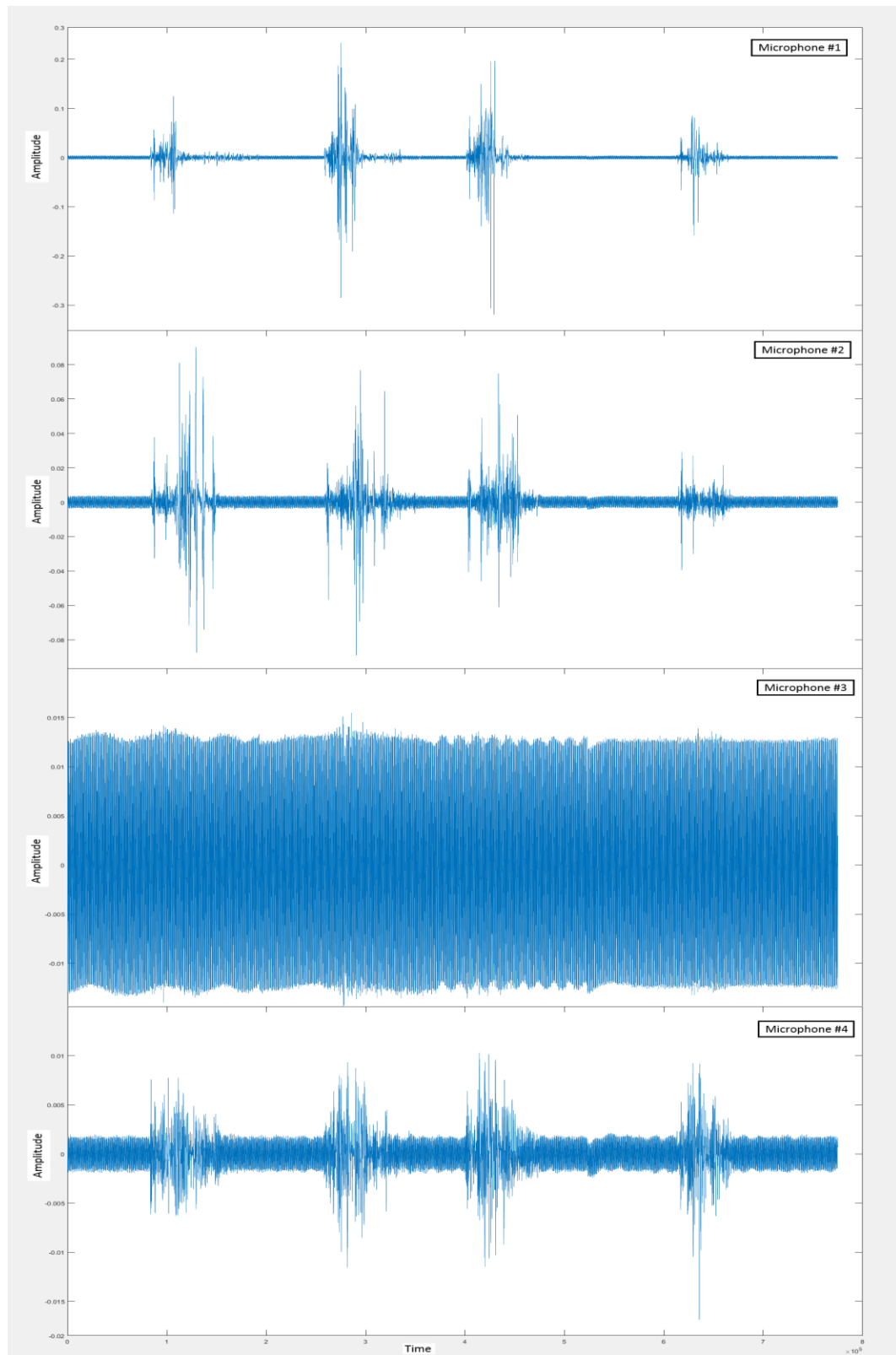


Fig. H14 - Tape No. 15, Blasts 1, 2, 3 and 4

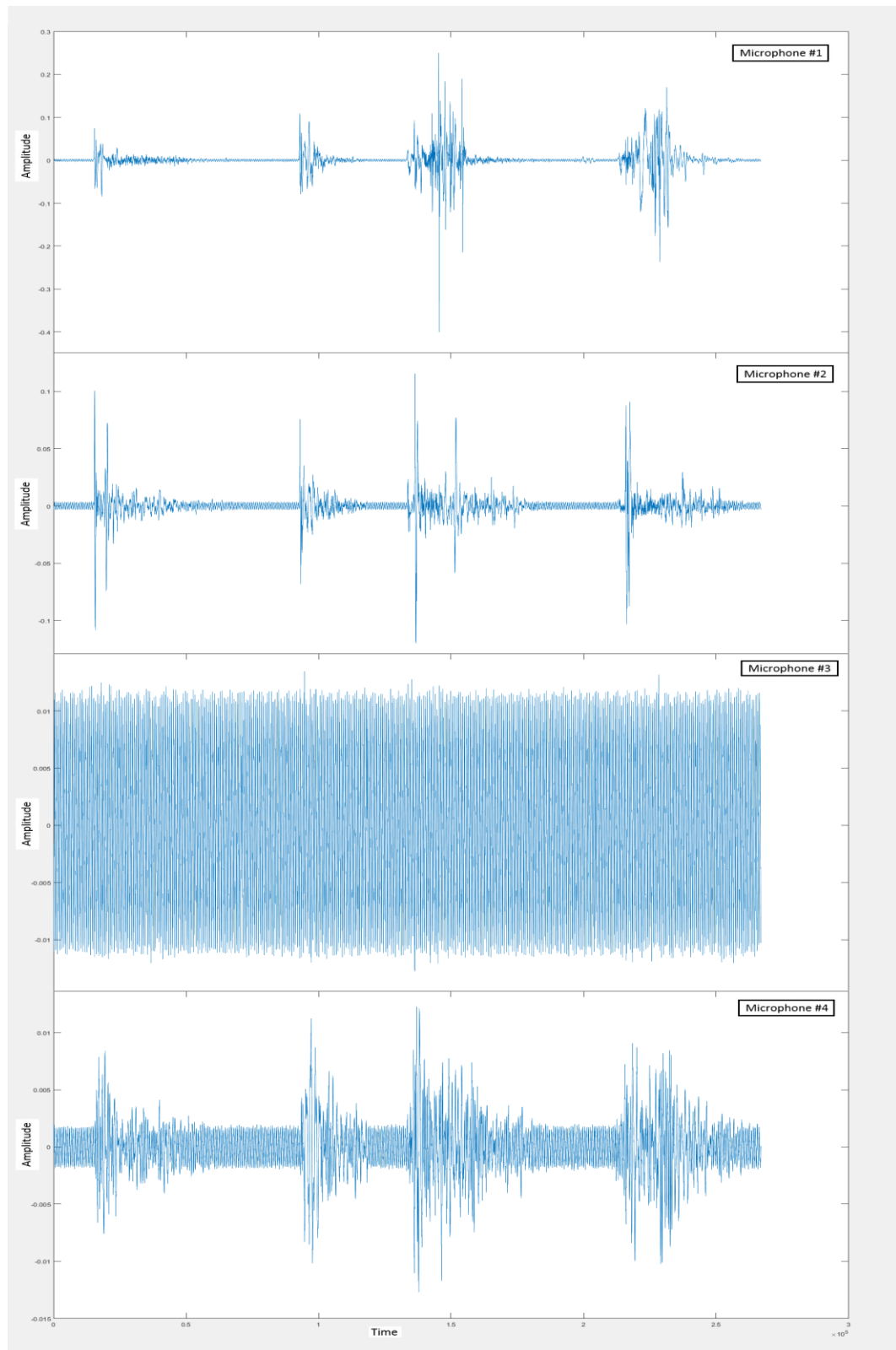


Fig. H15 - Tape No. 16, Blasts 1, 2, 3 and 4

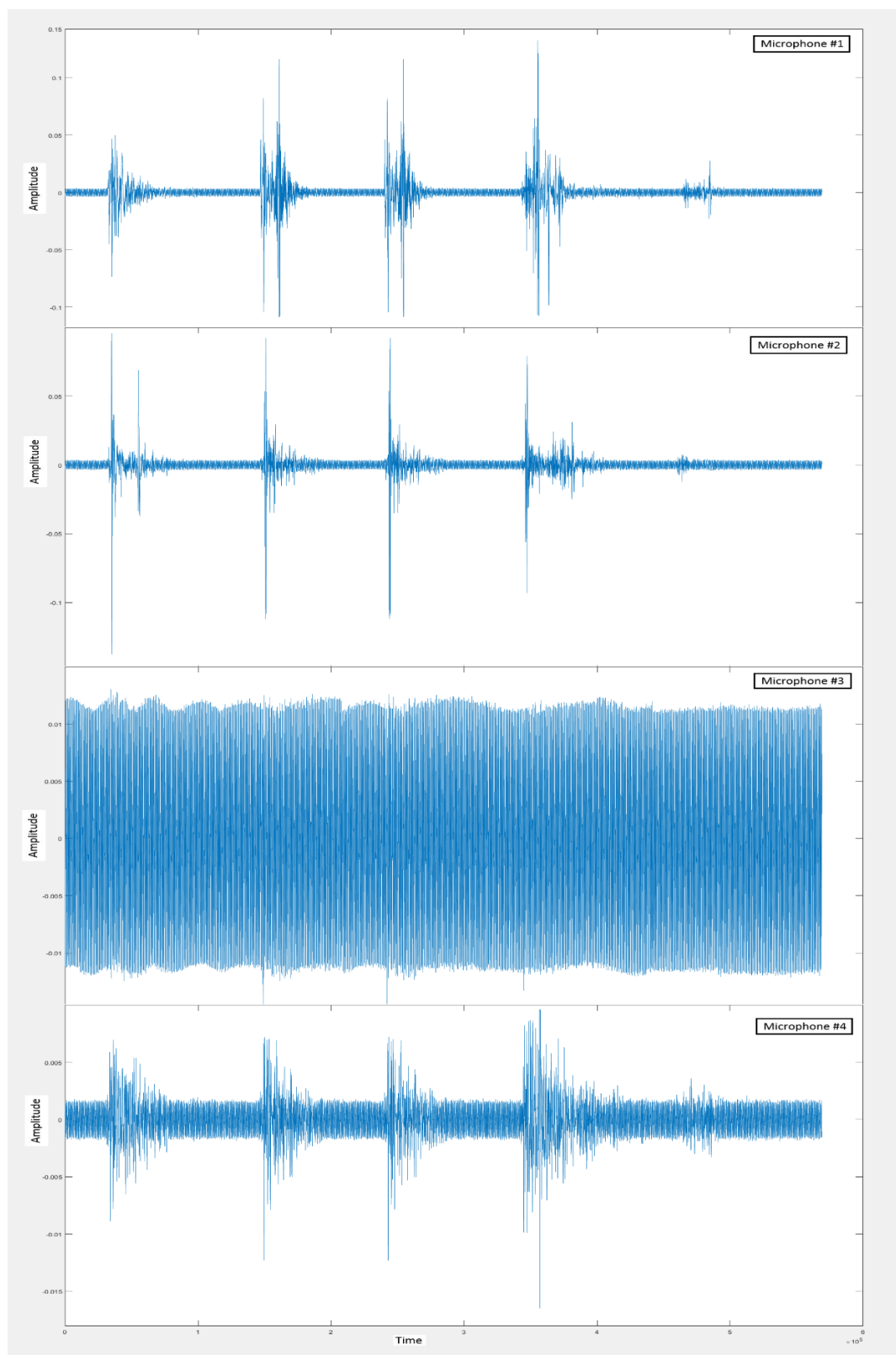


Fig. H16 - Tape No. 17, Blasts 1, 2, 3, 4 and 5

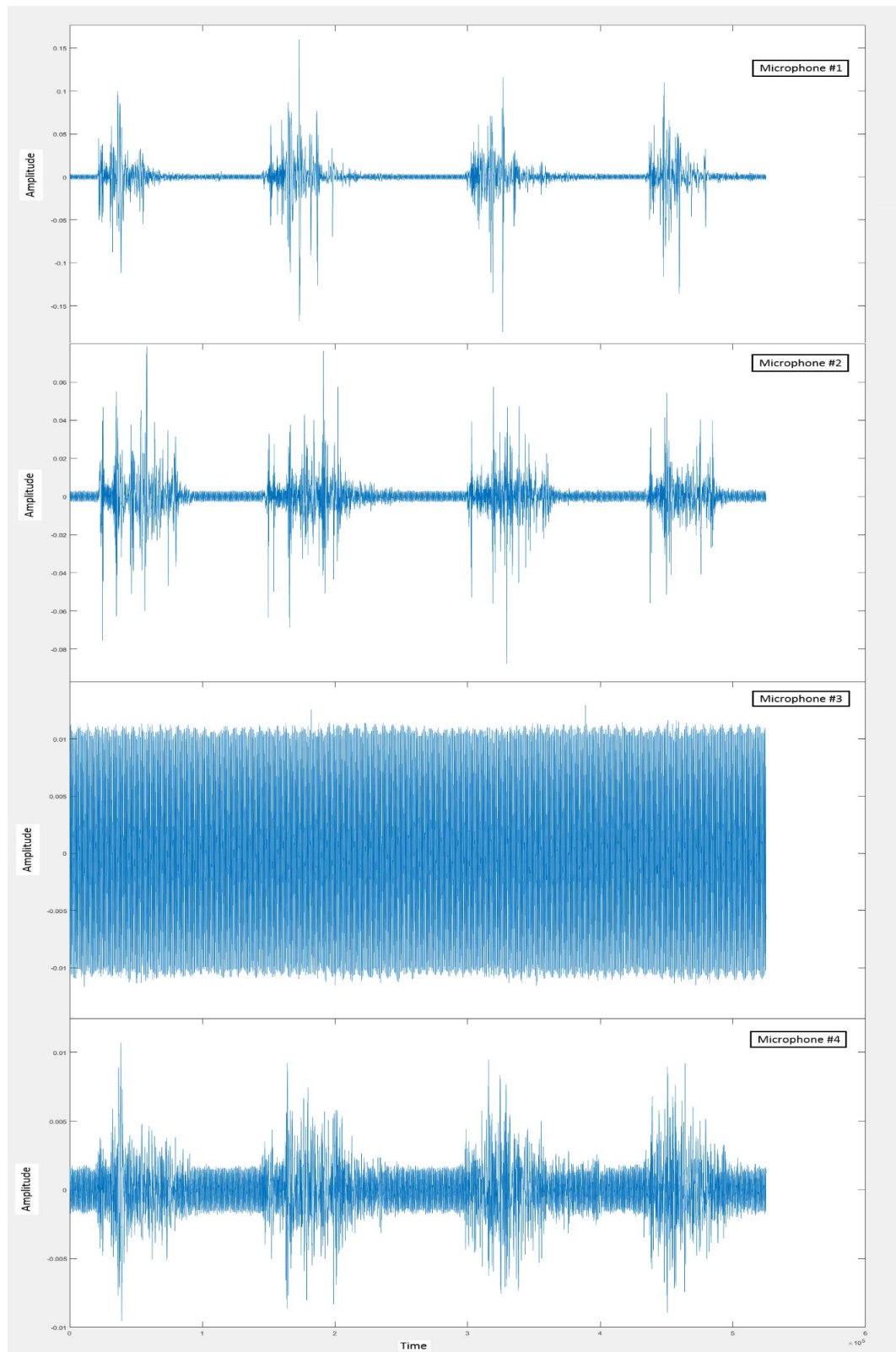
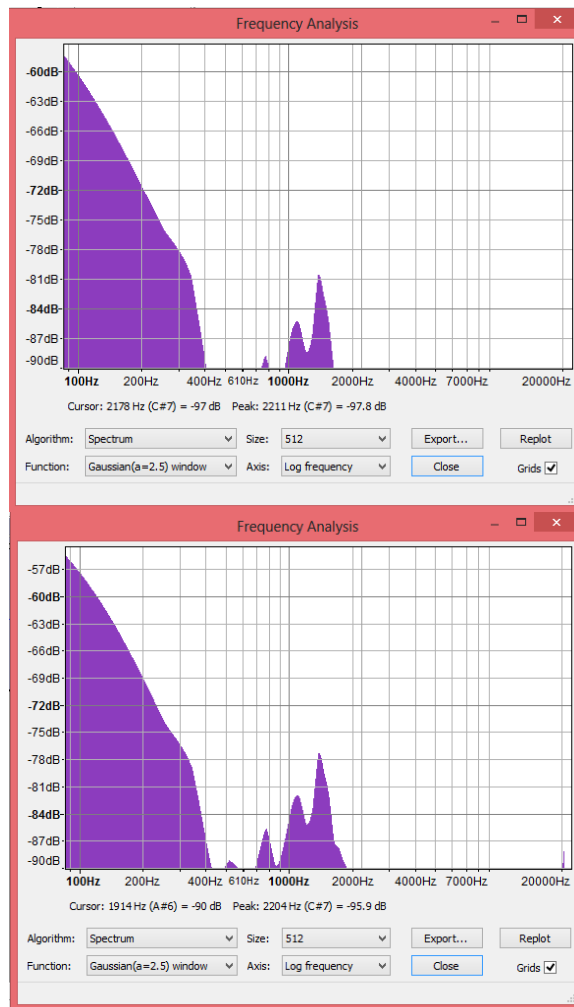


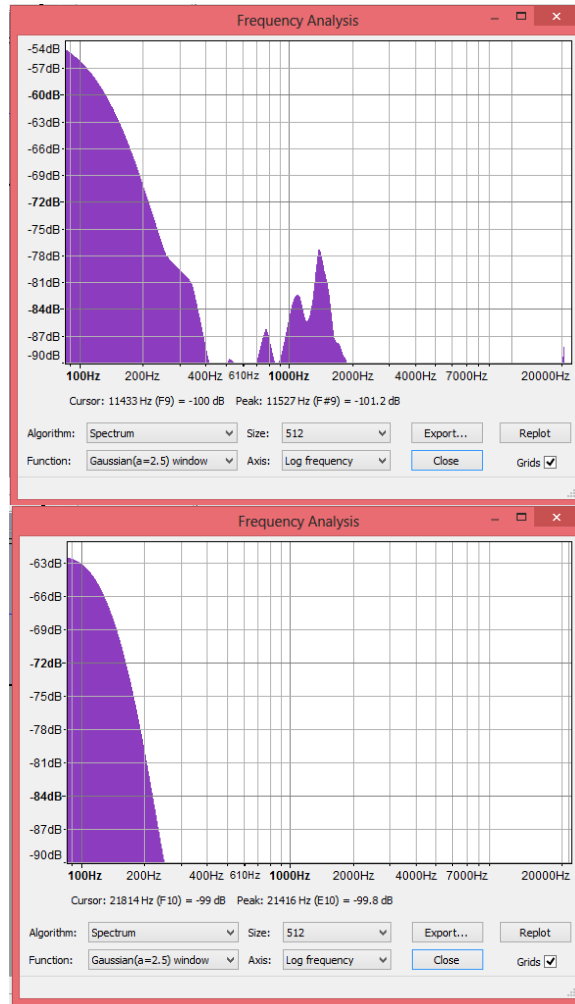
Fig. H17 - Tape No. 18, Blasts 1, 2, 3 and 4

Spectrum Frequency Plots



Tape 1 Blast 1 Mic. 1 (Ex1.1-01)

Tape 1 Blast 1 Mic. 2 (Ex1.1-02)



Tape 1 Blast 1 Mic. 3 (Ex1.1-03)

Tape 1 Blast 1 Mic. 4 (Ex1.1-04)

Fig. H18 - Gaussian Spectrum Log Plots of Tape 1 Blast 1 on all 4 Hydrophones

Corresponds to the pressure trace plot in Fig. H1 for the first of the three recorded blasts.

Appendix I: Results Description related to the Theorem of Buckingham Pi

Dimensional analysis is a means of simplifying a physical problem by appealing to dimensional homogeneity to reduce the number of relevant variables.

The theorem originates from the work of American engineer *E. Buckingham* who made use of the symbol, π , for the dimensionless variables in his original 1914 paper. The basic idea of the theorem is that relations between natural quantities can be expressed in an equivalent form that is comprised entirely of dimensionless quantities. It is particularly useful for:

- presenting and interpreting experimental data
- resolving problems not as manageable to a direct theoretical solution
- checking equations
- establishing the relative importance of particular physical phenomena
- *physical modelling*

In engineering, particularly in the field of Fluid Mechanics, as well as applied mathematics and physics, the Buckingham π theorem is a key theorem in dimensional analysis. It is a formalization of Rayleigh's method of dimensional analysis.

Loosely, the theorem states that if there is a physically meaningful equation involving a certain number, n , physical variables, it follows that the original equation can be reduced in terms of a set of $p = n - k$ dimensionless parameters named as $\pi_1, \pi_2, \dots, \pi_p$ constructed from these original variables, where k is the minimum number of reference dimensions needed to describe the variables. The dimensionless products are frequently referred to as “pi terms”.

The theorem can be seen as a scheme for non-dimensionalization because it provides a method for computing sets of dimensionless parameters from the given variables, even if the form of the equation is still unknown.

REFERENCES

Airy, George B. (1845), "On Tides and Waves," *Encyclopedia Metropolitana*, Vol. 5, Article 192, pp. 241 – 236, London.

Ang, Alfredo H-S, Tang, Wilson H., (1975), *Probability Concepts in Engineering Planning and Design*, John Wiley and Sons, Inc., New York (ISBN 0-47-03200-X)

ASTM (1963), "D-422," *Publication Standards*, Standard Test Method for Particle-Size Analysis of Soils, American Society of Testing Materials.

ASTM (2014), "D-638," *Publication Standards*, Standard Test Method for Tensile Properties of Plastics, American Society of Testing Materials.

ASTM (2015), "D-695," *Publication Standards*, Standard Test Method for Compressive Properties of Rigid Plastics, American Society of Testing Materials.

ASTM (1998), "D-2487 Unified Soil Classification System," *Publication Standards*, Standard Practice for Classification of Soils for Engineering Purposes, American Society of Testing Materials.

Ashford, Scott A., Rollins, Kyle M.; Lane, J. Dusty (2004), "Blast-Induced Liquefaction for Full Scale Foundation Testing," *Journal of Geotechnical and Geoenvironmental Engineering*, Vol. 130, No. 8, pp. 798-806.

Castro, G., (1969), *Liquefaction of Sands*, Ph.D. thesis, Harvard University. Harvard Soil Mechanics Series No. 81.

Clay, Clarence C., Medwin, Herman, (1977), *Acoustical Oceanography*, John Wiley and Sons, Inc., New York (ISBN 0-471-16041-5)

Elmore, William C., Herald, Mark A., (1985), *Physics of Waves*, Dover Publications, Inc., New York (ISBN 0-486-64926-1).

Fragaszy, Richard J, Voss, Michael E. (1981), “Laboratory Verification of Blast-Induced Liquefaction Mechanism,” *USAF – Office of Scientific Research, Grant No. AFOSR-81-0085; 52 pages.*

Gillmer, Thomas C., (1970, 1975), *Modern Ship Design*, Naval Institute Press, Annapolis, Maryland (ISBN 0-87021-388-1)

Hudson, Patrick J., (2001), *Wave-Induced Migration of Grounded Ships*, Ph.D. thesis, Johns Hopkins University, Baltimore, Maryland.

Hudson, Patrick J., McCormick, Michael E., Browne, Shannon T., (2001) “A Low-Cost Wave-Sediment-Towing Tank,” *Proceedings, Fourth International Symposium on Ocean Wave Measurement, ASCE Waves 2001 Ocean Wave Measurement and Analysis* pp. 1180-1189, San Francisco, California.

IPS Corporation (2002), *Weld-On # 16 Plexiglas Low VOC Fabrication Adhesive (for acrylics)*, Product Data Sheet, Crompton, CA

Kinsler, Lawrence E., Frey, Austin R., Coppens, Alan B., Sanders, James V. (1982), *Fundamentals of Acoustics*, John Wiley and Sons, Inc., Canada (ISBN 0-471-02933-5).

Kreysig, E., (1993), *Advanced Engineering Mathematics*, 7th Edition, John Wiley and Sons New York, New York (ISBN 0-471-55380-8).

Laine, L, Sandvick, A. (2001), “Derivation of Mechanical Properties for Sand” *4th Asia-Pacific Conference on Shock and Impact Loads on Structures (Singapore)*, pp. 361-368.

Loctite by Henkel Corporation (2013), *PL 300 Low VOC Foamboard Construction Adhesive*, Product Data Sheet, Rocky Hill, CT.

Mazzoni, Dominic, Dannenberg, Roger, (1999, 2000), *Audacity 2.1.2 Software*, Carnegie Mellon University, Creative Commons Attribution License Ver. 3.0.

McCarthy, David F. (1993), *Essentials of Soil Mechanics and Foundations*, Prentice Hall Career & Technology, New Jersey (ISBN 0-13-287814-3).

McCormick, Michael E. (1973), *Ocean Engineering Wave Mechanics*, John Wiley & Sons, Inc., New York (ISBN 0-471-58177-1).

McCormick, Michael E. (1979), *Anchoring Systems*, Pergamon Press, New York (ISBN 0-08-022694-9).

McCormick, Michael E. (1999), “On the Motions of Grounded Ships,” Johns Hopkins University Technical Report produced under NSWC Carderock Contract N00167-99-0226, Baltimore, Maryland.

McCormick, Michael E. (2010, 2014), *Ocean Engineering Mechanics*, Cambridge University Press, New York (ISBN 978-0-521-85952-3).

McCormick, Michael E. and Cerquetti, Jeffrey (2004), “Alternative Wave-Induced Force and Moment Expressions for a Fixed, Vertical, Truncated, Circular Cylinder in Waters of Finite Depth,” *Proceedings, Offshore Mechanics and Arctic Engineering (OMAE)*, Paper No. OMAE 2004-51330, pp. 673-680, Vancouver, British Columbia, Canada.

McCormick, Michael E. and Hudson, Patrick, J., (2001), “An Analysis of the Motions of Grounded Ships,” *International Journal of Offshore and Polar Engineering*, Vol. 11, No. 2, pp. 95-105.

McHendrie, G., (1988) sdsz, *A Program for Sediment Size Analysis: U.S. Geological Survey, Branch of Pacific Marine Geology*, Menlo Park, CA.

Naval Sea System Command, (1993) “*Ship Salvage Manual*,” United States Navy, Vol. 4.

Oelze, Michael L., O’Brian, William D., Darmody, Robert G., (2002), “Measurement of Attenuation and Speed of Sound in Soils,” *Soil Science Society of America Journal*, Vol. 66, pp.788-796.

Owens-Corning Foam Insulation, LLC (2011), *Foamular 150 Extruded Polystyrene (XPS) Rigid Foam Insulation*, Product Data Sheet, Toledo OH.

PPG Industries (2016), *Liquid Nails LN-604 Projects and Foamboard Latex Adhesive*, Technical Data Sheet, Cranberry, PA.

Rawson, K.J. Tupper, E.C., (1986), *Basic Ship Theory*, Longman Scientific and Technical w/John Wiley and Sons, Inc., New York (ISBN 0-470-20572-5)

Razdow, Allen (2010), *PTC MATHCAD Ver. 15 Software*, Parametric Technology Corporation, 140 Kendrick Street, Needham, MA.

Reddy, P.V., Swamidas, A.S.J., (2014), *Essentials of Offshore Structures*, CRC Press, Boca Raton, Florida (ISBN 978-1-4200-6882-5).

Rollins, Kyle M., Gerber, Travis M., Lane, Dusty J., Ashford, Scott A., (2005), "*Lateral Resistance of a Full-Scale Pile Group in Liquefied Sand*," *Journal of Geotechnical and Geoenvironmental Engineering*, Vol. 131, No. 1, pp. 115-125.

Scott-Russell, J. (1845), "Report on Waves," *Fourteenth Meeting, British Association of Advance Sci.*, pp. 311-390.

Seed, H. Bolton, Idriss, I.M. (1967), "*Analysis of Soil Liquefaction: Niigata Earthquake*," *Journal of Soil Mechanics and Foundations*, Division, ASCE Vol. 93, No. SM3, pp. 83-108.

Simonsen, Bo Cerup, Hansen, Peter Friis, (2000), "*Theoretical and Statistical Analysis of Ship Grounding Accidents*," *OMAE Division of the 18th International Symposium on Offshore Mechanics and Arctic Engineering. Proceedings of the American Society of Mechanical Engineering*, Vol. 122, pp. 200-207.

Terzaghi, K., Peck, R., Mesri, G. (1996), *Soil Mechanics in Engineering Practice*, John Wiley and Sons, New York, New York (ISBN 0-471-08638-4)

Tsinker, Gregory P. (2004), *Port Engineering*, John Wiley and Sons, Inc., New Jersey (ISBN 0-08-022694-9).

University of Connecticut, COSEE TEK., (2000), *Simple Hydrophone Design – Instructions*

Urick, Robert J., (1967), *Principles of Underwater Sound for Engineers*, McGraw-Hill, Inc., New York (Library of Congress Catalog Card Number 67-15040)

U.S. Navy Supervisor of Salvage, (1997), *U.S. Navy Salvage Engineer's Handbook, Volume 1 (Salvage Engineering)*, S0300-A8-HBK-010, Naval Sea Systems Command, Washington, DC.

Weaver, Thomas J., Ashford, Scott A., Rollins, Kyle M., (2005), “*Response of 0.6m Cast-In-Steel-Shell Pile in Liquefied Soil Under Lateral Loading*,” *Journal of Geotechnical and Geoenvironmental Engineering*, Vol. 131, No. 1, pp. 95-102.

Wiegel, Robert L., (1964), *Oceanographical Engineering*, Prentice-Hill, Englewood Cliffs, New Jersey (LOC Card No. 64-23185)

Zienkiewicz, O. C., Pande, G. N. (1982), *Soil Mechanics – Transient and Cyclic Loads*, John Wiley and Sons, Inc., Belfast (ISBN 0-471-010046-3)

PHOTO REFERENCES

- Fig. 1 Internet Image from France's Marine Nationale of TK Bremen grounding 2011
- Fig. 7 Internet Photo of SeaLand Express Grounding; Paul J. Gallie (2003)
- Fig. 8 Internet Photo of SeaLand Express Grounding; Paul J. Gallie (2003)
- Fig. 9 Internet Photo of SeaLand Express Grounding; Paul J. Gallie (2003)
- Fig. 10 Internet Photo of APL Panama; San Diego Tribune (2008)
- Fig. 11 Internet Photo of APL Panama; San Diego Tribune (2008)
- Fig. 12 Internet Photo of F/V Mar-Gun; N. Huddleson (2009)
- Fig. 14 Webpost Image from University of Washington – Dept. of Civil Eng. (2010)
- Fig. 43 Internet Photo of ARCA 1 Grounding; Fisheries and Oceans CA (2017)

REFERENCES (APPENDIX B)

Fig. B1 Internet Photo of Pasha Bulker grounding [1233 ABC Newcastle News](#), 2012

Fig. B2 Internet Photo of Pasha Bulker grounding [1233 ABC Newcastle News](#), 2012

Fig. B3 Internet Image from France's [Marine Nationale](#) of TK Bremen grounding 2011

Fig. B4 Internet Image from France's [Marine Nationale](#) of TK Bremen grounding 2011

Fig. B5 Internet Image from [World Maritime News](#) of the M/V Victoria grounding 2016

Fig. B6 Internet Image from [World Maritime News](#) of the M/V Victoria grounding 2016

The Daily Courier, (1999), "Grounding Incident of the M/V New Carissa off Coos Bay, Oregon," [*www.prescottaz.com*](http://www.prescottaz.com).

